

The Pennsylvania State University

The Graduate School

College of Engineering

**SIMULTANEOUS MONITORING OF OZONE DOSE AND RESPONSE**

**IN THE HUMAN RESPIRATORY TRACT**

A Dissertation in

Chemical Engineering

by

Timothy Brenza

© 2008 Timothy Brenza

Submitted in Partial Fulfillment  
of the Requirements  
for the Degree of

Doctor of Philosophy

December 2008

The dissertation of Timothy Brenza was reviewed and approved\* by the following:

James S. Ultman  
Distinguished Professor Emeritus of Chemical Engineering and Bioengineering  
Dissertation Advisor  
Co-Chair of Committee

Ali Borhan  
Professor of Chemical Engineering  
Co-Chair of Committee

Abdellaziz Ben-Jebria  
Professor of Chemical Engineering, Bioengineering, and Physiology

Darrell Velegol  
Associate Professor of Chemical Engineering

Rebecca Bascom  
Professor of Medicine

Andrew Zydney  
Walter L. Robb Chair and Professor of Chemical Engineering  
Head of the Department of Chemical Engineering

\*Signatures are on file in the Graduate School

## ABSTRACT

The goal of this research was to establish a relationship between the retained dose of O<sub>3</sub> and pulmonary response. Dose and response were measured through controlled exposure experiments on sixty test subjects. Test subjects were recruited based on their smoking status to evaluate the impact of smoking on O<sub>3</sub> sensitivity (30 smoking subjects, and 30 non-smoking subjects).

In the exposure session, the subjects exercised on a cycle ergometer at a workload that was adjusted to maintain their breathing at a constant ventilation rate for a one-hour period. During this exposure session the subject inhaled air that contained 0.3 ppm O<sub>3</sub>. Simultaneous measurements were made of flow, O<sub>3</sub> concentration and CO<sub>2</sub> concentration for the full session. From these measurements, the inhaled dose (D<sub>I</sub>) and the retained dose (D<sub>T</sub>) during complete respiratory cycles were computed.

Pulmonary response was measured by both static and dynamic methods. The static pulmonary response measurements were taken prior to and just after the O<sub>3</sub> exposure session at a fixed breathing condition, whereas the dynamic pulmonary response was measured simultaneous to the exposure. The statically measured parameters consisted of the forced expired volume (FEV<sub>1</sub>), the CO<sub>2</sub> dead space volume (V<sub>D</sub>), and the normalized slope of the CO<sub>2</sub> alveolar plateau (S<sub>N</sub>). The dynamically measured parameters included the tidal volume (V<sub>T</sub>), respiratory rate (RR), V<sub>D</sub>, and S<sub>N</sub>. An additional goal was to elucidate the course of response in these parameters during the exposure session.

Regional dose of O<sub>3</sub> was estimated by simulating the longitudinal distribution of O<sub>3</sub> within the respiratory tract during the breathing cycle. The liquid-phase reaction rate constant (k<sub>r</sub>) was used as an adjustable parameter in the model the fit the simulation to the experimentally measured uptake O<sub>3</sub> uptake efficiency (UE). The median values of k<sub>r</sub> were: 2.9 x 10<sup>6</sup> s<sup>-1</sup> for non-

smoking subjects,  $2.1 \times 10^6 \text{ s}^{-1}$  for smoking subjects,  $1.8 \times 10^6 \text{ s}^{-1}$  for female subjects, and  $2.4 \times 10^6 \text{ s}^{-1}$  for male subjects.  $D_T$  was partitioned into the regional dose ( $D_R$ ) within specific segments of the respiratory tract.  $D_I$ ,  $D_T$ , and  $D_R$  were compared to the response variables to determine the existence of correlations.

The dynamic values of  $\Delta V_T$  (difference between an air control and  $O_3$  exposure session at the same time point) and  $\Delta V_D$  were correlated with the retained dose ( $D_T$ ). Regression analysis determined a rate of change in  $\Delta V_T$  of  $-0.11 \pm 0.03 \text{ mL}/\mu\text{g}$  (mean  $\pm$  SD) and a rate of change in  $\Delta V_D$  of  $-0.014 \pm 0.005 \text{ mL}/\mu\text{g}$ . The smoking subjects exhibited the same dose-response relationships as the non-smoking subjects for these parameters.

The population average regional dose ( $D_R$ ) was:  $142 \pm 114 \mu\text{g}$  (mean  $\pm$  SD) in the upper airways (UA),  $549 \pm 115 \mu\text{g}$  in the conducting airways (CA), and  $97 \pm 113 \mu\text{g}$  in the respiratory airspaces (RA). No significant differences were observed between smoking and non-smoking subjects with respect to  $D_R$ . Significant differences were observed in  $D_R$  within the CA between female ( $487 \pm 88 \mu\text{g}$ ) and male ( $589 \pm 114 \mu\text{g}$ ) subjects, but not within the UA or RA. No correlations were determined between  $D_R$  and the statically evaluated percent change in  $FEV_1$ ,  $V_D$ , and  $S_N$ .

## TABLE OF CONTENTS

LIST OF FIGURES .....	vii
LIST OF TABLES .....	x
Chapter 1 Introduction .....	1
Chapter 2 Background .....	4
Response Measurements .....	4
Spirometry .....	5
Capnometry .....	5
Relating Exposure to Response .....	7
Indirect Method of Determining Inhaled O <sub>3</sub> Dose .....	7
Direct Method of Determining Inhaled O <sub>3</sub> Dose .....	12
Bolus Experiment .....	16
Uptake Simulation .....	17
Chapter 3 Experimental Methodology .....	24
Screening Protocol .....	24
Pulmonary Function Measurements .....	26
Continuous Exposure Experiment .....	28
Experimental Equipment .....	29
Continuous Experiment Procedure .....	35
Continuous Data Analysis .....	36
Determination of Individual Breaths .....	36
Determination of Single Breath Values .....	37
Minute Average Parameters .....	39
Bolus Experiment .....	40
Statistical Analysis .....	41
Chapter 4 Experimental Results .....	42
Subject Characteristics .....	42
Respiratory Flow .....	46
Effect of Smoking Status .....	46
Effect of Gender .....	52
Ozone Uptake .....	56
Effect of Smoking Status .....	56
Effect of Gender .....	59
Dynamic CO <sub>2</sub> Data .....	60
Effect of Smoking Status .....	60
Effect of Gender .....	63
Bolus Experiment Results .....	66
Chapter 5 Discussion .....	70

Total Retained Dose.....	70
Dynamic Changes with Dose.....	75
Simulation of Ozone Uptake.....	82
Single-Path Model.....	83
Modifications to Single-Path Model.....	88
Simulation Results.....	89
Regional Dose of O <sub>3</sub> .....	95
Partitioning Retained Dose Using Single-Path Model.....	96
Results of Retained Dose Partitioning.....	97
Comparison of Regional Dose to Pulmonary Response.....	100
Chapter 6 Summary and Future Work.....	106
Dose and Dose-Response Relationships.....	106
Influence of Smoking Status.....	107
Gender Differences.....	108
Future Work.....	108
Bibliography.....	110
Appendix A: Subject Specific Change in Tidal Volume with Respect to Retained Dose of O <sub>3</sub> .....	115
Appendix B: Subject Specific Change in Dead Space Volume with Respect to Retained Dose of O <sub>3</sub> .....	124
Vita.....	133

## LIST OF FIGURES

Figure 2-1: Sample Spirometric Result.....	5
Figure 2-2: Typical CO <sub>2</sub> Expirogram for an Extended Exhaled Breath. ....	6
Figure 2-3: Indirect Dose-Response Relationship. ....	9
Figure 2-4: Indirect Dose-Response Relationship, Male Subjects and Female Subjects.....	10
Figure 2-5: Indirect Dose-Response Relationship, Smoking Subjects and Non-Smoking Subjects. ....	11
Figure 2-6: Subject Variability in Direct Dose-Response Relationship for FEV <sub>1</sub> .....	14
Figure 2-7: Direct Dose-Response Relationship for S <sub>N</sub> and V <sub>D</sub> .....	15
Figure 2-8: Comparison of Simulation and Experimental Results for Regional O <sub>3</sub> Uptake Efficiency. ....	19
Figure 2-9: Comparison of Simulation and Experimental Results for Uptake Efficiency for Session Averaged Values. ....	20
Figure 2-10: Sensitivity of Simulation to the Reaction Rate Constant for O <sub>3</sub> Uptake Efficiency. ....	22
Figure 2-11: Comparison of Simulated Base Case, Simulated Adjusted and Experimental Results for Uptake Efficiency for Session Averaged Values.....	23
Figure 3-1: Sample CO <sub>2</sub> Expirogram with Parameters for an Extended Exhaled Breath. ....	28
Figure 3-2: Continuous Inhalation System. ....	29
Figure 3-3: Picture of Continuous Inhalation System.....	31
Figure 3-4: Breathing Mask Assembly.....	32
Figure 3-5: Fast Response O <sub>3</sub> Analyzer and Cardiopulmonary Unit.....	34
Figure 3-6: Example Flow-TimeWaveform. ....	38
Figure 3-7: Concentration Curve of an O <sub>3</sub> Bolus as a Function of Respired Volume. ....	41
Figure 4-1: Minute Volume During Air and Ozone Sessions for Smokers and Non- Smokers.....	47
Figure 4-2: Breathing Frequency During Air and Ozone Sessions for Smokers and Non- Smokers.....	48

Figure 4-3: Tidal Volume During Air and Ozone Sessions for Smokers and Non-Smokers.....	49
Figure 4-4: Minute Volume During Air and Ozone Sessions for Male Subjects and Female Subjects. ....	52
Figure 4-5: Breathing Frequency During Air and Ozone Sessions for Male Subjects and Female Subjects. ....	53
Figure 4-6: Tidal Volume During Air and Ozone Sessions for Male Subjects and Female Subjects. ....	54
Figure 4-7: O <sub>3</sub> Uptake Rate and O <sub>3</sub> Uptake Efficiency for Smokers and Non-Smokers. ....	57
Figure 4-8: O <sub>3</sub> Uptake Rate and O <sub>3</sub> Uptake Efficiency for Male Subjects and Female Subjects. ....	59
Figure 4-9: Dead Space Volume During Air and Ozone Sessions for Smokers and Non-Smokers.....	61
Figure 4-10: Normalized Slope During Air and Ozone Sessions for Smokers and Non-Smokers.....	62
Figure 4-11: Dead Space Volume During Air and Ozone Sessions for Male Subjects and Female Subjects. ....	64
Figure 4-12: Normalized Slope During Air and Ozone Sessions for Male Subjects and Female Subjects. ....	64
Figure 4-13: Longitudinal Distribution for Smokers and Non-Smokers. ....	67
Figure 4-14: V <sub>P50</sub> for Smokers and Non-Smokers. ....	67
Figure 4-15: Longitudinal Distribution for Male Subjects and Female Subjects. ....	68
Figure 4-16: V <sub>P50</sub> for Male Smoking Subjects, Female Smoking Subjects, Male Non-Smoking Subjects, and Female Non-Smoking Subjects. ....	69
Figure 5-1: Percent Change in FEV <sub>1</sub> with Respect to Minute Volume for Male Smoking Subjects, Female Smoking Subjects, Male Non-Smoking Subjects, and Female Non-Smoking Subjects.....	71
Figure 5-2: Percent Change in FEV <sub>1</sub> with Respect to Inhaled Dose of O <sub>3</sub> and Retained Dose of O <sub>3</sub> .....	72
Figure 5-3: Percent Change in V <sub>D</sub> and S <sub>N</sub> with Respect to Retained Dose of O <sub>3</sub> for Smokers and Non-Smokers.....	73

Figure 5-4: Percent Change in FEV <sub>1</sub> with Respect to Retained Dose of O <sub>3</sub> for Male Subjects and Female Subjects.....	75
Figure 5-5: Dynamic Change in V <sub>T</sub> with Respect to Retained Dose of O <sub>3</sub> for One Subject.....	77
Figure 5-6: Dynamic Change in V <sub>D</sub> with Respect to Retained Dose of O <sub>3</sub> for One Subject.....	78
Figure 5-7: Dynamic Change in S <sub>N</sub> with Respect to Retained Dose of O <sub>3</sub> for One Subject.....	79
Figure 5-8: Relationship Between S <sub>N</sub> and V <sub>T</sub> .....	80
Figure 5-9: Relationship Between S <sub>N</sub> and V <sub>T</sub> for One Subject.....	81
Figure 5-10: Relationship Between V <sub>D</sub> and V <sub>T</sub> for One Subject.....	82
Figure 5-11: Schematic of the Single-Path Model.....	83
Figure 5-12: Comparison of Measured Uptake Efficiency to the Predicted Values for Two Sample Subjects.....	90
Figure 5-13: Subject Specific k <sub>r</sub> Values by Smoking Category and by Gender.....	91
Figure 5-14: SSE Function for Sample Subjects with High, Average, and Low Fitted k <sub>r</sub> Multipliers.....	92
Figure 5-15: Time-Course of k <sub>r</sub> Value for Subject FPM074N.....	94
Figure 5-16: Comparison of Time Specific k <sub>r</sub> and Multiple Point Fitted k <sub>r</sub> Simulations for Subject FPM074N.....	95
Figure 5-17: Partitioning Factor for Regional Respiratory Compartment.....	98
Figure 5-18: Population Distribution of Retained Dose by Lung Region.....	100
Figure 5-19: Percent Change in FEV <sub>1</sub> with Respect to Regional Retained Dose of O <sub>3</sub> for Male Non-Smoking Subjects, Female Non-Smoking Subjects, Male Smoking Subjects, and Female Smoking Subjects.....	102
Figure 5-20: Percent Change in V <sub>D</sub> with Respect to Regional Retained Dose of O <sub>3</sub> for Male Non-Smoking Subjects, Female Non-Smoking Subjects, Male Smoking Subjects, and Female Smoking Subjects.....	103
Figure 5-21: Percent Change in S <sub>N</sub> with Respect to Regional Retained Dose of O <sub>3</sub> for Male Non-Smoking Subjects, Female Non-Smoking Subjects, Male Smoking Subjects, and Female Smoking Subjects.....	105

**LIST OF TABLES**

Table 4-1: Subject Characteristics.....	43
Table 4-2: Baseline Pulmonary Function Measurements.....	45
Table 4-3: Summary of ANCOVAs for Smoking Effects.....	51
Table 4-4: Summary of ANCOVAs for Gender Effects.....	55
Table 4-5: Summary of ANCOVAs for Ozone Uptake.....	58
Table 4-6: Summary of ANCOVAs for Smoking Status of Dynamic CO <sub>2</sub> Data.....	63
Table 4-7: Summary of ANCOVAs for Gender Difference of Dynamic CO <sub>2</sub> Data.....	65
Table 5-1: Subject Specific k <sub>r</sub> Values Determined Through Single-Breath and Multiple-Breath Fitting Procedures.....	89
Table 5-2: Retained Dose Partitioned into Lung Regions.....	98

## **Chapter 1**

### **Introduction**

Ground level ozone ( $O_3$ ) is an air pollutant generated by a photochemical reaction of oxygen with oxides of nitrogen ( $NO_x$ ) that is catalyzed by volatile organic compounds (VOC). The major sources for  $NO_x$  and VOC emissions are industrial factories, electric utilities, and automobile exhaust. National Ambient Air Quality Primary Standards are established by the US Environmental Protection Agency (EPA) to protect public health, including the health of “sensitive” populations. This year the EPA established a more stringent National Ambient Air Quality Primary Standard for  $O_3$  at 0.075 ppm over an 8-hour averaging time.

Short term health effects attributed to  $O_3$  exposure include: coughing, and pain when taking a deep breath; wheezing and breathing difficulties during exercise or outdoor activity; and aggravation of asthma. Laboratory studies of repeated exposure indicate that there is inflammation of the respiratory tract that is not attenuated over time [Ratto et al., 2006]. Epidemiological studies have correlated exposure to ambient  $O_3$  with increased daily morbidity and increased cardiovascular and respiratory morbidity [Bell et al., 2004].

The main function of the respiratory system is the transport of oxygen to the body and the elimination of carbon dioxide. The respiratory tract is typically divided into three regions: the upper conducting airways that include the oral cavity, the nasal cavities, the pharynx, and the larynx; the lower conducting airways that begins at the trachea and extends distally through a branching structure of the bronchi and continuing to bifurcate until ending at the bronchioles; and the respiratory airspaces where gas is exchanged across the alveoli. The conducting airways are

coated by an epithelial lining layer consisting of a mucous (gel) phase and an underlying aqueous (sol) phase. The mucous phase protects the airways from inhaled particulate matter by entrapping the particles and propelling them out of the conducting airways through the coordinated movement of hair-like cilia. Antioxidants contained in the epithelial liquid layer provide protection from oxidative pollutants [Pryor, 1994].

Ozone is a powerful oxidizing chemical that has a relatively low aqueous solubility but a very high reactivity with biochemical substrates, particularly those containing carbon-carbon double bonds. When  $O_3$  is inhaled, it is transported distally through the respiratory system by convection. Within the respiratory system,  $O_3$  diffuses into the epithelial lining layer where it is essentially neutralized before reaching the underlying tissue [Cvitas et al., 2005]. Therefore, the health effects of  $O_3$  are most probably caused by toxic intermediates such as peroxides formed when  $O_3$  reacts with polyunsaturated fatty acids in the epithelial lining fluid.

In this thesis, experimental measurements and a computer simulation were used to investigate the dose-response of  $O_3$  in the human respiratory tract. Of these sixty subjects that were studied in the laboratory, half were cigarette smokers and half were non-smokers. An approximately equal number of men and women participated. The experiments simultaneously measured retained  $O_3$  dose and pulmonary function. In addition to relating pre-to-post exposure decrements in pulmonary response measurements to retained  $O_3$  dose, the goal of the experiments was the incorporation of simultaneous, real time measurements of retained dose and pulmonary function. A third goal was to evaluate differences in respiratory susceptibility to  $O_3$  based on smoking status and on gender.

A mathematical model was used to estimate the dose distribution of  $O_3$  within the respiratory tract. The model incorporated the inhaled  $O_3$  concentration, the breathing pattern of the subject, and anatomical data. The respiratory tract geometry was simplified into a single representative path from the airway opening to the distal alveoli. The goal of the modeling work

was the estimation of the regional distribution of retained dose, and a comparison of these local doses to response measurements.

This thesis is composed of six chapters including this introduction. Chapter 2 reviews previously-established methods used to quantify response, previous experiments used to deduce the relationship between dose and response, and previous efforts to model the uptake of O<sub>3</sub> within the respiratory tract. The experimental methods used in the current study are detailed in Chapter 3. These include the static and dynamic determination of response measurements, and the dynamic measurement of retained dose of O<sub>3</sub>. Also contained in Chapter 3 is the statistical methodology used. Chapter 4 presents the results of the dose and response measurements with statistical analysis of the results. Chapter 5 discusses the relationship between the dose and response measurements. Also presented in Chapter 5 is the single-path model used for simulating respiratory O<sub>3</sub> transport and the application of this model to partition retained O<sub>3</sub> dose into its regional components. Chapter 6 describes the future work needed to further the understanding of the real-time dose-response data.

## **Chapter 2**

### **Background**

This chapter is divided into four sections and presents the historical efforts to deduce the relationship between exposure to ozone and responses. The focus of the research discussed is the clinical exposure of human subjects to ozone and the quantified pulmonary response to these exposures. Section 2.1 describes methods used to quantify human subject physiological responses to ozone exposure. Section 2.2 presents experiments that characterize human exposures to ozone with their measured responses. Section 2.3 describes the studies using the bolus experimental method to investigate ozone distribution in the human respiratory tract. Section 2.4 presents efforts to model the uptake of ozone within the human respiratory tract.

#### **2.1 Response Measurements**

To establish a relationship between ozone ( $O_3$ ) exposure and physiological responses, methods to quantify the response are necessary. Two of these methods of quantifying pulmonary response are discussed in this section: spirometry and capnometry. Spirometry is extensively used to characterize human responses to ozone exposure and relies solely on the measurement of airflow. Capnometry is less common and involves the measurement of the evolution of carbon dioxide ( $CO_2$ ) during the exhaled breath of the subject. These procedures are introduced in this section, but their methodology and analysis are described in more detail in Chapter 3.

### 2.1.1 Spirometry

Spirometry is the most common pulmonary function test and is used in the assessment of many respiratory conditions. The spirometric maneuver has the subject perform a maximal inhalation of air followed by a maximal forceful expiration of the air. The air flow is recorded throughout the procedure and used to determine specific pulmonary function parameters. The volume expired in the first second of the forceful exhalation is the forced expired volume in one second ( $FEV_1$ ). The total volume expired over the forceful exhalation is the forced vital capacity (FVC). These two values are shown graphically in Figure 2-1.

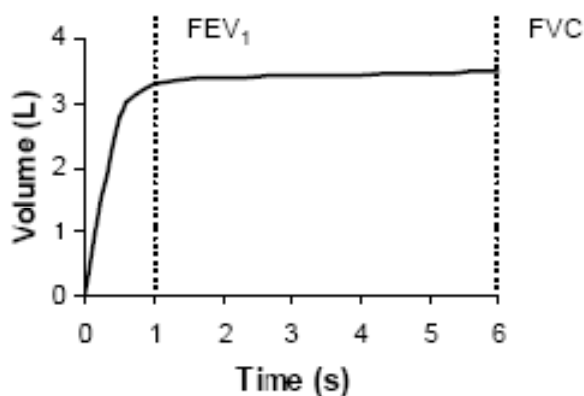


Figure 2-1: Sample Spirometric Result. Presented as a volume versus time curve. FVC determined as the volume at the end of the exhalation.  $FEV_1$  determined as the volume one second into the exhalation. For this sample the  $FEV_1$  is 3.3 L and FVC is 3.5 L.

### 2.1.2 Capnometry

Capnometry is similar to a more commonly used gas washout technique, as it is the measurement of the evolution of  $CO_2$  during exhalation. Capnometry depends on  $CO_2$  transport into the respiratory airspace across the alveoli from the bloodstream, whereas in traditional gas washout techniques, an inert gas confined to the airways is introduced into the mouth during

inhalation. The capnograph, which is a plot of expired  $\text{CO}_2$  concentration versus expired volume, has a sigmoidal shape that can be divided into three phases (Figure 2-2). Phase I corresponds to the initial expired gas that contains no  $\text{CO}_2$ . Phase II is the transition region where the  $\text{CO}_2$  concentration rapidly rises toward a plateau. Phase III is the alveolar plateau that is characterized by a shallow positive slope. The dead space ( $V_D$ ), which is the expired volume required to reach the concentration-weighted center of phase II [Fowler, 1948], reflects the volume of the conducting airways. The slope of phase III (S), or alveolar plateau, is a parameter that characterizes gas transfer in the respiratory zone.

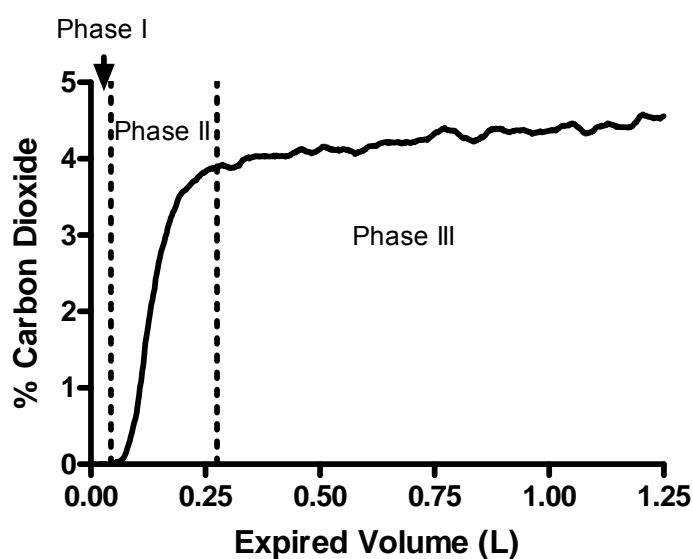


Figure 2-2: Typical  $\text{CO}_2$  Expirogram for an Extended Exhaled Breath.  $V_D$  is determined from the concentration-weighted center of Phase II. S is determined as the slope of Phase III.

## 2.2 Relating Exposure to Response

One of the first investigations into the pulmonary health effects of low concentration O<sub>3</sub> exposure on human subjects were the experiments conducted by Young, Shaw and Bates in 1964 [Young *et al.*, 1964]. In their work they showed that exposure to 0.6-0.8 ppm O<sub>3</sub> orally inhaled for a two hour period produced significant decrements in FVC and FEV<sub>0.75</sub>, forced expired volume in 0.75 seconds, of about 10%. Further studies based on these early health effect observations have investigated and quantified factors which effect pulmonary responses to O<sub>3</sub> exposure. The experimental methods of determining exposure have either involved the control of the ambient concentration of O<sub>3</sub>, the indirect method, or the measuring of the retained dose of O<sub>3</sub>, the direct method. Each method is reviewed in the following sections.

### 2.2.1 Indirect Method of Determining Inhaled O<sub>3</sub> Dose

The effective dose, or inhaled dose, was one of the first factors investigated as to the role it plays in the responses observed from O<sub>3</sub> exposure. In experiments conducted by Bates and coworkers, a population of subjects was exposed to 0.75 ppm O<sub>3</sub> while seated in an environmental chamber for two hours [Bates *et al.*, 1972]. A subset of the initial subjects also underwent a second exposure where they increased their breathing by intermittent exercise during the two hour exposure at the same O<sub>3</sub> concentration. The responses to the intermittent exercise resulted in a reduction in FEV<sub>1</sub> of 30.3% from pre-exposure values in the three subjects, while no significant changes were observed with the resting exposures. This experiment led to the hypothesis of a dose-response type of relationship between O<sub>3</sub> exposure and spirometric parameters.

Experiments were carried out controlling the duration of the exposure and varying the O<sub>3</sub> concentration to quantify this dose-response relationship [Silverman et al., 1976; Adams et al., 1981; McDonnell et al., 1983]. The work by Silverman and coworkers established a second order relationship between FEV<sub>1</sub> and effective dose. However, their definition of effective dose was a breathing rate weighted average concentration of O<sub>3</sub> and not an actual dose. For example exposure to 0.37 ppm O<sub>3</sub> over the two hour session at rest equaled an effective dose of 0.37, and exposure to the same concentration with an hour of exercise at 2.5 times the breathing rate and an hour of rest equaled an effective dose of 0.65 [Silverman et al., 1976].

Adams and coworkers determined an effective dose of ozone as the product of inhaled concentration and minute ventilation rate (ppm·l). In their experimental protocol, eight health male subjects completed 18 sessions with O<sub>3</sub> concentrations of 0, 0.20, 0.30 and 0.40 ppm. The subjects exercised continuously at one of two minute ventilation rates (33 or 66 L/min) for durations ranging from 30 to 80 min. In this fashion, the same effective dose was obtained during various concentrations of O<sub>3</sub> exposure. For example, a target effective dose of 800 ppm·L was achieved at 0.20 ppm O<sub>3</sub> with 60 min exercise at 66 l/min and at 0.40 ppm O<sub>3</sub> with 60 min exercise at 33 L/min. These results were compared to that of Silverman and coworkers and were found to be in good agreement [Adams et al., 1981].

The work of McDonnell and coworkers utilized the same exposure duration and breathing rate to investigate the influences of inhaled O<sub>3</sub> concentration on pulmonary function. Through regression analysis of their results a sigmoidal dose response relationship was determined for pulmonary functions, including FEV<sub>1</sub>, and O<sub>3</sub> concentration [McDonnell et al., 1983].

In order to compare studies that were conducted under various conditions, the inhaled dose of  $O_3$  ( $D_I$ ) was estimated using the concentration of  $O_3$  ( $C_{O_3}$ ), duration of exposure (Time), and minute ventilation ( $V_M$ ), through the following equation:

$$D_I = C_{O_3} [(Time_{tot} - Time_{ex}) V_{M_{rest}} + (Time_{ex}) V_{M_{ex}}] \quad [2-1]$$

To compare these studies  $D_I$  has been plotted against the response measurement  $FEV_1$  in Figure 2-3.

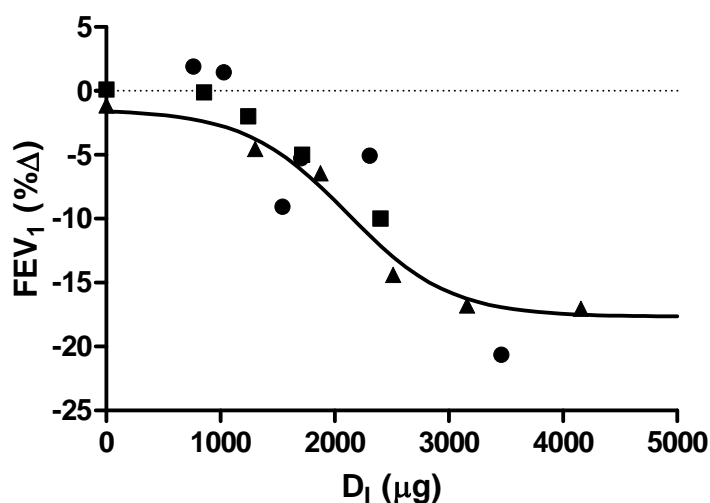


Figure 2-3: Indirect Dose-Response Relationship.  $D_I$  determined from Equation 2-1.  $V_{M_{rest}}$  estimated at 8 L/min in calculation of  $D_I$  from Silverman et al. (●), and McDonnell et al. (▲). Percent change in  $FEV_1$  (% $\Delta$ ) calculated as (post-exposure–pre-exposure)/pre-exposure for Adams et al. (■) and McDonnell et al. (▲).  $FEV_1$  (% $\Delta$ ) calculated as (exposure–control)/control for Silverman et al. (●). Solid line is sigmoidal dose response relationship established by McDonnell et al., converted to  $D_I$  by Equation 2-1 and  $FEV_1$  (% $\Delta$ ) by using population mean pre-exposure  $FEV_1$ .

Two of the previous studies, Adams et al. and McDonnell et al., explicitly studied healthy male non-smoking subjects. To understand the effects of gender on pulmonary function responses to  $O_3$  exposure, these studies have been compared with three studies on healthy female non-smoking subjects [Gibbons and Adams, 1984; Lauritzen and Adams, 1985; Messineo and Adams, 1990]. The  $FEV_1$  response has been plotted against  $D_I$ , calculated by Equation 2-1, in

Figure 2-4. The results suggest that for a given  $O_3$  dose, female subjects exhibit a greater decrement in pulmonary function than male subjects. To determine if the observed gender difference was a function of size, Messineo and Adams separated their female population by total lung capacity (TLC) and found no significant difference in responses based on lung capacity grouping, but observed nearly double the decrement in FEV1 when compared to a previously tested male population at the same conditions. However, in a study designed to address the gender and age effect, the dose of  $O_3$  administered to the subjects was normalized by their body surface area (BSA) through adjusting their ventilation rate [Hazucha et al., 2003]. No significant gender difference was observed when exposed to the normalized dose of  $O_3$ , suggesting that the difference observed was size related. Since each subject received an unique dose of  $O_3$  in the study by Hazucha et al., these data have not been included in Figure 2-4.

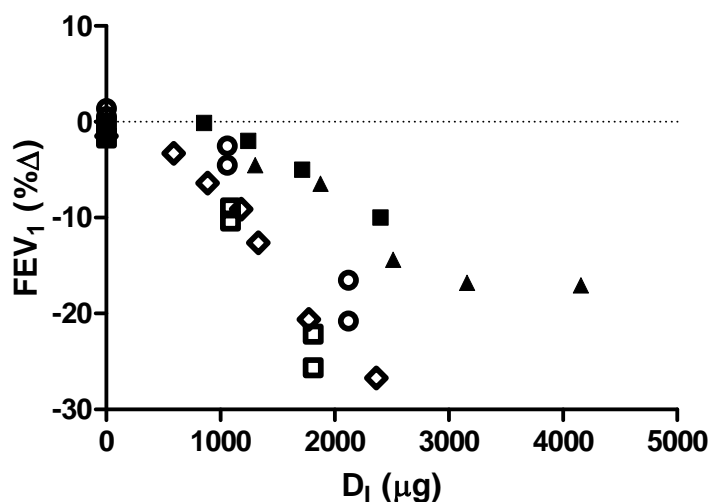


Figure 2-4: Indirect Dose-Response Relationship, Male Subjects (Adams et al. (■) and McDonnell et al. (▲)) and Female Subjects (Messineo and Adams (□), Lauritzen and Adams (◇), and Gibbons and Adams (○)).  $D_1$  determined from Equation 2-1.  $V_{M \text{ rest}}$  estimated at 8 L/min in calculation of  $D_1$  from McDonnell et al. (▲). Percent change in FEV<sub>1</sub> (% $\Delta$ ) calculated as (post-exposure – pre-exposure)/ pre-exposure.

The studies presented in Figure 2-4 are exclusively non-smoking subjects. It has been suggested that smoking subjects exhibit a reduced response to  $O_3$  in terms of pulmonary function [Kerr et al., 1975; Frampton et al., 1997]. The studies of Kerr and colleagues, Frampton and colleagues, and a study by Hazucha and coworkers paired populations of smoking subjects to subjects which did not smoke [Hazucha et al., 1973]. An additional study on the responsiveness of smoking subjects to ozone by Shephard and coworkers only included a smoking population [Shephard et al., 1983]. The exposure conditions in these studies have been converted to  $D_1$  and presented in Figure 2-5. There does not appear to be significant differences in the responsiveness of smokers to non-smokers, with the possible exception being at large values of  $D_1$  where there is limited data.

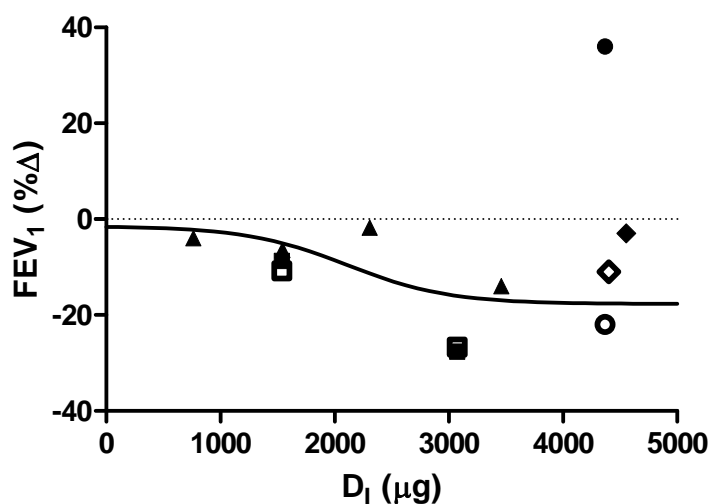


Figure 2-5: Indirect Dose-Response Relationship, Smoking Subjects (filled symbols) and Non-Smoking Subjects (open symbols).  $D_1$  determined from Equation 2-1.  $V_{M \text{ rest}}$  estimated at 8 L/min in calculation of  $D_1$  for all four studies: Kerr et al. (●, ○), Hazucha et al. (■, □), Frampton et al. (◆, ◇), and Shephard et al. (▲). Percent change in  $FEV_1$  (% $\Delta$ ) calculated as (post-exposure – pre-exposure)/ pre-exposure. Solid line is sigmoidal dose response relationship based on non-smoking subjects converted to  $D_1$  by Equation 2-1 and  $FEV_1$  (% $\Delta$ ) by using population mean pre-exposure  $FEV_1$  [McDonnell et al., 1983].

While forced spirometry is the most common quantification of pulmonary function decrement upon exposure to O<sub>3</sub>, there have been studies into changes in ventilation distribution related to exposure to O<sub>3</sub> through gas washout techniques. Silverman and colleagues utilized the nitrogen (N<sub>2</sub>) washout technique in a mixed population [Silverman et al., 1976]. At the highest exposure in their protocol, 0.75 ppm O<sub>3</sub> over 2 hours with 1 hour intermittent exercise to increase the minute volume by 2.5 times, the slope of the phase III plateau increased significantly, which provided evidence of responses to the O<sub>3</sub> exposure in the small airways.

In the experimental procedure of Hazucha and colleagues, they investigated changes in the closing capacity upon exposure to O<sub>3</sub> utilizing a Xenon (Xe) bolus technique [Hazucha et al., 1973]. The results showed a greater increase in closing capacity in the smoking population (10%) than the non-smoking population (2.7%) upon exposure to O<sub>3</sub>. The authors therefore hypothesized that smokers may exhibit an increased susceptibility of their peripheral airways to O<sub>3</sub>.

### **2.2.2 Direct Method of Determining Inhaled O<sub>3</sub> Dose**

Direct experimental measurements of the inhaled and exhaled O<sub>3</sub> concentration, required the change in O<sub>3</sub> sampling location from the environmental chamber to the subject airstream. In a study by Wiester and colleagues, two commercial O<sub>3</sub> analyzers were used to determine the percentage of O<sub>3</sub> uptake during resting conditions. The upstream and downstream sampling ports for O<sub>3</sub> were located approximately 1 m before and after the breathing port along a large-diameter supply tube. To combine the exhaled air and the excess air in the supply tube, a mixing chamber was positioned in the supply tube prior to the downstream sampling port. Determination of the percentage of O<sub>3</sub> uptake relied upon the measurement of time delay for both analyzers, the flow rate of the supplied airstream, and the measurement of minute volume obtained through the use of

a Respirtrace vest. During oral breathing the average percent of O<sub>3</sub> uptake was 76.5% with a range of approximately 50 to 90% for ten subjects [Wiester et al., 1996].

Measuring the inhaled dose of O<sub>3</sub>, and also the amount of O<sub>3</sub> retained by the subject, requires the use of an O<sub>3</sub> detector with a response suitable for the real-time analysis of O<sub>3</sub> concentration during the breathing cycle. The development of a respiratory analyzer by MacDougal and colleagues, with a response time of 0.07 s, enabled the measurement of inhaled dose directly from the subjects breathing pattern and inhaled O<sub>3</sub> concentration [MacDougal et al., 1998].

Direct measurements have been performed on ten non-smoking subjects to investigate the relationship between the inhaled dose of O<sub>3</sub> and the actual amount of O<sub>3</sub> retained by the subject [Rigas et al., 2000]. This report found that fractional absorption of O<sub>3</sub>, the amount of O<sub>3</sub> retained divided by the inhaled O<sub>3</sub> dose, ranged from 0.56 to 0.98 with a mean  $\pm$  SD of  $0.86 \pm 0.06$  for the pooled data from all subjects. This suggested that inter-subject variability in fractional absorbance of O<sub>3</sub> is greater than differences caused by changes in O<sub>3</sub> concentration, minute volume, or time. This was reinforced by another study investigating subject variability to O<sub>3</sub> exposure in which 60 non-smoking subjects were exposed to 0.25 ppm O<sub>3</sub> for one-hour while they exercised to achieve a minute ventilation rate of 30 L/min [Reeser et al., 2005]. The resulting uptake rate and change in FEV<sub>1</sub> is presented in Figure 2-6.

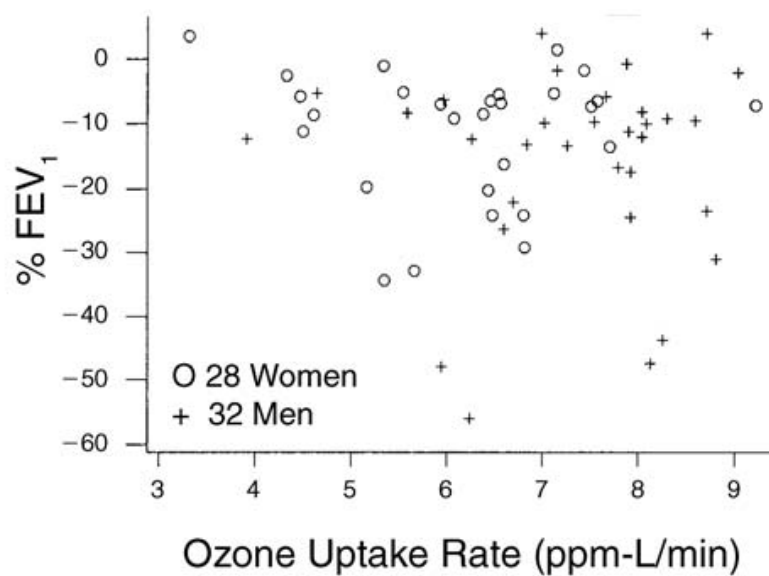


Figure 2-6: Subject Variability in Direct Dose-Response Relationship for FEV<sub>1</sub>. Each data point represents the behavior of one subject during O<sub>3</sub> exposure. Reproduced from Reeser et al., 2005.

Associated with the subject variability study, capnometry measurements were performed on a subset of subjects. The results indicated that there was a significant change in  $S$  ( $16.4 \pm 17.9$  % $\Delta$ ),  $S$  normalized by the amount of CO<sub>2</sub> exhaled ( $S_N$ ) ( $17.5 \pm 15.4$  % $\Delta$ ), and  $V_D$  ( $-4.2 \pm 5.1$  % $\Delta$ ) during O<sub>3</sub> exposure, but not during an air control session [Taylor et al., 2006]. The resulting changes in  $S_N$  and  $V_D$  with respect to O<sub>3</sub> uptake rate for the individual subjects are presented in Figure 2-7 [Ultman et al., 2004].

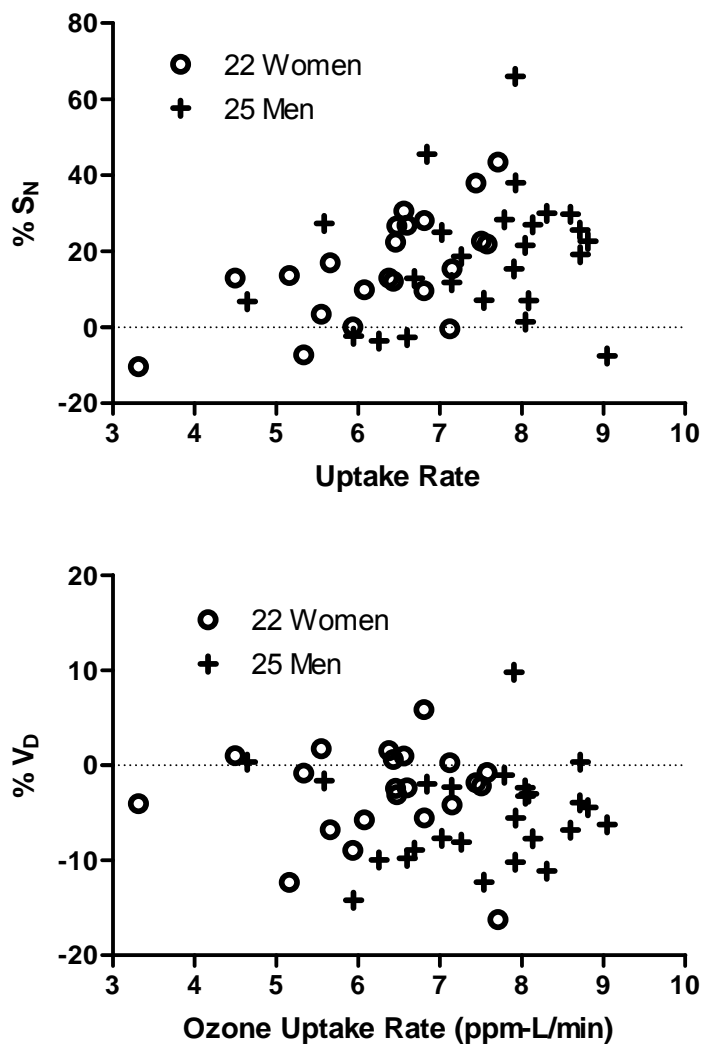


Figure 2-7: Direct Dose-Response Relationship for  $S_N$  and  $V_D$ . Each data point represents the behavior of one subject during  $O_3$  exposure.  $\%S_N$  and  $\%V_D$  calculated as  $100 \times (10 \text{ minutes post exposure} - \text{pre exposure}) / \text{pre exposure}$ . Reproduced from Ultman et al., 2004.

### 2.3 Bolus Experiment

A bolus inhalation technique for O<sub>3</sub> was developed to investigate the longitudinal distribution of O<sub>3</sub> uptake in the respiratory tract [Ben-Jebria et al., 1991]. This method was first applied to non-smoking human subjects by Hu and colleagues [Hu et al., 1992]. The longitudinal distribution was determined as the fractional absorption of O<sub>3</sub>,  $\Lambda$ , versus the volume the bolus penetrates into the respiratory tract, V<sub>P</sub>. At a respiration rate of 250 ml/s, the longitudinal distribution indicated that 50% of the inhaled O<sub>3</sub> was absorbed in the upper airways (V<sub>P</sub> up to 70 ml) and inhaled O<sub>3</sub> was almost completely absorbed in the conducting airways (V<sub>P</sub> up to 180 ml). This method has also been used to investigate the effects of flow, gender, inhaled O<sub>3</sub> concentration, and a continuous O<sub>3</sub> exposure on the longitudinal distribution.

In determining the effect of respiratory flow on the longitudinal distribution of O<sub>3</sub>, flow rates between 150 and 1,000 ml/s were investigated with the bolus technique [Hu et al., 1994]. This work showed that at a given V<sub>P</sub>,  $\Lambda$  decreased with increased flow rate. This corresponded to a greater amount of O<sub>3</sub> absorbed more distally in the respiratory tract when the bolus was inhaled at a greater flow rate.

In work investigating the role of lung anatomy and size on inter-subject variability in the longitudinal distribution of O<sub>3</sub>, Bush and colleagues determined that on average, women absorbed O<sub>3</sub> at a smaller V<sub>P</sub> than the men. Since the majority of inhaled O<sub>3</sub> in the bolus technique is absorbed in the conducting airways the authors normalized V<sub>P</sub> by a measure of V<sub>D</sub>. Using this as the independent variable, the difference in longitudinal distributions between the men and women were indistinguishable [Bush et al., 1996A].

In work investigating the differences in absorption between oral and nasal breathing, Kabel and colleagues demonstrated that the O<sub>3</sub> bolus technique was insensitive to the inhaled concentration of O<sub>3</sub> delivered in the bolus [Kabel et al., 1994]. An additional investigation

focused on changes to the longitudinal distribution after an exposure to O<sub>3</sub>. In this work, the subject established a baseline longitudinal distribution through the bolus technique. The subject was then exposed to ozone in a head-only chamber at 0, 0.12, or 0.36 ppm O<sub>3</sub> for 2 hours. During the exposure the subject was periodically removed from the O<sub>3</sub> to perform an abbreviated set of bolus maneuvers. The author concluded that continuous exposure to O<sub>3</sub> caused a dose-dependent decrease in the absorption efficiency [Asplund et al., 1996].

## 2.4 Uptake Simulation

Due to experimental limitations, the use of a mathematical model to understand the O<sub>3</sub> interactions with the different regions of the respiratory system is necessary. Simulations that utilized a one-dimensional unsteady state diffusion model were first applied to the bolus technique by Bush and colleagues [Bush et al., 1996B]. In this model, the complex tracheobronchial tree was replaced by a single path which represents all transport paths from the airway opening to the respiring airspace. This approach was first utilized for the modeling of insoluble inert gas by Scherer and colleagues [Scherer et al., 1972].

The simulation utilized the inhaled O<sub>3</sub> pattern, volumetric flow, and airway dead space that were measured in the O<sub>3</sub> bolus experiments. Anatomical details, gas-phase mass transfer coefficient, and dispersion coefficient were estimated from previously published measurements that were independent of the O<sub>3</sub> bolus study. The liquid-phase mass transfer coefficient through the mucous layer was approximated by a one-dimensional, steady state, model of simultaneous diffusion and homogeneous chemical reaction within the mucus layer. The simulated longitudinal distribution was close to the experimentally measured values [Bush et al., 1996B], but it was necessary to adjust the gas-phase and liquid-phase mass transfer coefficients to improve the simulation of data collected for both chlorine (Cl<sub>2</sub>) and O<sub>3</sub> [Bush et al., 2001].

To validate the single-path model with O<sub>3</sub> absorption data from an independent laboratory, the model was modified to account for a constant inhalation of O<sub>3</sub> [Bush et al., 2001]. The model was then used to simulate O<sub>3</sub> uptake efficiency under the experimental conditions of the work by Gerrity and colleagues. In this work, bronchoscopic positioning of the sampling in the respiratory tract enabled O<sub>3</sub> concentration measurements at these specific internal locations. The O<sub>3</sub> concentrations were monitored over the breathing cycle in healthy non-smoking male subjects. The concentration and flow results were used to determine the O<sub>3</sub> uptake efficiency within different regions within the respiratory tract for an entire respiratory cycle, inhalation and the subsequent exhalation [Gerrity et al., 1995]. As seen in Figure 2-8, the model simulation results closely matched the experimental measurements.

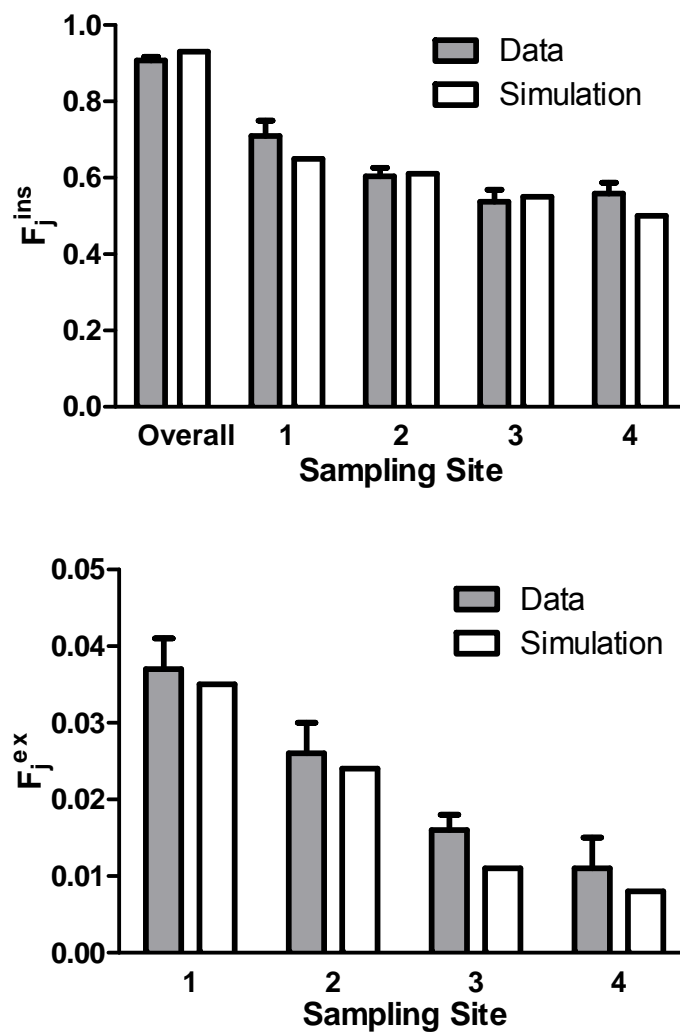


Figure 2-8: Comparison of Simulation and Experimental Results for Regional O<sub>3</sub> Uptake Efficiency.  $F_j^{ins}$  and  $F_j^{ex}$  are the fraction of inspired O<sub>3</sub> mass that passed the entrance to the pneumotach and reached site  $j$  during inspiration (ins) or expiration (ex). The four sites are: 1 above vocal cords; 2 below vocal cords; 3 just above main carina; and 4 midpoint of bronchus intermedius. The vertical bars represent the standard error of the experimental data. Reproduced from Bush et al., 2001.

This validated model has recently been used to investigate the inter-subject variability observed in responses to  $O_3$  exposure. In this work, the single-path model was compared to the experimental measurements of retained dose in 60 test subjects over an hour period during which the subjects exercised to achieve a target ventilation of 30 L/min while they inhaled a concentration of 0.3 ppm  $O_3$  [Reeser et al., 2005]. The model used anatomic parameters scaled for each subject by his or her measured  $V_D$  and FRC values. The breathing pattern for each subject was approximated as a square waveform using the session averaged values of tidal volume ( $V_T$ ) and respiratory rate (RR). The transport and reaction parameters used in this simulation were based on the simulation validation results by Zhang [Zhang, 2000]. The simulated uptake efficiency ( $U_E$ ) and experimentally measured  $U_E$  for the sixty test subjects in the variability study are presented in Figure 2-9 [Reeser, 2007].

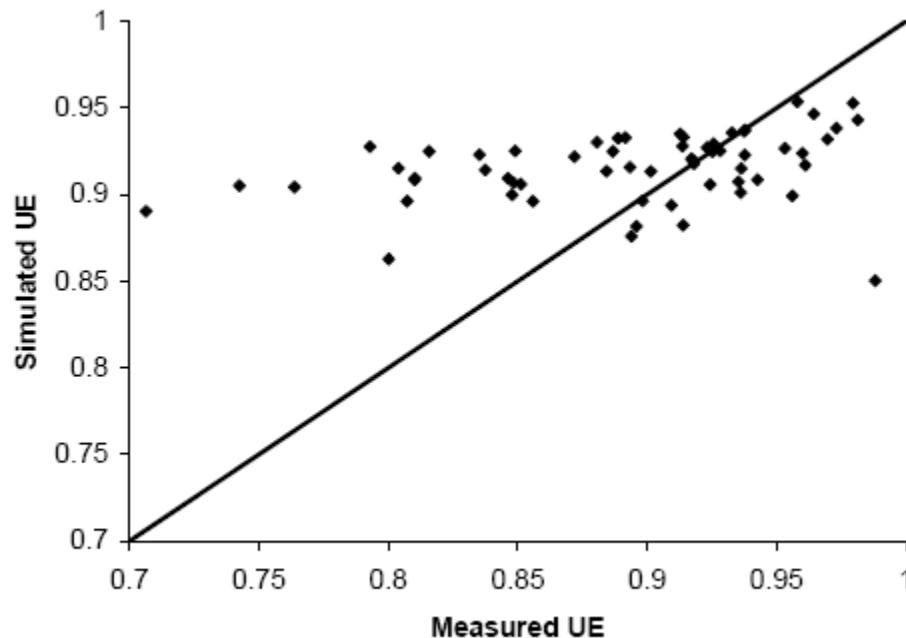


Figure 2-9: Comparison of Simulation and Experimental Results for Uptake Efficiency for Session Averaged Values. Each data point represents the behavior of one subject. The line of identity represents agreement between simulated and measured values. Reproduced from Reeser, 2007.

The impact of individual-subject modification of the following model parameters was investigated: the dispersion coefficient, the airway hydraulic diameter, the thickness of the mucus layer, and the pseudo first-order reaction rate constant. Since these parameters could also vary with longitudinal position, the impact of variation was analyzed over the whole lung and also within subsections of the respiratory tract. From this analysis, the simulation of uptake efficiency was found to be most sensitive to changes of the reaction rate constant. Presented in Figure 2-10 is the simulated uptake efficiencies for an “average man” (i.e., standard values of all the model parameters except for the reaction rate constant). Separate multipliers were applied to a base value of the reaction rate of  $3.0 \times 10^6 \text{ sec}^{-1}$  [Zhang, 2000] in order to fit the uptake efficiency for each subject. This procedure greatly reduced the difference between the simulated and the measured uptake efficiency was greatly reduced, as seen in Figure 2-11. The multipliers for the 60 test subjects ranged from  $10^{-5}$  to  $10^4$ .

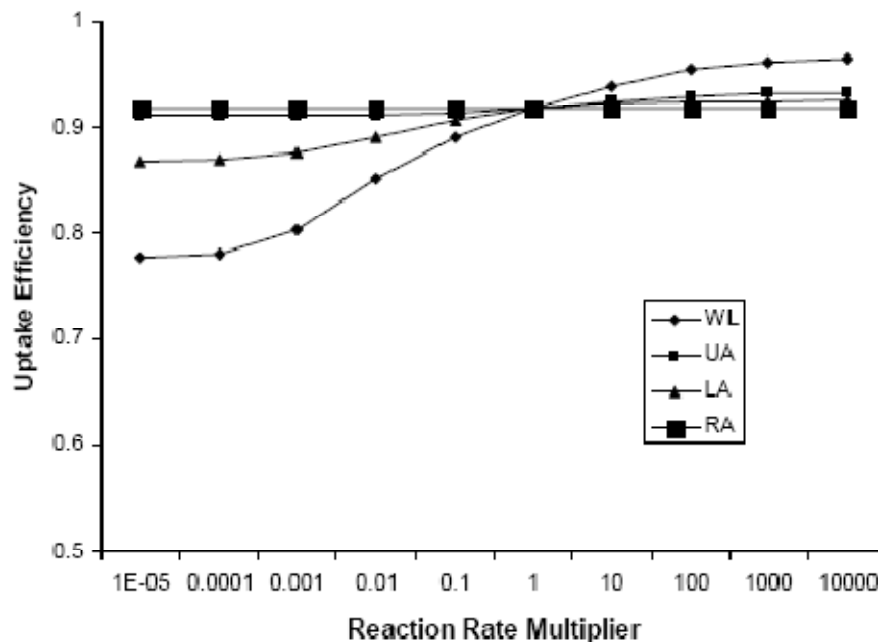


Figure 2-10: Sensitivity of Simulation to the Reaction Rate Constant for O<sub>3</sub> Uptake Efficiency. Simulation performed on “average man” with the following parameters: V<sub>D</sub> of 150 ml, FRC of 2.65 L, V<sub>T</sub> of 1 L, and RR of 30 breath/min. Multiplier applied to reaction rate for: whole lung (WL), upper airways (UA) including oral cavity, larynx, pharynx and trachea and Weibel lung model generations 1 through 3, lower airways (LA) include Weibel lung model generations 4 through 16, and respiratory airspace (RA) includes Weibel lung model generations 17 through 23. Reproduced from Reeser, 2007.

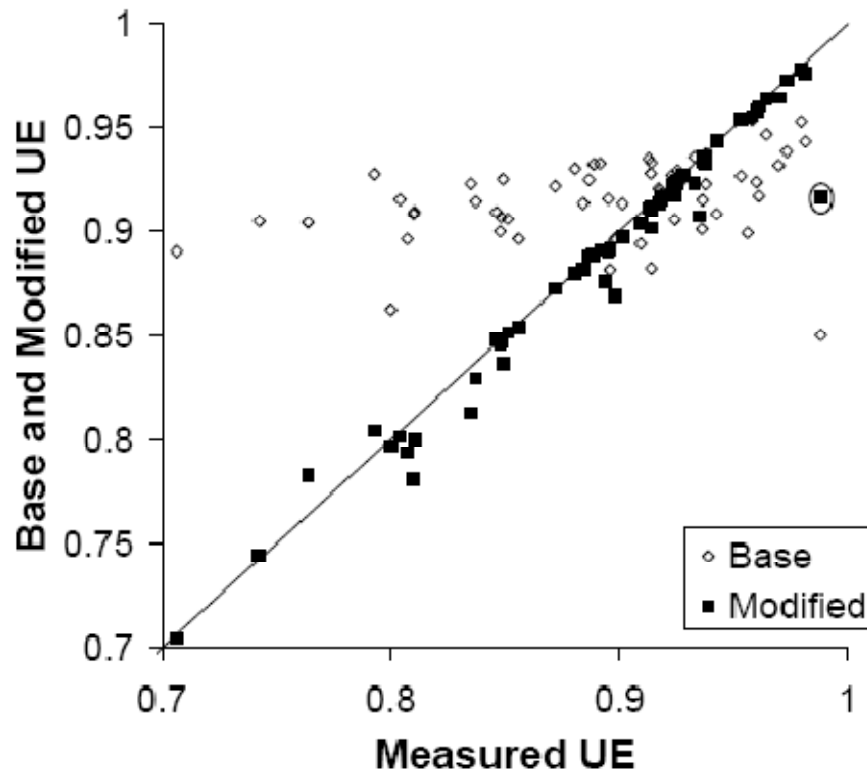


Figure 2-11: Comparison of Simulated Base Case, Simulated Adjusted and Experimental Results for Uptake Efficiency for Session Averaged Values. Each data point represents the behavior of one subject. The line of identity represents agreement between simulated and measured values. The circled value was identified as an outlier. Reproduced from Reeser, 2007.

## **Chapter 3**

### **Experimental Methodology**

Sixty healthy smokers and non-smokers were recruited without regard to race or ethnicity from the University Park campus and surrounding area. The experimental protocol consisted of two screening visits and three research sessions. The screening visits for the study protocol ensured that the subject had no apparent respiratory disease or cardiovascular risk. The three research sessions were executed in the same sequence for all subjects: the bolus experiment, the continuous air exposure, and the continuous ozone exposure. Each research session was conducted at least a week apart, thus separating the two sessions with O<sub>3</sub> exposure by a minimum of two weeks. All screening visits and research sessions were conducted at The Pennsylvania State University General Clinical Research Center (GCRC) at the University Park Campus and were carried out under the supervision of a clinician and nursing staff. The following sections describe the methodology used in the screening of subjects, the collection of response data, the continuous exposure sessions (air and O<sub>3</sub>), the bolus experiment, and the statistical methods used to analyze data.

#### **3.1 Screening Protocol**

To be scheduled for the first screening visit the potential subject first met with an investigator who explained the nature and the purpose of the study. If the subject was interested in participating, they were given an informed consent form to sign and scheduled for the first screening visit.

During the first screening visit, the subject completed a medical history questionnaire, a smoking history questionnaire, performed a clinical pulmonary function test (VMAX229 Legacy, SensorMedics, Yorba Linda CA), and had blood drawn. Subjects were excluded if they had: a history of cardiovascular, respiratory or other chronic diseases; regular medication usage (including over-the-counter pain relievers and anti-histamines but excluding hormonal birth control pills); pregnancy; and latex allergy. Based on their self-reported smoking history, subjects were categorized as smokers or non-smokers.

The pulmonary function test ensured that all subjects were able to meet or exceed the pulmonary function inclusion criteria which required a minimum of 80% of the predicted value for FEV<sub>1</sub> and a minimum of 0.7 for the FEV<sub>1</sub>/FVC ratio. For the predicted value of FEV<sub>1</sub> and FVC the Knudsen population was used [Knudsen et al., 1976]. The blood sample was processed by a commercial lab (QUEST Diagnostics) for clinical chemistry and blood count which were used in the evaluation of cardiac risk.

The second screening session took place only if the subject was at minimal risk for adverse cardiovascular events. This session consisted of a physician-administered medical examination, a pregnancy test for female subjects, and an exercise tolerance test. The medical examination included measurements of height, weight, blood pressure and a resting electrocardiogram. With a few exceptions subjects with a body mass index (BMI) greater than 30 were excluded. The exercise tolerance test was conducted on a bicycle ergometer. During this test, a commercial apparatus (VMAX229 Legacy, SensorMedics, Yorba Linda CA) monitored the subject's electrocardiogram, oxygen consumption rate (VO<sub>2</sub>), minute ventilation and pulse at graded exercise levels. The maximum oxygen consumption rate (VO<sub>2max</sub>) was determined when the subject indicated that they had reached maximal perceived exertion on the Borg scale.

After the subject successfully completed the two screening sessions, he/she was scheduled for the first experimental session.

### 3.2 Pulmonary Function Measurements

Prior to each experimental session, pulmonary function measurements were obtained. This was repeated at the end of the sessions to quantify the pulmonary response to the experiment. Pulmonary function was evaluated under resting conditions by a combination of forced expired spirometry and CO<sub>2</sub> expirometry.

A clinical-grade spirometer (KoKo Model and Pulmonary Data System, Ferraris Corp.) was used to measure pre- and post-exposure values of FEV<sub>1</sub> and FVC. This PC-based device allowed the evaluation of the quality of each breathing maneuver and the end-of-test criteria. The device was calibrated prior to each research session with a three liter syringe, and accounted for the temperature, humidity, and atmospheric pressure in the room. To perform the forced expiratory maneuver the subject first conducted four tidal breaths through the device and then a maximal inhalation and maximal exhalation. The subject repeated this maneuver until two matching tests were obtained. The quality of the test was evaluated according to the 1986 American Thoracic Society Guidelines for the measurement of lung volume.

Single-breath CO<sub>2</sub> expirograms were measured using dedicated equipment previously developed in our laboratory [Taylor *et al.*, 2006]. The subject breathed through a mouthpiece assembly in which CO<sub>2</sub> was monitored with an in-line capnometer (Model 47210A, Hewlett-Packard) and respiratory flow was monitored with a pneumotachometer (No.1, Fleisch, Lousanne, Switzerland). To insure consistency of these data both between and within subjects, the respired flow signal was displayed on a monitor and the subject was coached to maintain the signal at 250 ml/sec, which corresponded to quiet breathing. The full breathing maneuver consisted of a three second inhalation, three second exhalation (the conditioning breath), a three second inhalation, and a minimum of a five second exhalation (the extended breath). The maneuver was repeated until a minimum of four tests were recorded.

The pneumotachometer and capnometer were calibrated prior to each experimental session. The pneumotachometer was calibrated using an air stream at a set flowrate that was verified by an electronic mass flow meter (GFM-1133 Mass Flow Meter, Dwyer Instruments, Inc.). The capnometer was calibrated using a manufacturer supplied CO<sub>2</sub> cell.

The voltage signals from both the capnometer and the pneumotachometer were recorded by a data acquisition system at a sampling rate of 100 Hz on a personal computer. Data from the conditioning breath were discarded and the exhalation data of the extended breath were analyzed. The extended breath was first truncated at a volume of 1250 ml. Then the raw voltage data were analyzed based on the method described by Taylor and colleagues using an excel macro of our own design [Taylor et al., 2006]. This method involves the iterative solution of a numerical computation for V<sub>D</sub> which is equivalent to the graphical method first suggested by Aitken and Clarke-Kennedy [Aitken and Clarke-Kennedy, 1928], Equation 3-1.

$$V_D = -\frac{B}{S} + \sqrt{\left(\frac{B}{S}\right)^2 - \left(\frac{2A}{S} - V_{TE}^2 - \frac{2BV_{TE}}{S}\right)} \quad [3-1]$$

The symbols are defined as: A is the area under the entire expirogram curve found by numerical integration of the data; V<sub>TE</sub> is the total expired volume; S is the slope of the phase III plateau; and B is the intercept of the phase III plateau. These values along with the expired volume corresponding to the beginning of phase III (V<sub>II/III</sub>) are presented graphically in Figure 3-1.

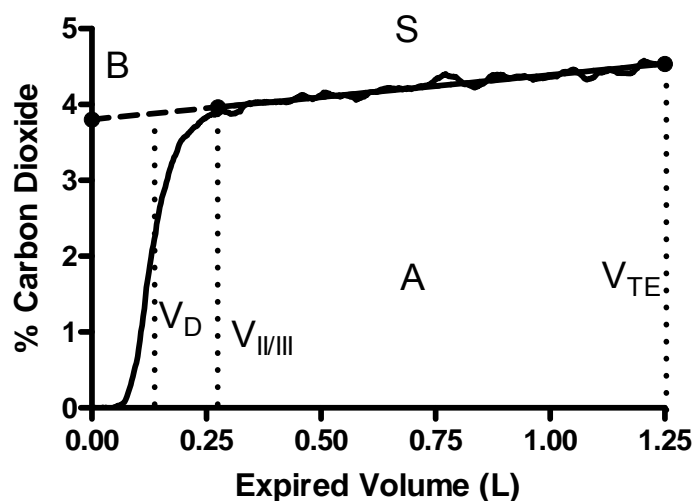


Figure 3-1: Sample CO<sub>2</sub> Expirogram with Parameters for an Extended Exhaled Breath.

An initial value for  $V_{II/III}$  was specified as twice the volume at which half the maximum CO<sub>2</sub> concentration occurred. A regression of the concentration data from  $V_{II/III}$  to  $V_{TE}$  provided the initial values for B and S. From equation 3-1 the initial value of  $V_D$  was then determined. An updated value for  $V_{II/III}$  was determined as two times the initial  $V_D$  value. This process was repeated until the value for  $V_D$  converged. The estimation of  $V_{II/III}$  as two times  $V_D$  was based on the findings of the single-breath nitrogen washout by Fowler [Fowler, 1948] and has been adopted in the work of other investigators [Neufeld et al., 1992; Schwardt et al., 1994]. Once the value of  $V_D$  was known, the normalized slope ( $S_N$ ) was determined as the slope of phase III (S) divided by the amount of exhaled CO<sub>2</sub> (A).

### 3.3 Continuous Exposure Experiment

The second and third research sessions involved a continuous one-hour exposure to room air (air session) or O<sub>3</sub>-enriched air (O<sub>3</sub> session) of a subject who was exercising on a cycle ergometer. Multiple data streams were recorded during the continuous sessions. The following

sections describe the experimental equipment, the procedure followed, and the analysis of the raw data.

### 3.3.1 Experimental Equipment

The experimental equipment was a slightly modified version of the Continuous Inhalation System previously developed by Rigas and colleagues and recently used by Reeser and colleagues [Rigas et al., 2000; Reeser et al., 2005; Reeser, 2007; Ultman et al., 2004]. A schematic of the system utilized in these experiments is presented in Figure 3-2.

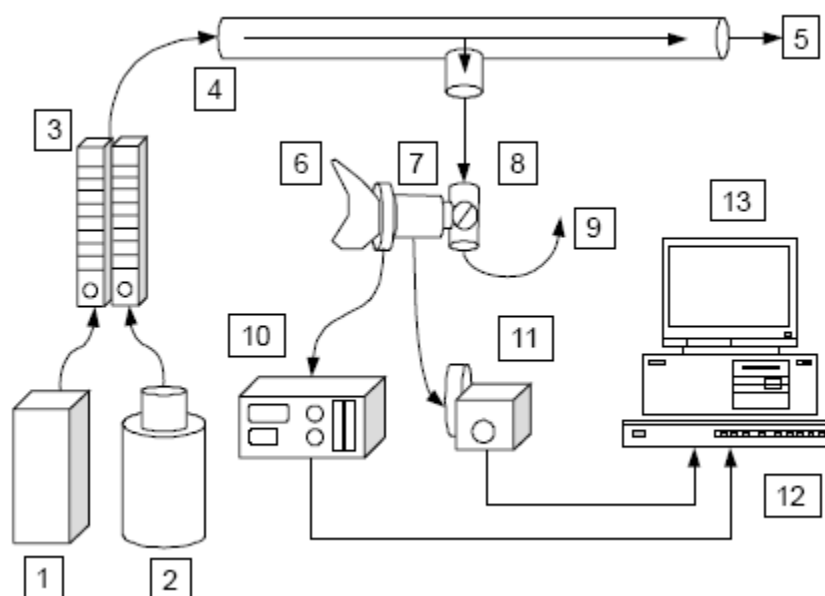


Figure 3-2: Continuous Inhalation System. 1. Ozone generator. 2. Vacuum blower. 3. Rotometer to regulate flow of air and  $O_3$ . 4. Stainless steel mixing tube with two outlet ports. 5. Exhaust to vacuum. 6. Silicone oral breathing mask. 7. In-line  $CO_2$ /flow sensor. 8. Two-way non-rebreathing valve. 9. Exhaust to room. 10. Fast response  $O_3$  analyzer. 11. Cardiopulmonary unit. 12. Data acquisition unit. 13. Personal computer.

Ozone was produced during the  $O_3$  session by a commercial ozone generator (Model O3V1-0, OREC, Phoenix, AZ). This concentrated stream of ozone was diluted with room air that

was provided by a commercial vacuum (Craftsman Wet/Dry). The air stream was monitored with an in-line rotometer (Dwyer Instruments, Inc.) and adjusted by a variable transformer connected to the vacuum power cord. The final concentration of O<sub>3</sub> in the mixed stream was controlled by adjusting the rotometer (ColeParmer) connected to the O<sub>3</sub>. A picture of this set-up is provided as Figure 3-3.

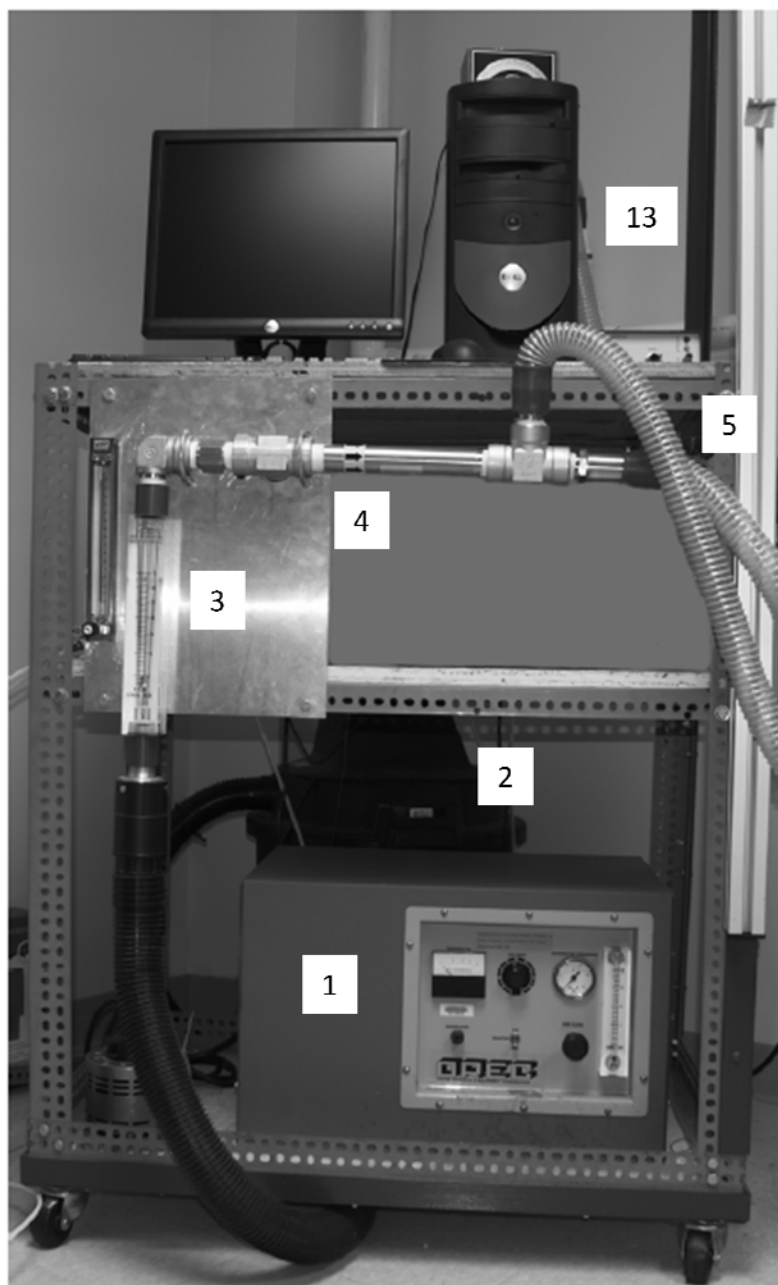


Figure 3-3: Picture of Continuous Inhalation System. Numbers correspond to Figure 3-2. 1. Ozone generator. 2. Vacuum blower. 3. Rotometer to regulate flow of air and  $O_3$ . 4. Stainless steel mixing tube with two outlet ports. 5. Exhaust to vacuum. 13. Personal computer.

The breathing mask assembly consisted of a silicone breathing mask that only allowed oral breathing (Series 7900, Hans Rudolph Inc., Kansas City, MO). A customized adaptor enabled the breathing mask to be connected to an in-line CO<sub>2</sub>/flow sensor (Respironics Novamatrix). The other port of this sensor was connected to a two way non-rebreathing valve (Model 2700, Hans Rudolph Inc., Kansas City, MO) that was supplied with air from the stainless steel mixing tube and exhausted into the room. A sampling tube for the O<sub>3</sub> analyzer was also connected to the mask adaptor, just proximal to the subject's lips. A picture of the breathing mask assembly is provided in Figure 3-4.

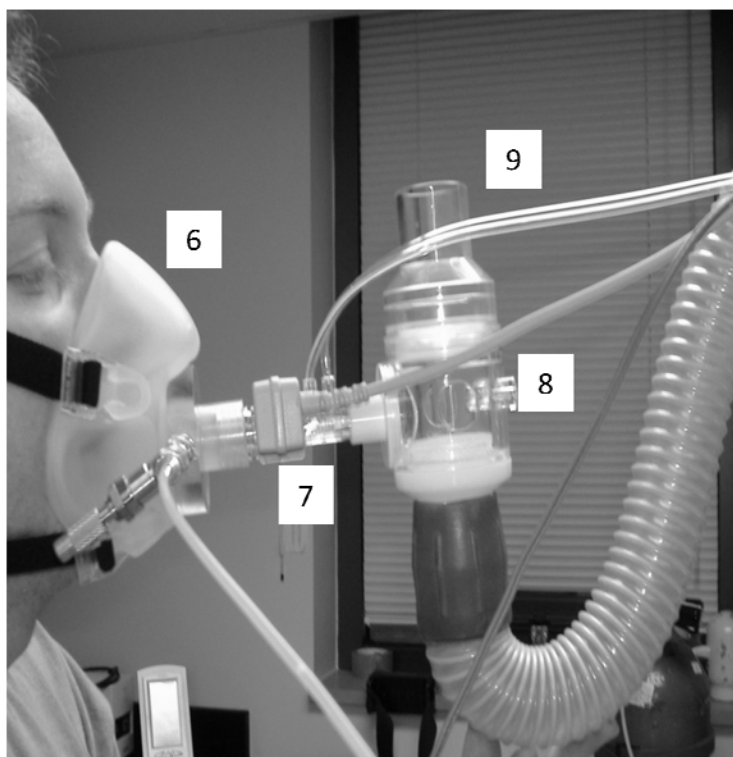


Figure 3-4: Breathing Mask Assembly. Numbers correspond to Figure 3-2. 6. Silicone oral breathing mask. 7. In-line CO<sub>2</sub>/flow sensor. 8. Two-way non-rebreathing valve. 9. Exhaust to room.

Air was drawn through the O<sub>3</sub> sampling tube from the breathing mask assembly to a rapidly responding chemiluminescent O<sub>3</sub> analyzer which was previously developed in our lab [MacDougal et al., 1998]. This analyzer utilized ethylene (C<sub>2</sub>H<sub>4</sub>) as the reactant gas and operated at the following conditions: reaction chamber pressure of 350 torr, ethylene to sample flow ratio of 4:1, and sample flow rate of 0.6 l/min. A picture of the O<sub>3</sub> analyzer is provided in Figure 3-5.

The O<sub>3</sub> analyzer was calibrated prior to each exposure session using a standard source approved by the US Environmental Agency (49PS, Thermo Environmental Instruments, Franklin MA). The sampling line of the analyzer was connected to the common port of a three-way stainless steel solenoid valve. The normally-open port was connected to room air while the normally-closed port was connected to the standard source which was set to a concentration of 1000 ppb O<sub>3</sub>. The solenoid valve was activated to produce a step response of O<sub>3</sub> through a computer controlled relay (PIO-8, Keithley Metrabyte, Cincinnati, OH). The delay time of the analyzer was determined as the time interval between the switching of the valve and an increased analyzer signal. The delay time, which depends on the sampling tube length, ranged from 320 to 650 ms.

The CO<sub>2</sub>/flow sensor calibration supplied by the manufacturer (NICO Cardiopulmonary Management System Model 7300, Respironics Novamatrix) was verified prior to each research session. The flow calibration of the sensor was checked with a 60 L/min air flow supplied through an electronic mass flow meter (GFM-1133 Mass Flow Meter, Dwyer Instruments, Inc.). The CO<sub>2</sub> output of the sensor calibration was verified using a nominal compressed gas mixture of 12% CO<sub>2</sub> in air. A picture of the cardiopulmonary system is included in Figure 3-5.

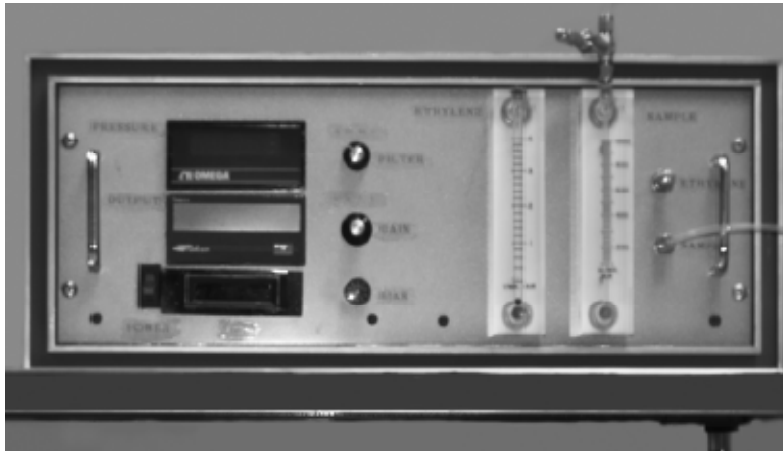


Figure 3-5: Fast Response O<sub>3</sub> Analyzer (left) and Cardiopulmonary Unit (right).

The analog output signals for O<sub>3</sub> concentration (from the O<sub>3</sub> analyzer), flow (from the cardiopulmonary unit), and CO<sub>2</sub> concentration (from the cardiopulmonary unit) were digitized at a sampling rate of 333 Hz and stored on a personal computer using a data acquisition system (DAS-1601, Keithley). Custom software developed using LabView version 7.1 (National Instruments) was used to control the data acquisition.

### **3.3.2 Continuous Experiment Procedure**

Upon arrival at the GCRC, the subject completed a symptom questionnaire, the forced expired spirometry test, and was checked by the nursing staff. Subjects that exhibited symptoms of a current upper or lower respiratory infection they were rescheduled. The subject then completed the CO<sub>2</sub> expirogram test, was fitted for the oral breathing mask and cycle ergometer, and resting data was observed visually on the computer screen from the data acquisition system program and on the cardiopulmonary system display.

The continuous air and ozone sessions required the participant to exercise for one hour while breathing either room air (air session) or room air containing O<sub>3</sub> (O<sub>3</sub> session). The subject was instructed to maintain a constant cadence on the cycle ergometer (60 rpm) while the workload was adjusted to elicit a subject specific target minute ventilation rate. The target minute ventilation rate of 15 L/(min · BSA).

The subject was taken from a resting condition to the desired minute volume rate through a gradual ramping of the workload on the cycle ergometer while maintaining their cadence. During this transition period, the subject inhaled room air through the mask assembly. Once the target minute ventilation rate was achieved, the subject was switched to the exposure air supply, and data monitoring was initiated. The minute ventilation during the session was monitored with

the cardiopulmonary system and periodic adjustments of the workload were made to maintain the target ventilation.

A nurse assessed the vital signs of the subject at 15 minute increments throughout the exposure. During the O<sub>3</sub> session the O<sub>3</sub> concentration in the exposure air was nominally 0.3 ppm. After completion of the exercise the breathing apparatus was removed and the subject was allowed a couple minutes of rest. Post-exposure measurements of pulmonary function were then performed.

### **3.3.3 Continuous Data Analysis**

The data analysis of the continuous air session and O<sub>3</sub> session data was accomplished using a suite of custom programs developed specifically for this experiment (LabView version 7.1, National Instrument). The analysis of the raw data was broken into three distinct steps: the determination of individual breaths from the continuous flow rate data; the determination of single breath parameters; and the analysis of the individual breath parameters to obtain respiratory and exposure quantities of interest.

#### ***3.3.3.1 Determination of Individual Breaths***

The automated detection of a complete breathing cycle is challenging since spontaneous breathing can include pauses, interrupted breaths, and coughs. To automate the analysis process to the fullest extent possible, a custom program was developed to determine the individual breaths from the continuous flow rate data.

The automated program used a moving average method originally developed to study the fractal dynamics of quiet breathing [Peng et al., 2002]. This approach was used to determine the

maximal volumes observed in the breathing pattern and incorporated two moving average windows. The width of the moving average was modified from the one used in the fractal dynamics work so that it would accommodate the shorter breath duration during exercise. The width of the long term average window was set at 90 samples, corresponding to 0.27 seconds, and the short term average window was set at 10 samples, corresponding to approximately 0.03 seconds.

The flow signal was numerically integrated to obtain volume. Then, the peak inspiratory volume (i.e., the end of inspiration) for a breath was located by determining the points where the short term average value crosses the long term average value. The local maximum between two such crossing points was the peak inspiratory volume. In their work on fractal dynamics, Peng and colleagues estimated that 1%-2% of the peaks identified with this automated algorithm required correction upon visual inspection. The corrections were mainly due to over-detection of peaks caused by transient interruptions in the breathing cycle.

The application of this algorithm to exercising conditions resulted in significant over-detection of peaks. The number of over-detected peaks was minimized by incorporating a zero-crossing of flow to identify the start of inhalation for each detected peak. Each uniquely identified start-of-inspiration point, or switch point, was then verified and/or adjusted through visual inspection of the time-flow waveform. These switch points were recorded for the entire one-hour stream of respiratory flow data during the continuous session.

### ***3.3.3.2 Determination of Single Breath Values***

Using the switch points to separate the data from the individual breaths, a custom program was developed to compute the inspired tidal volume ( $V_{Ti}$ ), the inspired dose of  $O_3$  ( $D_I$ ), the expired tidal volume ( $V_{Te}$ ), the expired dose of  $O_3$  ( $D_E$ ), the dead space volume ( $V_D$ ), and the

normalized slope of the alveolar plateau ( $S_N$ ). These breath-by-breath values were saved for further processing.

The complete set of data between two switch points was further separated into inspiration and expiration based on the zero-crossing of the flow (i.e., end of inspiration) between set points. For breaths in which multiple zero-crossing points existed between set points the actual separation between inhalation and exhalation was performed by visual inspection of the single breath time-flow waveform. Once separated into inspiration and expiration, each period of the breath was analyzed to determine the tidal volume and  $O_3$  dose associated with the respective period. The exhaled period of the breath was further evaluated to determine the capnometry parameters for the breath.

$V_{Ti}$  was obtained by numerical integration of the flow-time curve from the initial switch point to the zero-crossing point. This value was converted to BTPS based on the room temperature and relative humidity at the time of the continuous session.  $V_{Te}$  was the numerical integration of the flow-time curve from the zero-crossing point to the final switch point. Figure 3-6 shows an example flow-time waveform with switch points and zero-crossing point identified.

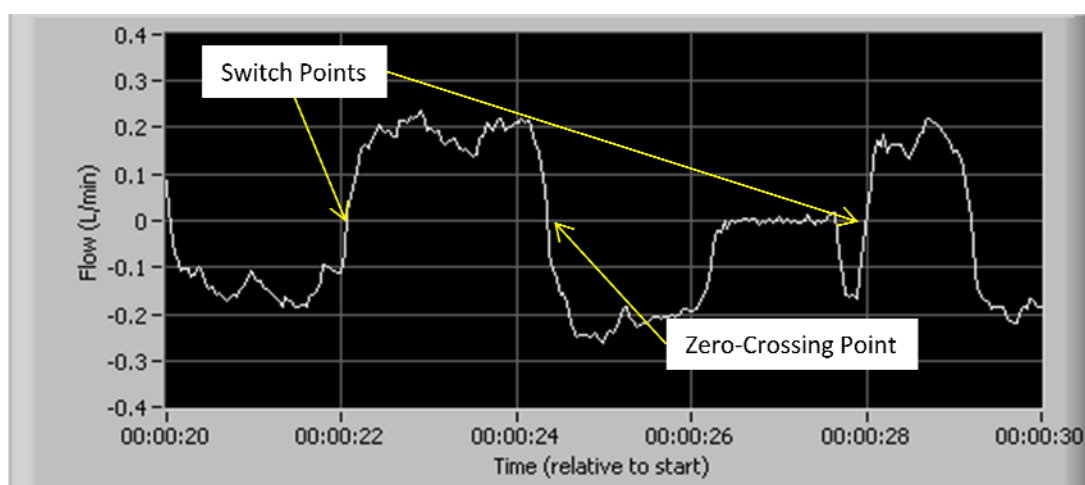


Figure 3-6: Example Flow-Time Waveform. Switch points and zero-crossing point identified for one complete breathing cycle.

The data from the ozone analyzer was shifted forward in time to account for the delay of the O<sub>3</sub> analyzer that was determined at the beginning of each continuous experimental session. The inhaled dose (D<sub>I</sub>) and exhaled dose (D<sub>E</sub>) were then determined as the numerical integration of the flow times concentration-time data during the appropriate half-cycles of each breath. The capnometry parameters, V<sub>D</sub> and S<sub>N</sub>, were determined using the same methodology as described in section 3.2.

### 3.3.3.3 Minute Average Parameters

A custom program was developed to determine minute averaged parameters from the breath-by-breath data. The respiratory rate (RR) of the subject was determined as the total number of completed breathes within a minute period. The minute volume (V<sub>M</sub>) was determined as the sum of V<sub>Ti</sub> of completed breathes within the minute period.

The ozone uptake rate (UR) was determined as:

$$UR = \sum (D_I - D_E) \quad [3-2]$$

The uptake efficiency (UE) was determined as:

$$UE = \frac{\sum (D_I - D_E)}{\sum D_I} \quad [3-3]$$

The cumulative amount of O<sub>3</sub> (D<sub>T</sub>) at the end of the continuous session was determined as the sum of UR over the entire session.

The capnometry parameters, V<sub>D</sub> and S<sub>N</sub>, were evaluated and averaged on a minute-to-minute bases. To ensure that the alveolar plateau was sufficiently long to indentify the slope originating from the distal lung breathes were removed where the tidal volume was less than half that of the average tidal volume for the session. Additionally, where there were multiple zero crossings during the breath, the breath was removed from the capnometry parameter averages.

### 3.4 Bolus Experiment

The bolus experiment session lasted approximately two hours during which the distribution of ozone within the subject's respiratory tract was measured using equipment previously developed in our lab [Hu et al., 1994]. While breathing through a mouthpiece, the participant initiated two to three bolus test breaths per minute while controlling their inspired and their expired flow at 1.0 L/s. A 20-mL bolus of ozonated air was injected into each test breath, and the timing of the injection was varied by the experimenter until 60-80 breaths ranging from penetration volumes of 40 and 300 mL had been recorded for further analysis. A similar number of breaths that did not fall within 15% of the targeted 1.0 L/s flow were discarded. Throughout each bolus test breath, respiratory flow rate and O<sub>3</sub> concentration were continuously monitored just proximal to the mouth. Absorbed fraction ( $\Lambda$ ) was calculated as 1 minus the ratio of the integrals of the inspired and expired O<sub>3</sub> concentration-volume curves. Penetration volume ( $V_p$ ) was computed as the mean volume of the inhaled O<sub>3</sub> concentration-volume curve relative to the end of inspiration (Figure 3-7).

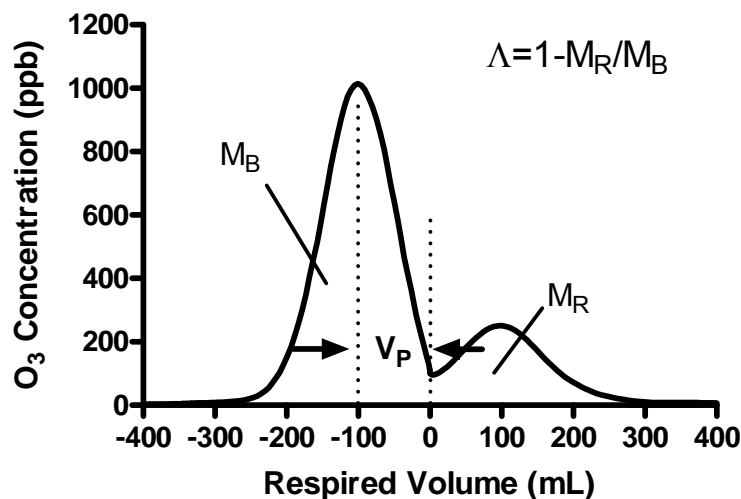


Figure 3-7: Concentration Curve of an O<sub>3</sub> Bolus as a Function of Respired Volume.  $M_B$  and  $M_R$  represent the inhaled and exhaled dose of O<sub>3</sub>, calculated by integrating the inhaled and exhaled concentrations as a function of volume. The penetration volume ( $V_P$ ) is indicated as the midpoint of the inspiratory concentration profile relative to the end of inspiration.

### 3.5 Statistical Analysis

Two main types of statistical analyses were utilized to analyze the collected dose and response data. Two-tailed Student's t-tests were used to analyze differences in a single parameter between two fixed factors. Analyses of Covariance's (ANCOVAs) were applied to analyze the progression of various variables with time or with dose during a session. In these measurements time or dose was applied as the covariate, gender or smoking status was a fixed factor, and subject was included as a random factor. In all statistical tests, the level of significance was set at  $P = 0.05$ . Statistical analyses were performed using a commercially available statistical software package (Minitab 15).

## **Chapter 4**

### **Experimental Results**

The experimental methodology detailed in Chapter 3 was applied to sixty subjects. Presented in this chapter are the results of the experiments and a statistical analysis of the data. The subject characteristics and baseline pulmonary function measurements are presented in Section 4.1. The analyzed flow rate data for the continuous air and ozone sessions are presented in Section 4.2. Presented in Section 4.3 are the analyzed ozone concentration data from the continuous ozone session. The analyzed carbon dioxide concentration data collected during the continuous air and ozone sessions are presented in Section 4.4. The results of the bolus exposure session are presented in Section 4.5.

#### **4.1 Subject Characteristics**

A total of 60 subjects, 30 smoking and 30 non-smoking, completed all three experimental procedures. However, ozone concentration could not be recorded during the ozone exposure session for one male smoking subject. Therefore, the data for this subject has been removed from the results and discussion in this thesis. The smoking status of the subject was based on their self-reported smoking history. Summary subject characteristic data on the two populations and four sub-populations are presented in Table 4-1.

Table 4-1: Subject Characteristics.

	Non-Smokers			Smokers		
	Men	Women	Combined	Men	Women	Combined
Number	17	13	30	18	11	29
Age (yr)	26 (7)	23 (5)	25 (6)	24 (4)	24 (4)	24 (4)
Height (cm)	179.3 (6.3)	163.9 (5.5) <sup>+</sup>	172.6 (9.7)	179.7 (6.3)	165.1 (5.0) <sup>+</sup>	174.1 (9.2)
Weight (kg)	81.7 (12.9)	61.6 (11.3) <sup>+</sup>	73.0 (15.7)	78.1 (11.0)	68.3 (16.1)	74.4 (13.8)
BMI	25.3 (2.7)	22.8 (3.2) <sup>+</sup>	24.2 (3.2)	24.2 (2.7)	25.0 (5.3)	24.5 (3.8)
BSA (m <sup>2</sup> )	2.0 (0.2)	1.7 (0.2) <sup>+</sup>	1.9 (0.2)	2.0 (0.2)	1.7 (0.2) <sup>+</sup>	1.9 (0.2)
Smoking History						
Pack/Week	0 (0)	0 (0)	0 (0)	4 (2)	5 (3)	4 (2)
Years	0 (0)	0 (0)	0 (0)	7 (4)	7 (3)	7 (4)

Values are mean ( $\pm$ SD)

Pack/Week and Year represent values self reported

<sup>+</sup> Male subjects different than female subjects

A two-sample t-test was performed on the two populations (non-smokers and smokers) for age, height, and weight. There were no significant differences between these two populations in age, height, or weight. Two-sample t-tests were performed on sub-populations of subjects as well. Comparison of the male and female non-smoking subjects showed significant differences in height, weight, BMI, and BSA ( $P < 0.001$ ). This trend is consistent with previous clinical experiments in our lab. Comparison of the male and female smoking subjects showed a significant difference existed in height ( $p < 0.001$ ), but not weight ( $P = 0.096$ ). No significant differences existed between the female non-smoking sub-population and the female smoking sub-population or the male non-smoking sub-population and the male smoking sub-population in terms of height, weight, BMI, BSA or age.

The subject performed pre-exposure forced expired spirometry and  $\text{CO}_2$  expirogram measurements in each of the three experimental sessions. Previous measurements of baseline parameters from the  $\text{CO}_2$  expirogram in healthy non-smoking subjects showed significant differences between the male and female subjects, but no significant differences on measurements performed on the same subjects on separate days [Taylor et al., 2006]. Average pre-exposure values of  $\text{FEV}_1$ ,  $V_D$  and  $S_N$  were considered to be the baseline values of these parameters for the subjects. The population and sub-population averages of these baseline data are presented in Table 4-2.

Table 4-2: Baseline Pulmonary Function Measurements.

	Non-Smokers (n=30)			Smokers (n=29)		
	Men (n=17)	Women (n=13)	Combined	Men (n=18)	Women (n=11)	Combined
FEV <sub>1</sub> (L)	4.44 (0.59)	3.07 (0.31) <sup>+</sup>	3.85 (0.84)	4.55 (0.63)	3.4 (0.56) <sup>+</sup>	4.11 (0.82)
V <sub>D</sub> (mL)	175.9 (23.8)	133.7 (15.3) <sup>+</sup>	157.6 (29.4)	171.2 (23.9)	136.9 (22.6) <sup>+</sup>	158.2 (28.6)
S <sub>N</sub> (L <sup>-1</sup> )	0.133 (0.025)	0.162 (0.030) <sup>+</sup>	0.145 (0.031)	0.137 (0.020)	0.145 (0.025) <sup>+</sup>	0.140 (0.022)

Values are mean ( $\pm$ SD)

<sup>+</sup> Male subject different than female subject

ANOVAs using smoking category as the fixed factor indicated that the baseline values of  $FEV_1$ ,  $V_D$  and  $S_N$  were not significantly different between the non-smokers and smokers.

ANOVAs on the sub-populations indicated significant differences in the parameters  $FEV_1$ ,  $V_D$  and  $S_N$  between male and female non-smoking subjects, and  $FEV_1$  and  $V_D$  between male and female smoking subjects. Baseline values of  $FEV_1$ ,  $V_D$  and  $S_N$  were not significantly different between the three sessions. No significant differences were found between male non-smokers and smokers or female non-smokers and smokers with respect to the baseline values of  $FEV_1$ ,  $V_D$  and  $S_N$ .

## **4.2 Respiratory Flow**

The subject exercised at an intensity required to obtain a target minute ventilation rate based on the size of the subject during the continuous air and continuous ozone sessions. Measurements of the flow rate of the subject were recorded throughout these sessions. Over each minute of the continuous sessions, the breathing frequency (RR) and average inhaled tidal volume ( $V_T$ ) were determined. The product of the breathing frequency and tidal volume provided the inhaled minute ventilation rate for that subject.

### **4.2.1. Effect of Smoking Status**

Presented in Figure 4-1 is the minute ventilation rate for the air and ozone sessions for the smoking and non-smoking populations. The minute ventilation rate appeared to be consistent over the air and ozone session. There was some separation in the minute ventilation between smokers and non-smokers, particularly during the air control session.

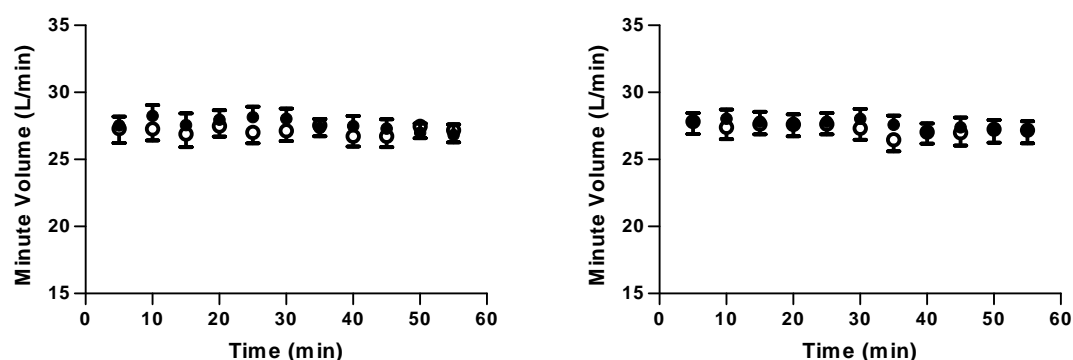


Figure 4-1: Minute Volume During Air (left) and Ozone (right) Sessions for Smokers (●) and Non-Smokers (○). These data were time averaged every 5 minutes across the subject populations. Vertical bars represent the standard error.

To determine the significance of changes in minute volume over time a series of four ANCOVAs were performed. Each ANCOVA corresponded to a specific combination of smoking status and session: smoking subject during air session; smoking subject during ozone session; non-smoking subject during air session; and non-smoking subject during ozone session. Subject was a random factor and time was the covariate in all of the analyses. The resulting initial value (i.e., the intercept) and slope of the minute volume with respect to time and their standard errors are summarized in Table 4-3.

These ANCOVAs tested the hypothesis of a linear relationship between minute volume and time, shown in Table 4-3 as a slope that is significantly different from zero. The t-statistics from the ANCOVAs were also used to determine if significant differences existed between smoking and non-smokers during the same session (e.g. smoker/air session compared to non-smoker/air session), and between session for the same smoking status (e.g. smoker/air session compared to smoker/O<sub>3</sub> session).

Time had a significant negative correlation with minute volume for the smoking subjects in both the air and O<sub>3</sub> sessions, and the non-smoking subjects in the O<sub>3</sub> session. However, the greatest change in  $V_M$  over a one-hour session (slope of -0.0235 L/min for the smoking subject in

the air session) was only 1.52 L or 5.4% of its intercept value. A significant difference in the intercept value of  $V_M$  existed between the air session, 28.3 L/min for smokers and 27.2 L/min for non-smokers. No differences existed between sessions for the same smoking status.

The minute volume is the product of the breathing frequency (RR) and the tidal volume ( $V_T$ ). The time course of the breathing frequency is presented for the air and ozone sessions in Figure 4-2. The breathing frequency appeared to increase in both sessions with the increase in the ozone session being greater than that in the air session. During the ozone session the non-smoking subjects consistently exhibited a higher breathing frequency than the smoking subjects. The time course of the tidal volume is presented for the air and ozone sessions in Figure 4-3. The trends observed in tidal volume were opposite those found in breathing frequency which lead to the maintenance of the minute volume.

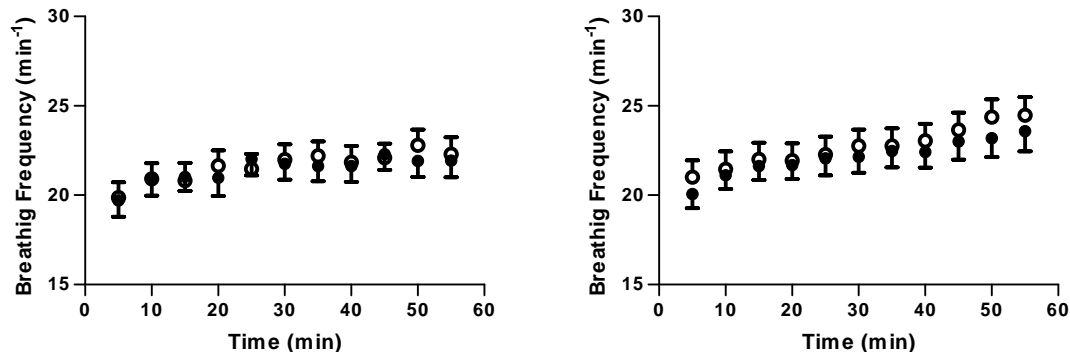


Figure 4-2: Breathing Frequency During Air (left) and Ozone (right) Sessions for Smokers (●) and Non-Smokers (○). These data were time averaged every 5 minutes across the subject populations. Vertical bars represent the standard error.

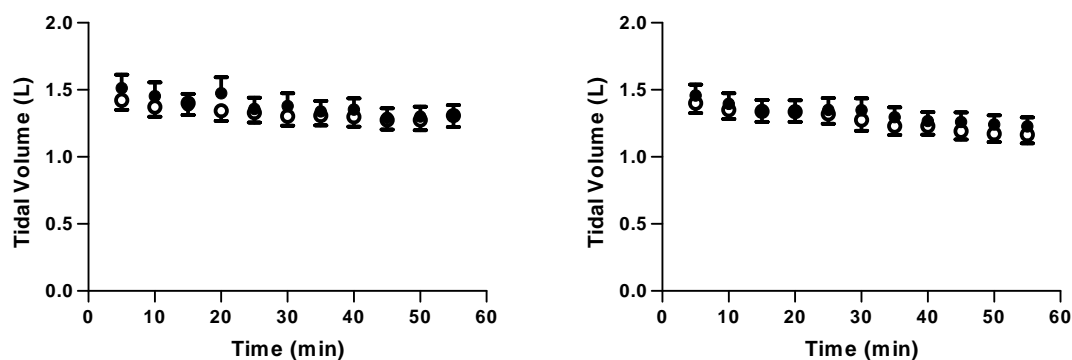


Figure 4-3: Tidal Volume During Air (left) and Ozone (right) Sessions for Smokers (●) and Non-Smokers (○). These data were time averaged every 5 minutes across the subject populations. Vertical bars represent the standard error.

To determine the significance of changes in respiratory rate and tidal volume over time a series of four ANCOVAs were performed for each parameter. The resulting initial value and slope of RR and  $V_T$  with respect to time and their standard errors are summarized in Table 4-3.

Time had a significant positive correlation with respiratory rate for the smoking subjects in both the air and O<sub>3</sub> sessions, and the non-smoking subjects in both the air and O<sub>3</sub> sessions. The change in RR over a one-hour session resulted in increases in smoking subjects of 10% (air session) and 17% (O<sub>3</sub> session); and in non-smoking subjects of 13% (air session) and 19% (O<sub>3</sub> session) of their respective intercept values. No differences existed in the intercept value between smoking status for the same session. No differences existed in the intercept value between sessions for the same smoking status.

Time had a significant negative correlation with tidal volume for the smoking subjects in both the air and O<sub>3</sub> sessions, and the non-smoking subjects in the O<sub>3</sub> session. The change in  $V_T$  over a one-hour session resulted in increases in smoking subjects of 16% (air session) and 17% (O<sub>3</sub> session); and in non-smoking subjects of 11% (air session) and 20% (O<sub>3</sub> session). The difference in the rate of change in  $V_T$  for the non-smoking subjects was significant between

sessions. A significant difference in the intercept value of  $V_T$  existed for the air session between smoking subjects (1.50 L) and non-smoking subjects (1.41 L).

Table 4-3: Summary of ANCOVAs for Smoking Effects.

Smoking Status	Session	$V_M$ (L/min)		RR (breath/min)		$V_T$ (L)	
		Initial Value	Slope	Initial Value	Slope	Initial Value	Slope
Smoker	Air	28.322 ± 0.207 <sup>+</sup>	-0.0235 ± 0.0061 <sup>°</sup>	20.388 ± 0.201	0.0353 ± 0.0059 <sup>°</sup>	1.498 ± 0.023 <sup>+</sup>	-0.0040 ± 0.0007 <sup>°</sup>
	O <sub>3</sub>	28.108 ± 0.205	-0.0172 ± 0.0061 <sup>°</sup>	20.392 ± 0.208	0.0578 ± 0.0061 <sup>°</sup>	1.444 ± 0.015	-0.0041 ± 0.0004 <sup>°</sup>
Non-Smoker	Air	27.227 ± 0.260 <sup>+</sup>	-0.0023 ± 0.0077	20.296 ± 0.231	0.0445 ± 0.0068 <sup>°</sup>	1.410 ± 0.016 <sup>+</sup>	-0.0026 ± 0.0005 <sup>°#</sup>
	O <sub>3</sub>	27.752 ± 0.224	-0.0148 ± 0.0066 <sup>°</sup>	20.690 ± 0.200	0.0666 ± 0.0059 <sup>°</sup>	1.419 ± 0.013	-0.0048 ± 0.0004 <sup>°#</sup>

Values are mean ± SE

<sup>°</sup> Value of slope significantly different than zero

<sup>+</sup> Significantly different between smokers and non-smokers for the same session

<sup>#</sup> Significantly different between air session and ozone session for the same smoking status

#### 4.2.2 Effect of Gender

Presented in Figure 4-4 is the minute volume data for the air and ozone sessions for the male and female populations. The minute ventilation rate appeared to be consistent over the air and ozone sessions. There is significant separation between genders, which is consistent with the normalization of ventilation rate to the subject size.

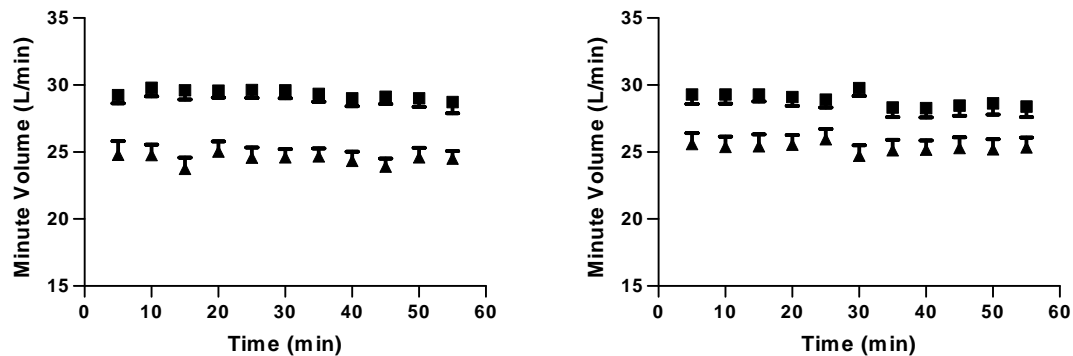


Figure 4-4: Minute Volume During Air (left) and Ozone (right) Sessions for Male Subjects (■) and Female Subjects (▲). These data were time averaged every 5 minutes across the subject populations. Vertical bars represent the standard error.

To determine the significance of changes in minute volume over time a series of four ANCOVAs were performed. Each ANCOVA corresponded to a specific combination of gender and session: female subject during air session; female subject during ozone session; male subject during air session; and male subject during ozone session. Subject was a random factor in the analysis and time was the covariate. The resulting initial value and slope of minute volume with respect to time and their standard errors are summarized in Table 4-4.

Time had a significant negative correlation with minute volume for the male subjects in both the air and O<sub>3</sub> sessions, but not the female subjects in either session. However, the magnitude of the change in V<sub>M</sub> over the one-hour session for the greatest slope (-0.0217 L/min

for the male subjects in the O<sub>3</sub> session) resulted in a reduction in V<sub>M</sub> of only 4.4% of its intercept value. A significant difference existed between gender for the same session for the initial value of V<sub>M</sub> in both the air and ozone sessions. A significant difference existed between sessions for the male subjects in the intercept value of V<sub>M</sub>.

The time course of the breathing frequency is presented for the air and ozone sessions in Figure 4-5. The breathing frequency appeared to increase consistently in both sessions for the female subjects, while the male subjects exhibited an increase in the ozone session greater than that in the air session. In both sessions the female subjects consistently exhibited a higher breathing frequency than the male subjects.

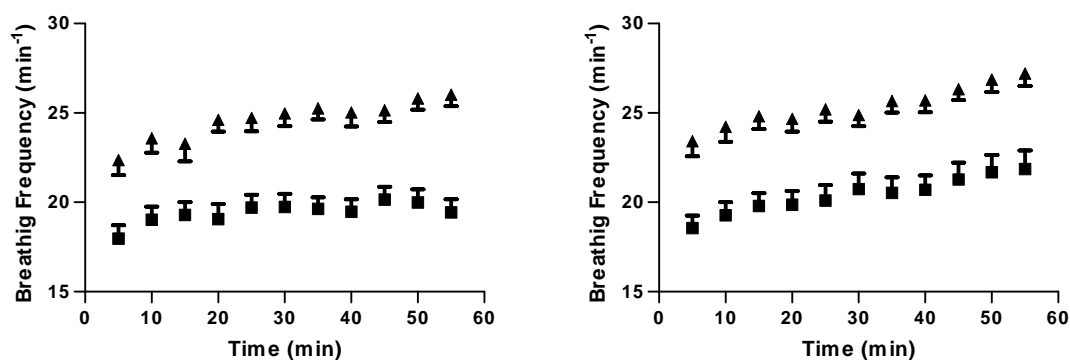


Figure 4-5: Breathing Frequency During Air (left) and Ozone (right) Sessions for Male Subjects (■) and Female Subjects (▲). These data were time averaged every 5 minutes across the subject populations. Vertical bars represent the standard error.

To determine the significance of changes in breathing frequency over time a series of four ANCOVAs were performed. The resulting initial value and slope of RR with respect to time and their standard errors are summarized in Table 4-4.

Time had a significant positive correlation with respiratory rate for female subjects in both the air and O<sub>3</sub> sessions, and male subjects in both the air and O<sub>3</sub> sessions. The change in RR over a one-hour session resulted in increases in female subjects of 16% (air session) and 17% (O<sub>3</sub> session); and in non-smoking subjects of 8% (air session) and 19% (O<sub>3</sub> session) of their

respective intercept values. The difference in the rate of change in RR for the male subjects was significant between sessions. The difference in the rate of change in RR for the air session was significant between genders. A significant difference in the intercept value of RR existed for the between gender for both the air and O<sub>3</sub> session. A significant difference in the intercept value of RR existed between sessions for the female subjects.

The time course of the tidal volume is presented for the air and ozone sessions in Figure 4-6. The trends observed in tidal volume were opposite those found in breathing frequency which lead to the maintenance of the minute volume.

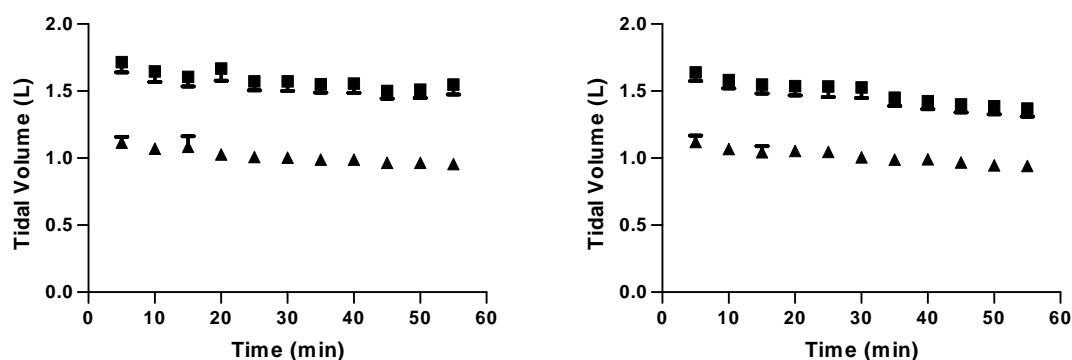


Figure 4-6: Tidal Volume During Air (left) and Ozone (right) Sessions for Male Subjects (■) and Female Subjects (▲). These data were time averaged every 5 minutes across the subject populations. Vertical bars represent the standard error.

Time had a significant negative correlation with tidal volume for female subjects in the air and O<sub>3</sub> sessions, and male subjects in the air and O<sub>3</sub> sessions. The change in  $V_T$  over a one-hour session resulted in decreases in female subjects of 17% (air session) and 18% (O<sub>3</sub> session); and in non-smoking subjects of 12% (air session) and 19% (O<sub>3</sub> session) of their respective intercept values. The difference in the rate of change in  $V_T$  for the ozone session was significant between genders. A significant difference in the intercept value of  $V_T$  existed for the between gender for both the air and O<sub>3</sub> session. No differences existed in the intercept value between sessions for the same gender.

Table 4-4: Summary of ANCOVAs for Gender Effects.

Gender	Session	$V_M$ (L/min)		RR (breath/min)		$V_T$ (L)	
		Intercept Value	Slope	Intercept Value	Slope	Intercept Value	Slope
Female	Air	24.660 ± 0.303 <sup>+#</sup>	-0.0052 ± 0.0089	22.751 ± 0.277 <sup>+#</sup>	0.0623 ± 0.0082 <sup>°+</sup>	1.108 ± 0.015 <sup>+</sup>	-0.0031 ± 0.0004 <sup>°</sup>
	O3	25.577 ± 0.182 <sup>+#</sup>	-0.0076 ± 0.0054	23.366 ± 0.194 <sup>+#</sup>	0.0665 ± 0.0057	1.113 ± 0.009 <sup>+</sup>	-0.0033 ± 0.0003 <sup>°+</sup>
Male	Air	29.893 ± 0.190 <sup>+</sup>	-0.0178 ± 0.0056 <sup>°</sup>	18.692 ± 0.171 <sup>+</sup>	0.0245 ± 0.0050 <sup>°+#</sup>	1.690 ± 0.021 <sup>+</sup>	-0.0035 ± 0.0006 <sup>°</sup>
	O3	29.538 ± 0.224 <sup>+</sup>	-0.0217 ± 0.0066 <sup>°</sup>	18.608 ± 0.204 <sup>+</sup>	0.0594 ± 0.0154 <sup>°#</sup>	1.649 ± 0.015 <sup>+</sup>	-0.0053 ± 0.0005 <sup>°+</sup>

Values are mean ± SE

<sup>°</sup> Value of slope significantly different than zero

<sup>+</sup> Significantly different between female and male subject for the same session

<sup>#</sup> Significantly different between air and O<sub>3</sub> session for same gender

### **4.3 Ozone Uptake**

During the exposure session the measurement of flow and O<sub>3</sub> concentration were monitored throughout the session. These values were used to determine the cumulative dose of O<sub>3</sub> (D<sub>T</sub>), the rate of O<sub>3</sub> uptake (UR), and the individual subject retained and the efficiency at which the subject retained O<sub>3</sub> (UE). The cumulative dose of O<sub>3</sub>, and time course of UR and UE are described in the following section that investigates the differences between the smoking and non-smoking populations and the gender differences in these measurements.

#### **4.3.1 Effect of Smoking Status**

The cumulative dose of ozone retained by the two populations was  $793 \pm 143 \mu\text{g}$  (mean  $\pm$  SD) for the smoking population and  $795 \pm 116 \mu\text{g}$  for the non-smoking population. No differences were observed between these populations with respect to D<sub>T</sub>. The time course of the parameters UE and UR is presented in Figure 4-7.

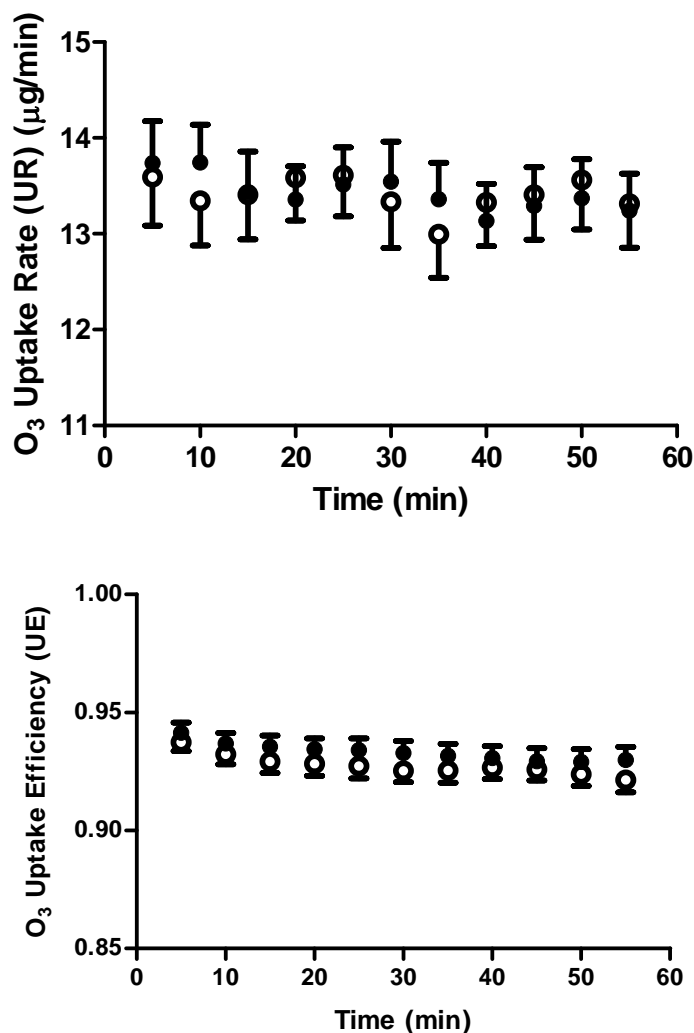


Figure 4-7: O<sub>3</sub> Uptake Rate (above) and O<sub>3</sub> Uptake Efficiency (below) for Smokers (●) and Non-Smokers (○). These data were time averaged every 5 minutes across the subject populations. Vertical bars represent the standard error.

To determine the significance of changes in UR and UE over time a series of two ANCOVAs were performed for each parameter. Each ANCOVA corresponded to a specific subject category: smoking subject; and non-smoking subject. Subject was a random factor and time was the covariate in all of the analyses. The resulting initial value (i.e., the intercept) and slope of UR and UE with respect to time and their standard errors are summarized in Table 4-5.

These ANCOVAs tested the hypothesis of a linear relationship between UR or UE and time, shown in Table 4-5 as a slope that is significantly different from zero. The t-statistics from the ANCOVAs were also used to determine if significant differences existed between subject category (e.g. smoker compared to non-smoker).

Time had a significant negative correlation with UR for the smoking subjects but not the non-smoking subjects. However, the rate of change in UR in the smoking subjects was only 4% of its intercept value. No differences existed for the rate of change in UR or the initial value of UR between smoking and non-smoking subjects. Time had a significant negative correlation with UE for the smoking and non-smoking subjects. However, the rate of change in UE in both the smoking and non-smoking subjects was less than 2% of its intercept value. No differences existed for the rate of change in UE between smoking and non-smoking subjects. A significant difference in the intercept value of UE existed between smoking and non-smoking subjects, 0.940 for smokers and 0.935 for non-smokers.

Table 4-5: Summary of ANCOVAs for Ozone Uptake.

Subject Category	UR ( $\mu\text{g}/\text{min}$ )		UE	
	Intercept Value	Slope	Intercept Value	Slope
Female	12.00 $\pm$ 0.10 <sup>#</sup>	-0.0018 $\pm$ 0.0028	0.928 $\pm$ 0.001 <sup>#</sup>	-0.00024 $\pm$ 0.00003 <sup>o</sup>
Male	14.70 $\pm$ 0.11 <sup>#</sup>	-0.0089 $\pm$ 0.0031 <sup>o</sup>	0.943 $\pm$ 0.001 <sup>#</sup>	-0.00021 $\pm$ 0.00003 <sup>o</sup>
Smoker	13.70 $\pm$ 0.10	-0.0091 $\pm$ 0.0030 <sup>o</sup>	0.940 $\pm$ 0.001 <sup>#</sup>	-0.00021 $\pm$ 0.00003 <sup>o</sup>
Non-Smoker	13.50 $\pm$ 0.11	-0.0030 $\pm$ 0.0032	0.935 $\pm$ 0.001 <sup>#</sup>	-0.00024 $\pm$ 0.00003 <sup>o</sup>

Values are mean  $\pm$  SE

<sup>o</sup> Value of slope significantly different than zero

<sup>#</sup> Significantly different between gender or between smoking status

### 4.3.2 Effects of Gender

The cumulative dose of ozone retained by the male subjects was  $853 \pm 117 \mu\text{g}$  (mean  $\pm$  SD) and  $708 \pm 95 \mu\text{g}$  for the female subjects. A two-sample t-test confirmed the significance of the gender difference on cumulative uptake. The time course of the parameters UR and UE is presented in Figure 4-8.

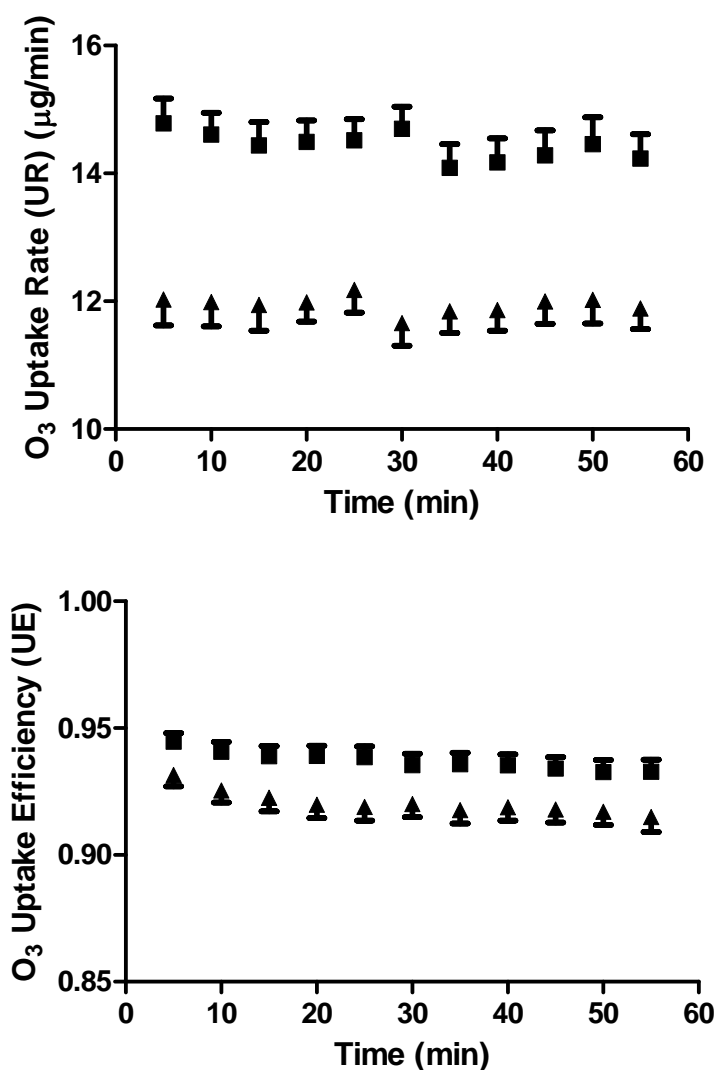


Figure 4-8: O<sub>3</sub> Uptake Rate (above) and O<sub>3</sub> Uptake Efficiency (below) for Male Subjects (■) and Female Subjects (▲). These data were time averaged every 5 minutes across the subject populations. Vertical bars represent the standard error.

Time had a significant negative correlation with UR for the male subjects but not the female subjects. However, the rate of change in UR in the male subjects was only 4% of its intercept value. No differences existed for the rate of change in UR between female and male subjects. A significant difference in the intercept value of UR existed between female and male subjects, 12.0 for female subjects and 14.7 for male subjects. Time had a significant negative correlation with UE for both female and male subjects. However, the rate of change in UE in both female and male subjects was less than 2% of its intercept value. No differences existed for the rate of change in UE between female and male subjects. A significant difference in the intercept value of UE existed between female and male subjects, 0.928 for female subjects and 0.943 for male subjects.

#### **4.4 Dynamic CO<sub>2</sub> Data**

During both the air and ozone sessions, measurements of the CO<sub>2</sub> concentration were recorded along with the flow data. This enabled the analysis of the continuous session data to determine  $V_D$  and  $S_N$  at exercise conditions. The influence of smoking status and gender on these parameters is described in the following sections.

##### **4.4.1 Effect of Smoking Status**

Presented in Figure 4-9 is the dead space volume ( $V_D$ ) from the CO<sub>2</sub> expirogram for the air and ozone sessions for the smoking and non-smoking populations. The  $V_D$  appeared to decrease in the O<sub>3</sub> session for the smoking population. There was significant separation in  $V_D$  between smokers and non-smokers in both sessions.

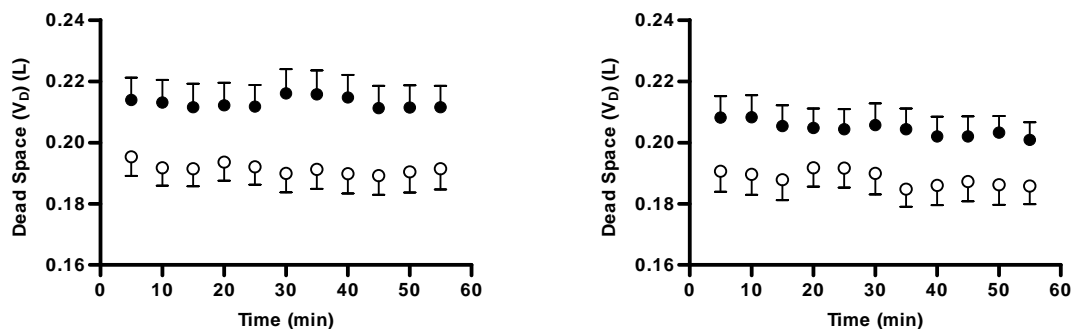


Figure 4-9: Dead Space Volume During Air (left) and Ozone (right) Sessions for Smokers (●) and Non-Smokers (○). These data were time averaged every 5 minutes across the subject populations. Vertical bars represent the standard error.

To determine the significance of changes in  $V_D$  over time a series of four ANCOVAs were performed. The resulting initial value and slope of  $V_D$  with respect to time and their standard errors are summarized in Table 4-6.

Time had a significant negative correlation with  $V_D$  for smoking subjects in the air session, and non-smoking subjects in both the air and  $O_3$  sessions. However, the rate of change in  $V_D$  in all cases was less than 4% of its intercept value. A significant difference in the intercept value of  $V_D$  existed for the between smoking status for both the air and  $O_3$  session. A significant difference in the intercept value of  $V_D$  existed between sessions for smoking subjects.

Presented in Figure 4-10 is the normalized slope ( $S_N$ ) for the air and ozone sessions for the smoking and non-smoking populations. The  $S_N$  appeared to increase in both sessions for both smoking and non-smoking subjects. There was separation in  $S_N$  between smokers and non-smokers in the air session and initial period of the  $O_3$  session.

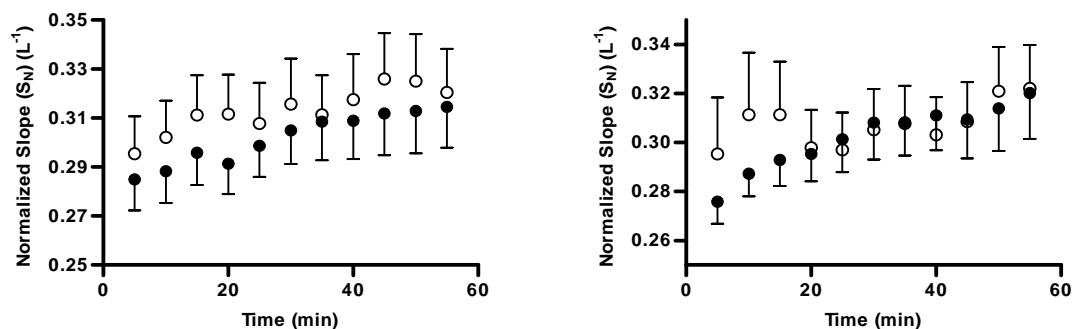


Figure 4-10: Normalized Slope During Air (left) and Ozone (right) Sessions for Smokers (●) and Non-Smokers (○). These data were time averaged every 5 minutes across the subject populations. Vertical bars represent the standard error.

To determine the significance of changes in  $S_N$  over time a series of four ANCOVAs were performed. The resulting initial value and slope of  $S_N$  with respect to time and their standard errors are summarized in Table 4-6.

Time had a significant positive correlation with  $S_N$  for smoking subjects in the air and  $O_3$  sessions, and non-smoking subjects in both the air and  $O_3$  sessions. The change in  $S_N$  over a one-hour session resulted in increases in smoking subjects of 13% (air session) and 16% ( $O_3$  session); and in non-smoking subjects of 10% (air session) and 7% ( $O_3$  session) of their respective intercept values. A significant difference in the intercept value of  $S_N$  existed for between smoking status for both the air and  $O_3$  session.

Table 4-6: Summary of ANCOVAs for Smoking Status of Dynamic CO<sub>2</sub> Data.

Smoking Status	Session	V <sub>D</sub> (L)		S <sub>N</sub> (L <sup>-1</sup> )	
		Intercept Value	Slope	Intercept Value	Slope
Smoker	Air	0.214 ± 0.001 <sup>+ #</sup>	-0.00002 ± 0.00003	0.283 ± 0.003 <sup>+</sup>	0.00062 ± 0.00010 <sup>°</sup>
	O <sub>3</sub>	0.208 ± 0.001 <sup>+ #</sup>	-0.00013 ± 0.00004 <sup>°</sup>	0.279 ± 0.004 <sup>+</sup>	0.00076 ± 0.00011
Non-Smoker	Air	0.194 ± 0.001 <sup>+</sup>	-0.00007 ± 0.00003 <sup>°</sup>	0.298 ± 0.003 <sup>+</sup>	0.00050 ± 0.00010 <sup>°</sup>
	O <sub>3</sub>	0.191 ± 0.001 <sup>+</sup>	-0.00011 ± 0.00004 <sup>°</sup>	0.297 ± 0.005 <sup>+</sup>	0.00034 ± 0.00016 <sup>°</sup>

Values are mean ± SE

<sup>°</sup> Value of slope significantly different than zero

<sup>+</sup> Significantly different between smokers and non-smokers for the same session

<sup>#</sup> Significantly different between air and O<sub>3</sub> session for same smoking status

#### 4.4.2 Effect of Gender

Presented in Figure 4-11 is the dead space volume (V<sub>D</sub>) from the CO<sub>2</sub> expirogram for the air and ozone sessions for female and male populations. The V<sub>D</sub> appeared to decrease in the O<sub>3</sub> session for the male population. There was significant separation in V<sub>D</sub> between genders in both sessions.

To determine the significance of changes in V<sub>D</sub> over time a series of four ANCOVAs were performed. The resulting initial value and slope of V<sub>D</sub> with respect to time and their standard errors are summarized in Table 4-7. Time had a significant negative correlation with V<sub>D</sub> for male subjects in the O<sub>3</sub> session, and female subjects in both the air and O<sub>3</sub> sessions. However, the rate of change in V<sub>D</sub> in all cases was less than 5% of its intercept value. A significant

difference in the intercept value of  $V_D$  existed for the between gender for both the air and  $O_3$  session.

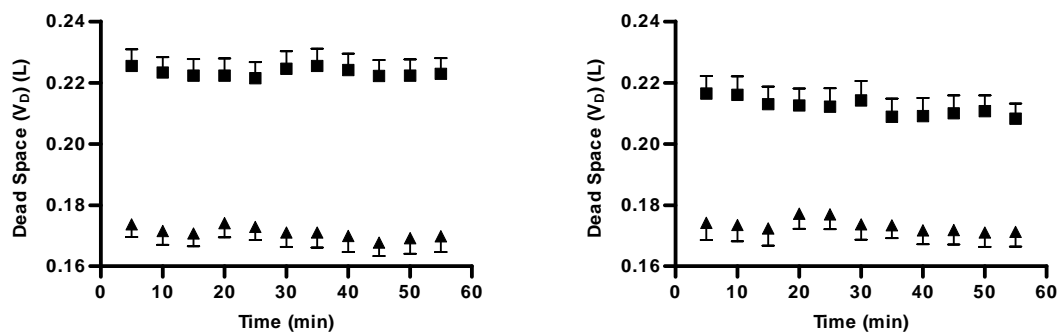


Figure 4-11: Dead Space Volume During Air (left) and Ozone (right) Sessions for Male Subjects (■) and Female Subjects (▲). These data were time averaged every 5 minutes across the subject populations. Vertical bars represent the standard error.

Presented in Figure 4-12 is the normalized slope ( $S_N$ ) for the air and ozone sessions for the smoking and non-smoking populations. The  $S_N$  appeared to increase dramatically in the air sessions for female subjects, and a less dramatic increase in the  $O_3$  session. There was separation in  $S_N$  between gender in both sessions.

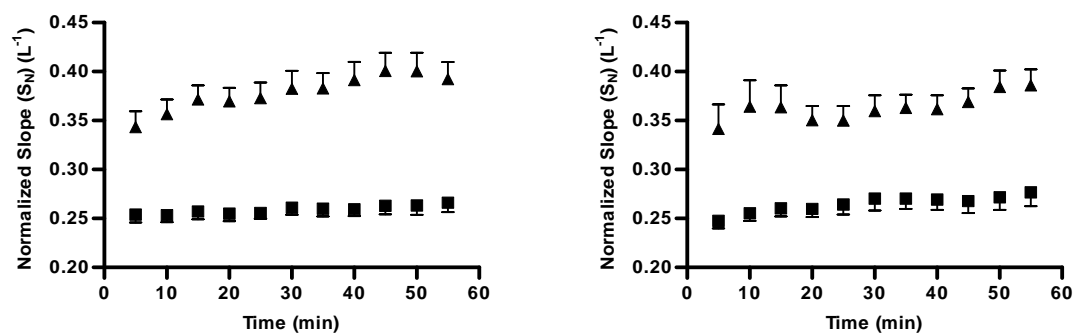


Figure 4-12: Normalized Slope During Air (left) and Ozone (right) Sessions for Male Subjects (■) and Female Subjects (▲). These data were time averaged every 5 minutes across the subject populations. Vertical bars represent the standard error.

To determine the significance of changes in  $S_N$  over time a series of four ANCOVAs were performed. The resulting initial value and slope of  $S_N$  with respect to time and their standard errors are summarized in Table 4-7. Time had a significant positive correlation with  $S_N$  for female subjects in the air and  $O_3$  sessions, and male subjects in both the air and  $O_3$  sessions. The change in  $S_N$  over a one-hour session resulted in increases in female subjects of 18% (air session) and 11% ( $O_3$  session); and in male subjects of 6% (air session) and 11% ( $O_3$  session) of their respective intercept values. A significant difference in the intercept value of  $S_N$  existed for between gender for both the air and  $O_3$  session.

Table 4-7: Summary of ANCOVAs for Gender Difference of Dynamic  $CO_2$  Data.

Gender	Session	$V_D$ (L)		$S_N$ ( $L^{-1}$ )	
		Intercept Value	Slope	Intercept Value	Slope
Female	Air	0.174 ± 0.001 <sup>+</sup>	-0.00009 ± 0.00003 <sup>°</sup>	0.348 ± 0.005 <sup>+</sup>	0.00102 ± 0.00015 <sup>°+</sup>
	$O_3$	0.176 ± 0.001 <sup>+</sup>	-0.00007 ± 0.00003 <sup>°</sup>	0.344 ± 0.007 <sup>+</sup>	0.00064 ± 0.00020 <sup>°</sup>
Male	Air	0.224 ± 0.001 <sup>+</sup>	-0.00002 ± 0.00003	0.252 ± 0.002 <sup>+</sup>	0.00024 ± 0.00006 <sup>°+</sup>
	$O_3$	0.216 ± 0.001 <sup>+</sup>	-0.00015 ± 0.00004 <sup>°</sup>	0.251 ± 0.003 <sup>+</sup>	0.00047 ± 0.00009 <sup>°</sup>

Values are mean ± SE

<sup>°</sup> Value of slope significantly different than zero

<sup>+</sup> Significantly different between female and male subjects for the same session

#### 4.5 Bolus Experiment Results

The results of the bolus session are presented to compare the smoking population to the non-smoking population and the male subjects to the female subjects in this section. The longitudinal distribution has been compared qualitatively, while the volume at which half the inhaled ozone is absorbed ( $V_{P,50}$ ) has been compared quantitatively.

Presented in Figure 4-13 are the population averaged longitudinal distributions for the smoking and non-smoking subjects. The data in this figure represents the average  $\Lambda$  value within 10 ml increments of  $V_P$  obtained from separately pooling the data for smokers and non-smokers. As seen in Figure 4-13, the longitudinal distributions for smokers and non-smokers are virtually superimposed. Presented in Figure 4-14 are the individual subject values of  $V_{P50}$ . The mean value for the smoking subjects was  $111 \pm 19$  ml (mean  $\pm$  SD) and for the non-smoking population was  $110 \pm 19$  ml. No significant differences were observed when comparing  $V_{P50}$  between smoking and non-smoking populations.

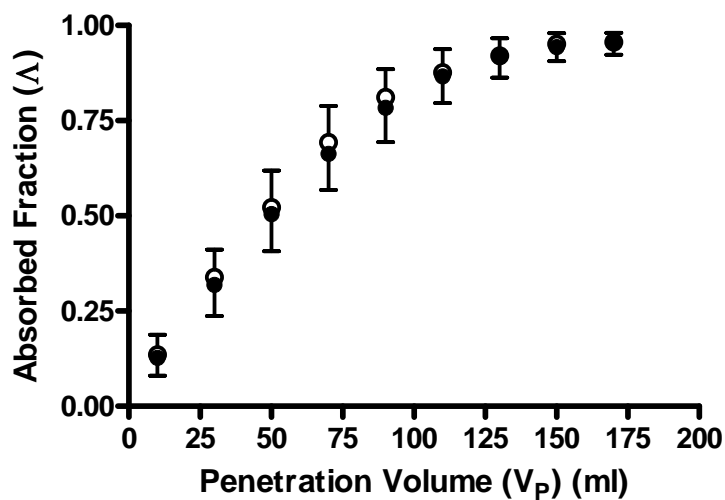


Figure 4-13: Longitudinal Distribution for Smokers (●) and Non-Smokers (○). Data points are population average  $\Delta$  value for 10 ml bin of  $V_p$ . The upper airway volume ( $V_{p0}$ ) has been subtracted from  $V_p$ . Bars are standard error of the population average.

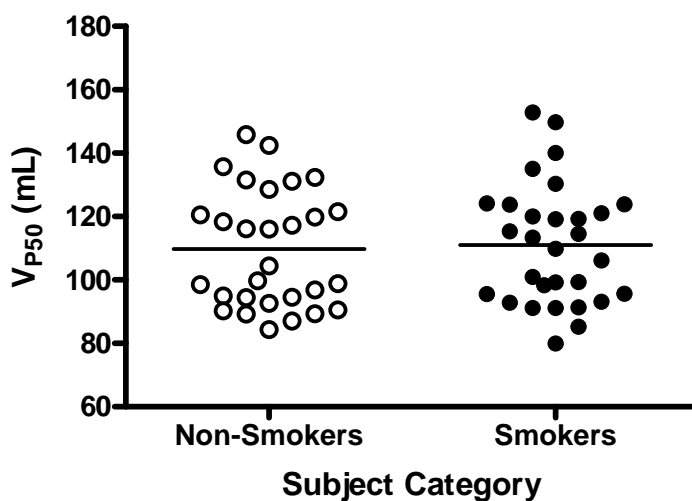


Figure 4-14:  $V_{p50}$  for Smokers (●) and Non-Smokers (○). The population mean value is indicated by the horizontal bars.

Presented in Figure 4-15 are the gender averaged longitudinal distributions.

Qualitatively, the female subjects consistently showed a greater fractional absorbance of  $O_3$  at the same penetration depth than the male subjects. Presented in Figure 4-16 are the individual subject  $V_{P50}$  values, grouped by gender and smoking status. Significant differences between the male and female subjects were observed ( $P < 0.05$ ).

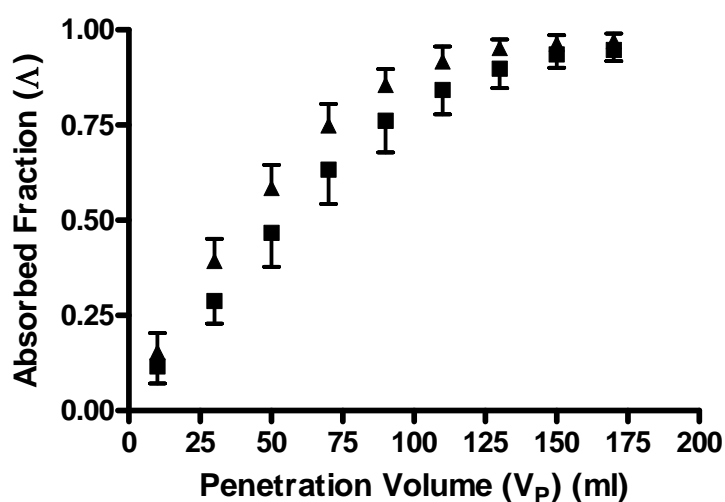


Figure 4-15: Longitudinal Distribution for Male Subjects (■) and Female Subjects (▲). Data points are population average  $\Lambda$  value for 10 ml bin of  $V_p$ . The upper airway volume ( $V_{P0}$ ) has been subtracted from  $V_p$ . Bars are standard error of the population average.

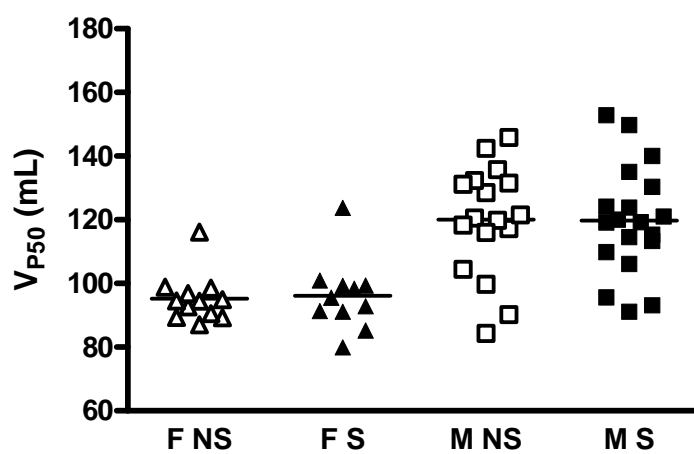


Figure 4-16:  $V_{P50}$  for Male Smoking Subjects (■), Female Smoking Subjects (▲), Male Non-Smoking Subjects (□) and Female Non-Smoking Subjects (Δ). The population mean value is indicated by the horizontal bars.

## Chapter 5

### Discussion

Because of its ease in measurement, the majority of the O<sub>3</sub> literature uses the inhaled dose of O<sub>3</sub> (D<sub>I</sub>) to construct dose-response relationships. In contrast, this chapter explores how the observed responses in breathing pattern, FEV<sub>1</sub>, and capnometry parameters are affected by the retained O<sub>3</sub> dose. Presented in Section 5.1 is the relationship between pre and post exposure static (pre-to-post exposure) response measurements with respect to the total retained dose of ozone for the subject. The dependence of dynamic (simultaneous with exposure) response measurements on retained dose is presented in Section 5.2. Through the use of a single-path model of O<sub>3</sub> uptake in the human respiratory tract, the retained dose of O<sub>3</sub> has been partitioned into a localized dose in specific respiratory compartments. The results and analysis of the partitioned O<sub>3</sub> doses are presented in Section 5.3.

#### 5.1 Total Retained Dose

Through the experiments outlined in Chapter 3, the inhaled dose of O<sub>3</sub> (D<sub>I</sub>) and total retained dose of O<sub>3</sub> (D<sub>T</sub>) during a continuous O<sub>3</sub> exposure session was quantified. To quantify changes in respiratory parameters, pulmonary function measurements were collected just prior to and immediately following the O<sub>3</sub> exposure. The results were analyzed to determine if the retained dose of O<sub>3</sub> provides an indicator of changes in pulmonary function.

McDonnell and colleagues have established a model that predicts O<sub>3</sub>-induced changes in FEV<sub>1</sub> as a function of concentration, minute volume (V<sub>M</sub>), duration of exposure, and age [McDonnell et al., 1997]. The model parameters were determined through a cross-validation with the results of eight experimental chamber exposure studies, which consisted of 485 non-smoking

subjects. Figure 5-1 compares the percent change in FEV<sub>1</sub> in response to O<sub>3</sub> exposure in the current study to the model prediction for 24.4 year old subjects exposed to 0.30 ppm O<sub>3</sub> for a one-hour duration (the population average and experimental conditions of the current study). The mean response data obtained in the current study are consistent with the predictive model with considerable inter-subject variability.

The exposure conditions of the current study compared well with the one-hour intermittent moderate exercise with 0.30 ppm O<sub>3</sub> exposure conditions in McDonnell's work. The responses measured in the current study (mean of -8.86 and range from 6.71 to -40.37 %ΔFEV<sub>1</sub>) are consistent with those observed in the comparable group from McDonnell's work (mean -5.6 and range from about 5 to -30).

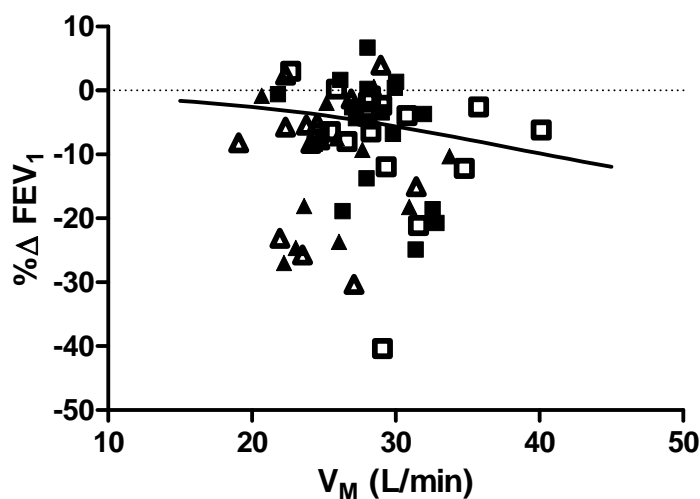


Figure 5-1: Percent Change in FEV<sub>1</sub> with Respect to Minute Volume for Male Smoking Subjects (■), Female Smoking Subjects (▲), Male Non-Smoking Subjects (□) and Female Non-Smoking Subjects (Δ). Each symbol represents an individual subject. Percent change in FEV<sub>1</sub> (%Δ) calculated as (post-exposure – pre-exposure)/ pre-exposure. Solid line is sigmoidal dose response relationship based on predictive response model by McDonnell et al., 1997.

The individual subject results for change in  $FEV_1$  with respect to  $D_I$  and  $D_T$  are presented in Figure 5-2. Whereas  $D_R$  accounts for the effect of the subject-specific uptake efficiency, the  $D_I$  does not. Thus, in principle, inter-subject variability in pulmonary response compared to  $D_I$  is amplified relative to the inter-subject variability in pulmonary response compared to  $D_T$ , suggesting that  $D_T$  is a stronger predictor of response than  $D_I$ . However,  $D_T$  was highly correlated with  $D_I$  (Figure 5-3), indicating a population-average uptake efficiency (UE) of 0.971.

An ANCOVA with  $D_T$  as a covariate and smoking status as a fixed factor indicated that  $D_T$  is not predictive of the change in  $FEV_1$  and differences due to smoking status were not significant.

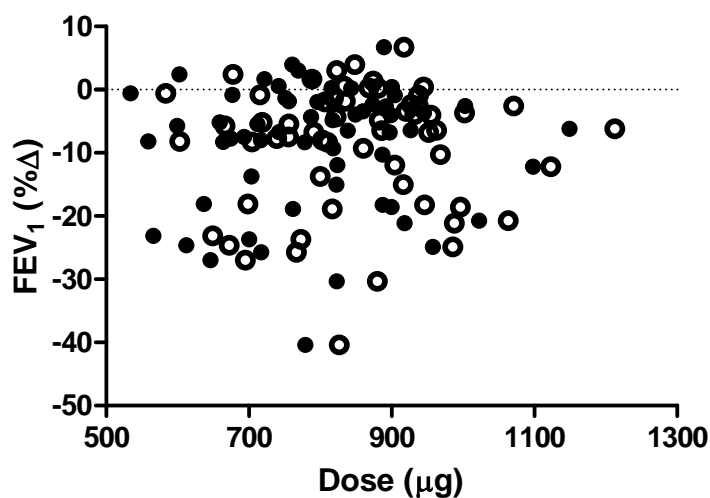


Figure 5-2: Percent Change in  $FEV_1$  with Respect to Inhaled Dose of  $O_3$  (o) and Retained Dose of  $O_3$  (●). Each symbol represents an individual subject. Percent change in  $FEV_1$  (%Δ) calculated as (post-exposure – pre-exposure)/ pre-exposure.

Pre and post exposure measurements of  $V_D$  and  $S_N$  were also obtained for each subject.

Figure 5-3 presents the relative percent change in these parameters with respect to the retained dose. ANCOVAs with  $D_T$  as a covariate and smoking status as a fixed factor indicated that  $D_T$  is

not predictive of the change in  $V_D$  or  $S_N$  and differences due to smoking status were not significant.

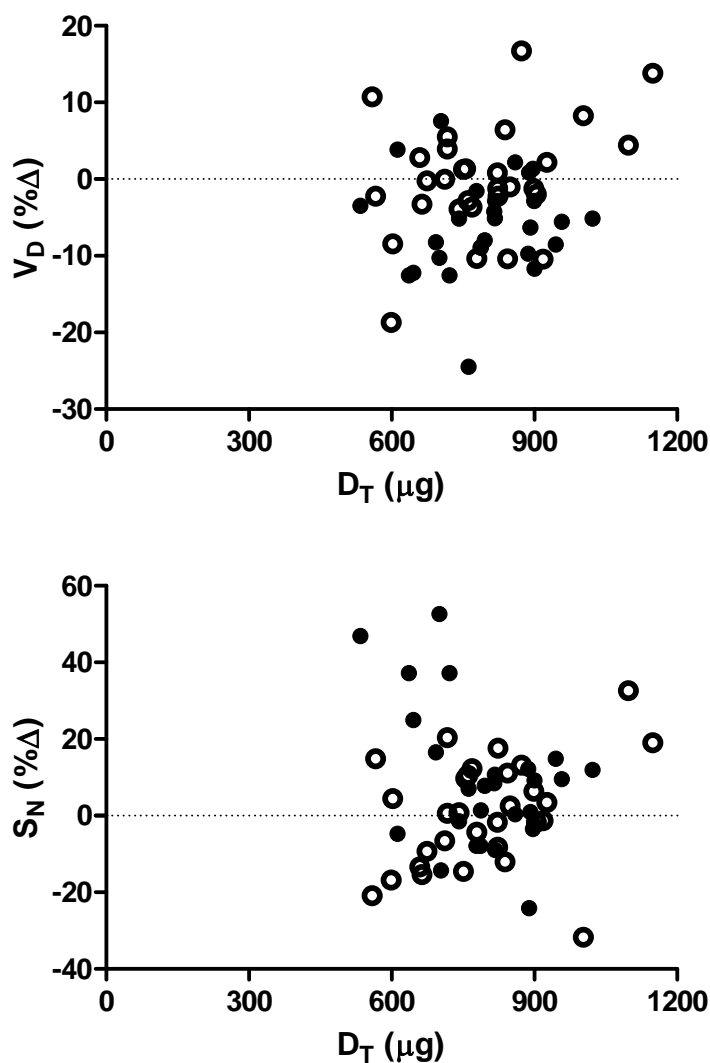


Figure 5-3: Percent Change in  $V_D$  and  $S_N$  with Respect to Retained Dose of  $O_3$  ( $D_T$ ) for Smokers (●) and Non-Smokers (○). Each symbol represents an individual subject. Percent change (% $\Delta$ ) calculated as (post-exposure – pre-exposure)/ pre-exposure.

Hazucha and colleagues concluded that “with minute ventilation during exercise normalized for BSA, young men and women are on average about equally responsive to a moderately intense exposure to  $O_3$ , though the responses significantly deviated from a normal

distribution” [Hazucha et al., 2003]. The experimental protocol utilized by Hazucha and colleagues used intermittent exercise (60 total minutes of exercise and 30 total minutes of rest) at a minute ventilation of 20 L/(min·m<sup>2</sup>) and a concentration of 0.42 ppm O<sub>3</sub>. The current procedure used the same one-hour exercise duration as Hazucha, a reduced minute ventilation of 15 L/(min·m<sup>2</sup>) and a concentration of 0.3 ppm O<sub>3</sub>. Presented in Figure 5-4 are the gender results from the current protocol. Hazucha reported decrements in FEV<sub>1</sub> of -16.6% (range +2 to -53%) for male subjects less than 35 years in age and -16.3% (range +1 to -44%) for young female subjects of a similar age. In the present study, the average change in FEV<sub>1</sub> was -7.2% (range 6.7 to -40.4%) for male subjects and -11.3% (range 4.0 to -30.3%) for female subjects.

The D<sub>R</sub> for the two genders was significantly different with the male population retaining 853 ± 117 µg O<sub>3</sub> (mean ± SD) and the female population retaining 708 ± 95 µg O<sub>3</sub>. However, the ventilation of the subject was normalized by BSA resulting in size normalized D<sub>I</sub>. The relationship between UE and gender was presented in Figure 4-8. The gender difference in UE suggests a functional difference between male and female subjects, with the male subjects exhibiting an increased UE. Thus male subjects would have a higher D<sub>R</sub> for a given D<sub>I</sub> than female subjects.

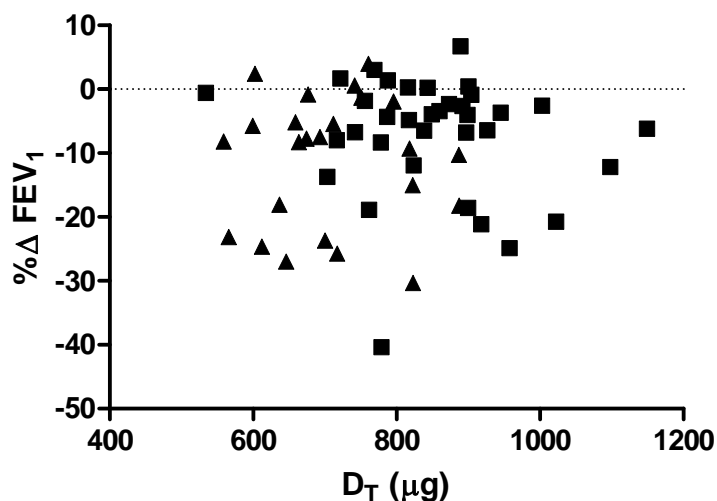


Figure 5-4: Percent Change in FEV<sub>1</sub> with Respect to Retained Dose of O<sub>3</sub> ( $D_T$ ) for Male Subjects (■) and Female Subjects (▲). Each symbol represents an individual subject. Percent change in FEV<sub>1</sub> ( $\% \Delta$ ) calculated as (post-exposure – pre-exposure)/ pre-exposure.

## 5.2 Dynamic Changes with Dose

Several investigators have observed changes in the respiratory pattern of subjects during exposure to O<sub>3</sub>. Some have observed an increase in frequency and a decrease in tidal volume with increasing O<sub>3</sub> concentration [Gibbons and Adams, 1984; Lauritzen and Adams, 1985; Messineo and Adams, 1990]. Recently, the onset of this rapid shallow breathing pattern has been attributed to the cumulative dose of O<sub>3</sub> received by the subject before tachypnea was initiated [Schelegle et al., 2007].

In the work by Schelegle and colleagues, the results from four previously-published and two unpublished studies were used to determine the time course of tachypnea with O<sub>3</sub> exposure. The data that was analyzed included subject characteristics (age, height, weight, BSA, baseline FVC, baseline FEV<sub>1</sub>/FVC), exposure parameters (O<sub>3</sub> concentration, inhaled dose rate, total inhaled dose, and length of exposure) and response measurements (time to onset, percent change

in frequency, tidal volume, FVC, FEV<sub>1</sub>, and FEV<sub>1</sub>/FVC). Regression analysis indicated that significant associations existed between time to onset of tachypnea and BSA, O<sub>3</sub> concentration, breathing frequency prior to onset, and tidal volume prior to onset. The product of time to onset, O<sub>3</sub> concentration, frequency prior to onset, and tidal volume prior to onset is equivalent to the inhaled dose of O<sub>3</sub> prior to onset. Significant associations were also determined between percent change in breathing frequency (pre-to-post exposure) and O<sub>3</sub> inhaled dose rate and percent change in tidal volume and O<sub>3</sub> inhaled dose rate (pre-to-post exposure).

A subset of subjects (20 of 157) did not display tachypnea. In these cases, however, the cumulative inhaled dose of O<sub>3</sub> for the entire exposure period was less than the cumulative inhaled dose of O<sub>3</sub> required to achieve tachypnea in the same subjects under different exposure conditions. All subjects in these studies were healthy non-smoking subjects.

In the current study (Section 4.2) we observed a significant increase in RR and decrease in V<sub>T</sub> over the course of the continuous O<sub>3</sub> session. These changes were significant for all the subject populations grouped by both smoking status and gender. However, significant changes in RR and V<sub>T</sub> were also determined during the continuous air session for all populations. Only the non-smoking subjects exhibited a significant difference in the rate of change in V<sub>T</sub> between the air and O<sub>3</sub> session with respect to time (Table 4-3).

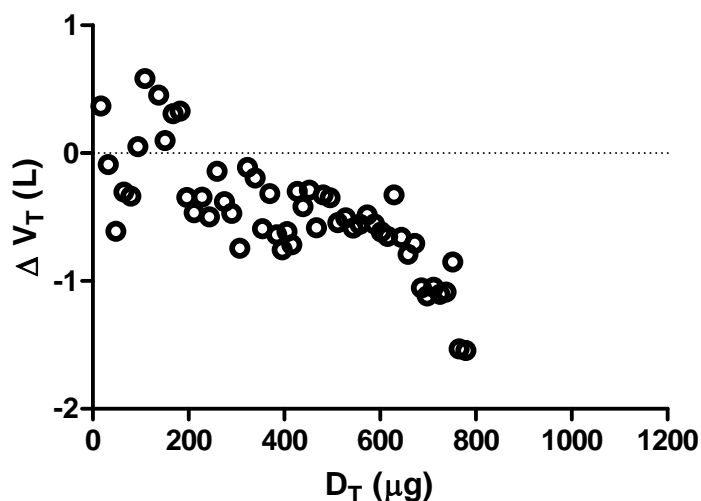


Figure 5-5: Dynamic Change in  $V_T$  with Respect to Retained Dose of  $O_3$  ( $D_T$ ) for One Subject (MPM080N). Change in  $\Delta V_T$  calculated as the minute averaged  $V_T$  for ozone-exposure minus the minute averaged  $V_T$  for air-exposure.

To determine the dependence of the change in  $V_T$  on the retained dose of  $O_3$ , the change in  $V_T$  between the air and ozone sessions ( $\Delta V_T$ ) was first determined. The  $\Delta V_T$  with respect to  $D_T$  for one sample non-smoking subjects is presented in Figure 5-5. This subject exhibited the greatest decrease in  $\Delta V_T$  as the retained dose increased over the exposure session. The subject specific plots of  $\Delta V_T$  with respect to  $D_T$  are presented in Appendix A.

An ANCOVA showed that  $D_T$ , the covariate in the analysis, was a significant factor for  $\Delta V_T$ . Smoking status and gender were not significant factors. The constant value in the regression analysis was not significantly different from zero, which indicated that the difference between the initial  $V_T$  in the air and ozone sessions were not different for the overall population. The regression coefficient describing the change in  $\Delta V_T$  with respect to  $D_T$  had a value of  $-0.11 \pm 0.03$  mL/ $\mu\text{g}$ .

The capnometry parameters,  $V_D$  and  $S_N$ , were determined over the time course of the continuous air and continuous ozone sessions. To determine if a relationship existed between the

change in these parameters and the retained dose of  $O_3$ , the change in  $V_D$  and  $S_N$  between the air and ozone sessions ( $\Delta V_D$  and  $\Delta S_N$ ) was first determined. The  $\Delta V_D$  and  $\Delta S_N$  are presented with respect to  $D_R$  for one sample subject in Figures 5-6 and 5-7. The subject specific plots of  $\Delta V_D$  with respect to  $D_T$  are presented in Appendix B.

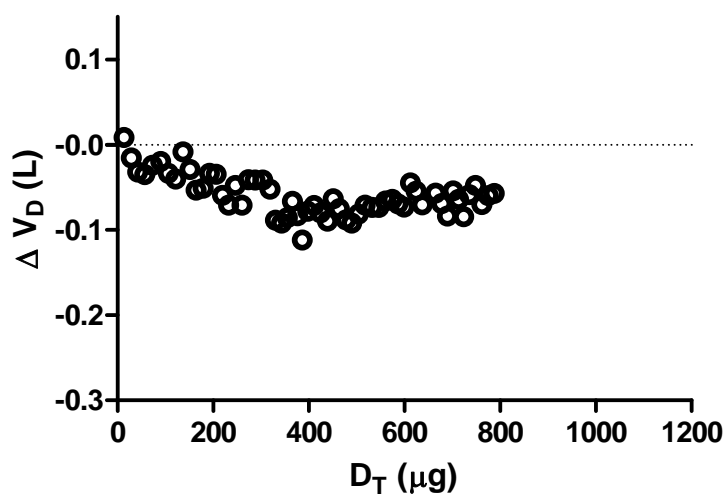


Figure 5-6: Dynamic Change in  $V_D$  with Respect to Retained Dose of  $O_3$  ( $D_T$ ) for One Subject (MPM022S). Change in  $\Delta V_D$  calculated as the minute averaged  $V_D$  for ozone-exposure minus the minute averaged  $V_D$  for air-exposure.

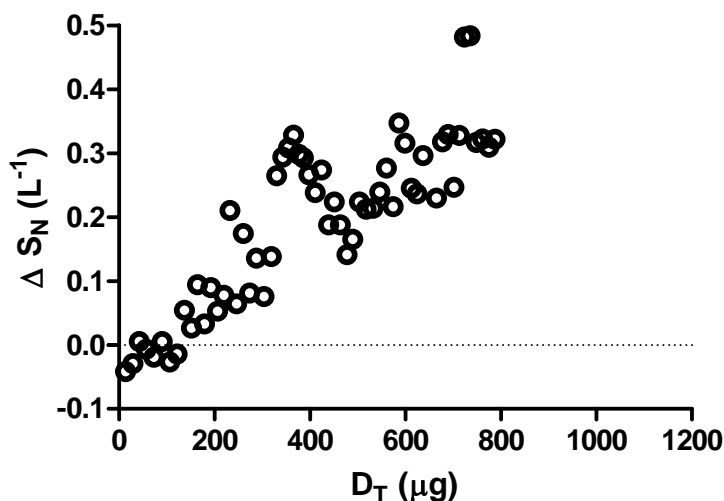


Figure 5-7: Dynamic Change in  $S_N$  with Respect to Retained Dose of  $O_3$  ( $D_T$ ) for One Subject (MPM022S). Change in  $\Delta S_N$  calculated as the minute averaged  $S_N$  for ozone-exposure minus the minute averaged  $S_N$  for air-exposure.

Subject MPM022S exhibited a decrease in  $\Delta V_D$  and an increase in  $\Delta S_N$  between the start and end of the session. The magnitude of the changes in these parameters was the greatest observed in the study population. However,  $\Delta V_D$  and  $D_T$  did not appear to be linearly related, whereas  $\Delta S_N$  and  $D_T$  appeared to be linearly related for this subject.

An ANCOVA established that  $D_T$ , the covariate in the analysis, and gender were significant factors for  $\Delta V_D$ , while smoking status was not a significant factor. The constant value in the regression analysis was not significantly different from zero, which indicated that the difference between the initial  $V_D$  in the air and ozone sessions was not different for the overall population. The regression coefficient describing the change in  $\Delta V_D$  with respect to  $D_T$  had a value of  $-0.014 \pm 0.005$  mL/ $\mu$ g.

An ANCOVA showed that  $D_T$  was not a significant factor for  $\Delta S_N$ . This showed that changes in  $S_N$  with both time and retained ozone dose, are indistinguishable between the air session and ozone session.

Although the capnometry parameters of  $V_D$  and  $S_N$  were evaluated as a dynamic measure of pulmonary function, the time-course measurements can be influenced by the dynamic breathing pattern during the session. The significance of breathing pattern on these measurements was investigated by Neufeld and colleagues [Neufeld et al., 1991]. The measurement of  $S_N$  was significantly increased when subjects used a rapid breathing pattern compared to a normal breathing pattern. No significant differences were observed in the measurement of  $V_D$  between breathing patterns. Figure 5-8 presents the relationship between  $S_N$  and  $V_T$  from the results of the experiments conducted by Neufeld and colleagues. In an experimental protocol by Kars and colleagues,  $CO_2$  expirogram measurements were collected from subjects breathing at increasing respiratory rates [Kars et al., 1997]. This study showed a significant negative correlation between the slope of phase III of the expirogram and  $V_T$ , and a positive correlation between dead space volume measurements and  $V_T$ .

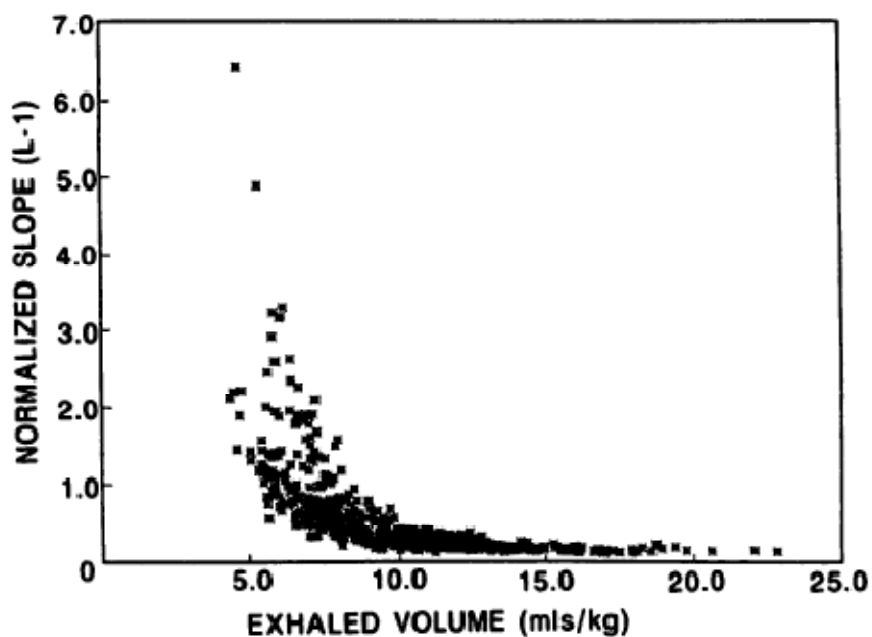


Figure 5-8: Relationship Between  $S_N$  and  $V_T$ . Illustrated are all 663 breaths measured in six stages of the study by Neufeld and colleagues, 1991.

Presented in Figure 5-9 is the relationship between  $S_N$  and  $V_T$  for the air session for one subject. This subject exhibited the largest decrement in  $V_D$  and increase in  $S_N$  during the  $O_3$  session. This subject (MPM020S) exhibited a similar increase in normalized slope with decreasing tidal volume as seen in Figure 5-8, but was fairly consistent across the higher values of  $V_T$ . Figure 5-10 presents  $V_D$  with respect to  $V_T$  for the same subject.  $V_D$  was observed to increase at higher values of  $V_T$ , but was consistent across the lower values of  $V_T$ . Therefore, the impact of the decreasing tidal volume upon exposure to  $O_3$  had a greater impact on the value of  $S_N$  than that of  $V_D$ .

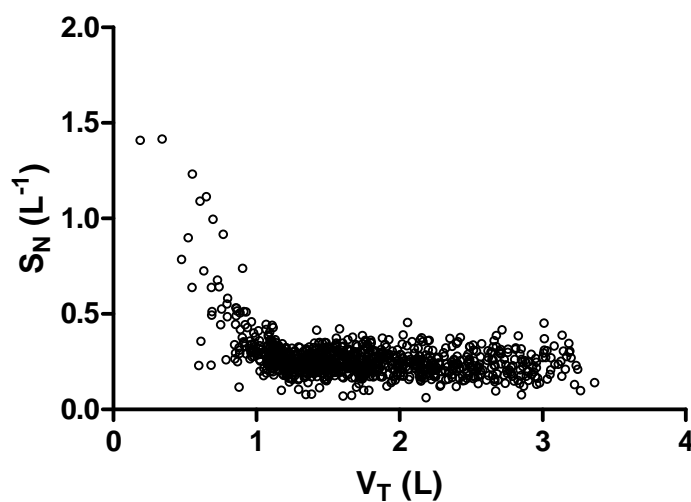


Figure 5-9: Relationship Between  $S_N$  and  $V_T$  for One Subject (MPM022S). Presented are all 920 breaths during the air session. Included in the figure are data points with tidal volume less than half the average tidal volume for the session.

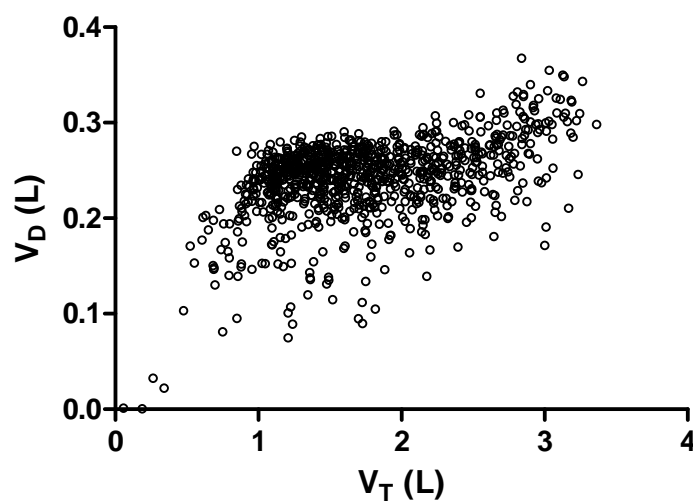


Figure 5-10: Relationship Between  $V_D$  and  $V_T$  for One Subject (MPM022S). Presented are all 920 breaths during the air session. Included in the figure are data points with tidal volume less than half the average tidal volume for the session.

### 5.3 Simulation of Ozone Uptake

The distribution of the retained dose within the human respiratory tract was estimated by mathematical modeling. This enabled the investigation of dose-response relationship on the level of localized dose of  $O_3$  within respiratory compartments.

A single path model developed for the uptake of  $O_3$  had been previously developed and documented [Bush et al., 1996A; Bush, 1999; Bush et al., 2001; Zhang, 2000; Reeser, 2007]. The description of the original single-path model, modifications to this model, simulation results, and implications of the local dose estimates on pulmonary response are presented in this section.

### 5.3.1 Single-Path Model

In a single path model, the transport of air through the respiratory tract is estimated by modeling the airway geometry by a series of bifurcating generations, each containing identical branches of the equal lengths and diameters. The single-path model used for simulations assumed that the air was radially homogenous in composition and flowed through the airways with a flat velocity profile. Thus, all transport paths from the airway opening to the alveolar sacs were identical, and the airway system could be modeled as a single conduit which, at any particular axial location, had a cross-sectional area equal to the summed area of the airway branches at that location. A schematic representation of the single-path model is presented in Figure 5-11. Shown in the schematic is the expanding cross-sectional area ( $A$ ) as a function of longitudinal distance ( $y$ ). The model allowed for the presence of alveoli in the respiratory airspaces by the inclusion of the peripheral cross-section  $A^*$ . The single-path model adjusts the baseline respiratory dimensions in an isotropic manner based on the subject specific  $V_D$  and functional residual capacity (FRC).

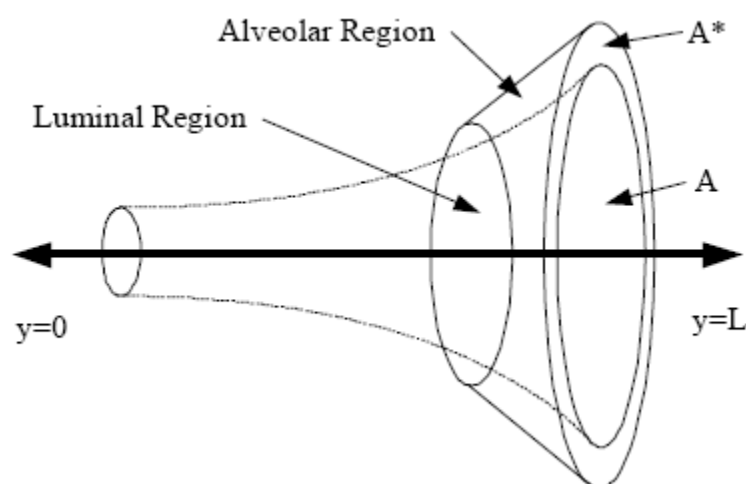


Figure 5-11: Schematic of the Single-Path Model. The luminal region is a tube of expanding cross-section that represents the conducting airways: oral cavity, larynx, pharynx and generations 1 to 16 of the Weibel lung model. The alveolar region represents the respiratory airspaces of generations 17 through 23 of the Weibel lung model and expands and contracts during the

respiratory cycle. Figure adapted from Taulbee and Yu, 1975.

The single-path model accounted for the transport of O<sub>3</sub> through axial convection, axial dispersion, and radial absorption into the fluid lining the airway epithelium. These processes were accounted for in the following species conservation equation:

$$\frac{\partial C}{\partial t} = -\left(\frac{\dot{V}}{A^*}\right) \frac{\partial C}{\partial y} + \frac{1}{A^*} \frac{\partial}{\partial y} (D A) \frac{\partial C}{\partial y} - K \left(\frac{A}{d}\right) \left(\frac{A}{A^*}\right) C \quad [5-1]$$

where:

- y is the axial position;
- t is time;
- C(y,t) is the concentration of O<sub>3</sub> in air;
- $\dot{V}(y,t)$  is the respiratory flow rate;
- A(y) is the central cross-section through which dispersion occurs;
- A\*(y,t) is the total summed cross-section;
- K(y) is the overall mass transfer coefficient;
- D(y) is the axial dispersion coefficient; and
- d(y) is the local hydraulic diameter.

The initial and boundary conditions used to integrate this equation were as follows:

- 1) Prior to inhalation the residual air in the respiratory tract was free of O<sub>3</sub>

$$t=0, y=y \quad C(t=0)=0; \quad [5-2]$$

- 2) At the distal end of the respiratory system (y=L), the axial flux was purely diffusive and equaled the absorptive flux through the gas-liquid interface

$$t=t, y=L \quad -D \left(\frac{\partial C}{\partial y}\right) = K C; \quad [5-3]$$

- 3) At the airway opening (y=0), a constant inhaled concentration of O<sub>3</sub> was specified during inspiration

$$t \leq t_1, y=0 \quad C(y=0)=C_1; \text{ and} \quad [5-4]$$

4) Axial dispersion was neglected during expiration,

$$t \geq t_i, y=0 \quad -D \left( \frac{\partial C}{\partial y} \right) = 0 \quad [5-5]$$

where  $L$  is the total longitudinal length;  
 $C_i$  is the inspired concentration of  $O_3$ ; and  
 $t_i$  is the time of inspiration.

A modified Crank-Nicolson finite difference technique was used to solve the species conservation equation, since an analytical solution does not exist. A more detailed description of the numerical solution was provided by Bush [Bush, 1999].

The values for the dispersion coefficient ( $D$ ) used in the single-path model were obtained depending on the longitudinal position along the respiratory tract and the direction of airflow. The relationships for determining  $D$  in the upper airways was from the work of Ben-Jebria and colleagues [Ben-Jebria et al., 1982]. Through a radioactive bolus inhalation method during inhalation and exhalation, the correlations for  $D$  in the upper airways during inhalation is

$$D = D_g + 3.2 \text{ Pe } D_g \quad [5-6]$$

and exhalation is

$$D = D_g + 0.51 \text{ Pe } D_g \quad [5-7]$$

where  $D_g$  is the molecular diffusivity of  $O_3$  in air of  $1.95 \text{ cm}^2/\text{s}$  [Cussler, 1984]; and  
 $\text{Pe}$  is the Peclet number.

The relationship for determining  $D$  in the lower airways and airspaces was from the work of Scherer and colleagues [Scherer et al., 1975]. Through studies on longitudinal mixing in a symmetrical glass model of the tracheobronchial tree during inhalation and exhalation, the correlations for  $D$  in the lower airways and airspaces during inhalation is

$$D = D_g + 1.08 \text{ Pe } D_g \quad [5-8]$$

and exhalation is

$$D=D_g+0.37 Pe D_g \quad [5-9]$$

Individual mass transfer coefficients in the gas phase boundary layer and the epithelial lining layer were used in determining the value of the overall mass transfer coefficient (K). The single path model combined the individual resistances to mass transfer into the overall mass transfer coefficient through the following equation.

$$\frac{1}{K} = \frac{1}{k_g} + \frac{\lambda_{gt}}{k_t} \quad [5-10]$$

where:  $k_g$  is the gas-phase mass transfer coefficient;  
 $\lambda_{gt}$  is the concentration partition coefficient for O<sub>3</sub> between the gas-phase and the liquid-phase; and  
 $k_t$  represents the mass transfer coefficient in the liquid-phase.

The gas-phase mass transfer coefficient ( $k_g$ ) used in the single-path model was dependent on the axial location in the model, the flow direction, and the magnitude of the flow. Nuckols used experiments with a physical model of the upper and lower airways to establish dimensionless correlations for heat transfer. By applying the analogy between heat and mass transfer the following correlations were determined [Nuckols, 1981]:

Upper airways during inhalation

$$Sh=0.035 (Re Sc)^{0.804} \quad [5-11]$$

Upper airways during exhalation

$$Sh=0.035 (Re Sc)^{0.804} \quad [5-12]$$

Lower airways during inhalation

$$Sh=0.035 (Re Sc)^{0.804} \quad [5-13]$$

Lower airways during exhalation

$$Sh=0.035 (Re Sc)^{0.804} \quad [5-14]$$

where:  $Sh$  is the Sherwood number ( $Sh = \frac{k_g d_T}{D_g}$ );

Re is the Reynolds number ( $Re = \frac{\rho u d_T}{\mu}$ );

Sc is the Schmidt number ( $Sc = \frac{\mu}{\rho D_g}$ );

$d_T$  is the tracheal diameter;

$\mu$  is the gas viscosity;

$\rho$  is the density of the gas stream; and

$u$  is the mean velocity of the gas stream.

As Re becomes very small,  $k_g$  would approach zero. To remedy this artifact Condorelli and George theoretically determined that  $k_g$  approaches a finite asymptotic limit as the gas flow becomes negligible [Condorelli and George, 1999]. The value of  $k_g$  at this limit is

$$k_g = \frac{6 D_g}{d} \quad [5-15]$$

where  $d$  is the diameter of the airways.

The liquid-phase mass transfer coefficient was estimated from a quasi-steady solution to the reaction-diffusion equation in a static liquid film:

$$k_t = \sqrt{k_r D_{O_3}} \coth \left( \sqrt{\frac{k_r}{D_{O_3}}} \delta_m \right) \quad [5-16]$$

where:  $k_r$  is the pseudo first-order reaction rate constant;

$D_{O_3}$  is the estimated diffusion coefficient of  $O_3$  in the liquid-phase [Bush, 1999]; and

$\delta_m$  is the thickness of the liquid-film.

The use of the pseudo first-order reaction rate constant assumed that the biochemical substrates in the liquid-phase are in excess.

### 5.3.2 Modifications to Single-Path Model

Reeser (1997) used the single-path model to establish subject specific values for the  $O_3$  reaction rate constant ( $k_r$ ). Model simulations of  $O_3$  uptake efficiency that used the observed tidal volume and respiratory rate were matched to the session-averaged data by using  $k_r$  as a fitting parameter. These values were used along with subject-specific values of  $V_D$  and functional residual capacity (FRC). To determine the subject-specific value for  $k_r$ , the single-path model was run ten times with a multiplier for  $k_r$  ranging from  $10^{-5}$  to  $10^4$ . The actual  $k_r$  value for the subject was determined through interpolation of the minimum error of uptake efficiency between the simulated and experimental results [Reeser, 2007].

The first modification to the single-path model used by Reeser was the use of a value for FRC based on the subject's characteristics. This was necessary because the current experiential protocol did not include a method to measure the FRC. The height, age and gender were used to determine subject specific values for FRC [Cotes, 1993].

The second modification improved upon the method used to estimate the subject specific value of  $k_r$ . The original program was modified to incorporate a variation of the Levenberg-Marquardt algorithm to minimize the squared error between the predicted and measured UE with respect to  $k_r$ . As in Reeser's study,  $k_r$  was assigned a fixed, standard value of  $3 \times 10^6 \text{ s}^{-1}$  [Zhang, 2000] and variation of  $k_r$  within the error minimization algorithm was accomplished by using a variable multiplication factor.

The third modification increased the volume of UE, tidal volume, and respiratory rate data used in the determination of the subject-specific  $k_r$  values. Reeser used a single session-averaged value to determine the subject-specific  $k_r$  value. However, significant changes in both tidal volume and respiratory rate occur over the course of the  $O_3$  exposure session, shown in Section 4.2. Thus, in the present study the  $k_r$  value was determined based on a multiple-breath

simulation, consisting of eleven points each representing a 5-minute averaged value for UE, tidal volume, and respiratory rate. The multiple breath simulation assured that best fit  $k_r$  value included the experimental UE under changing respiratory conditions.

### 5.3.3 Simulation Results

The data for three subjects were examined to determine the effect simulating only one breath employing the session-averaged  $V_T$  and RR as Reeser has done, compared to inputting multiple values of  $V_T$  and RR and then performing multiple-breath simulations throughout the exposure period. These subjects were chosen to represent the range in  $k_r$  multiplier values from a high multiplier (FPM104S), an average multiplier (FPM074N), and a low multiplier (MPM069N). Summarized in Table 5-1 are the subject-specific  $k_r$  values estimated for the one-breath simulations (60-min averaged breathing and uptake data) and for the multiple-breath simulations (5-min averaged breathing and uptake data). Differences between the one-breath and multiple-breath simulation fitting procedures are only observed for one of the three sample subjects, FPM074N.

Table 5-1: Subject Specific  $k_r$  Values Determined Through Single-Breath and Multiple-Breath Fitting Procedures.

Subject	$k_r$ Multiplier Value	
	Single Point Fitting	Multiple Point Fitting
FPM074N	0.770	1.050
FPM104S	12.312	12.414
MPM069N	0.027	0.0270

The experimental uptake efficiency data and the two simulated results are presented in Figure 5-12. The differences between the two simulations for subject FPM074N, in terms of the summed squared error (SSE) from the experimental values, are 0.0268 for the fitting procedure

for the single point simulation and 0.0258 for the fitting procedure using multiple points. There was no difference in SSE between the two simulations for subject FPM104S. Therefore, the use of the multiple-breath simulation method only yielded a slight improvement in agreement between the simulated UE and the experimental measurements. The difference between simulated and experimental UE for subject FPM074N suggested that there may have been physiological changes in addition to breathing pattern changes.

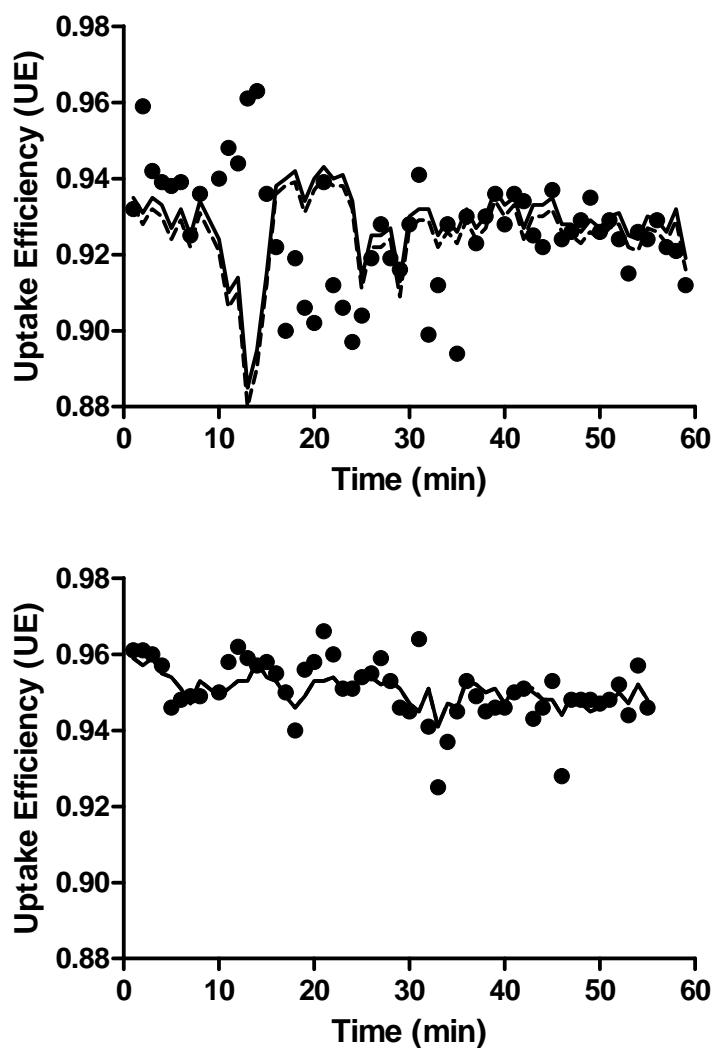


Figure 5-12: Comparison of Measured Uptake Efficiency (•) to the Predicted Values for Two Sample Subjects (FPM074N (top) and FPM104S (bottom)). Predicted UE are based on  $k_r$  values for single-breath simulation method (dashed line) and multiple-breath simulation method (solid

line). The single-breath and multiple breath simulation method for FPM104S are superimposed.

The  $k_r$  multipliers resulting from the multiple-breath fitting procedure is shown for all subjects in Figure 5-13. The population average  $k_r$  multiplier values are  $6.8 \pm 19.1$  (mean  $\pm$  SD) for the non-smoking subjects,  $32.6 \pm 107.6$  for the smoking subjects,  $17.2 \pm 53.2$  for the male subjects, and  $22.9 \pm 103.8$  for the female subjects. A two-sample t-test resulted in no significant differences in average  $k_r$  multiplier values between smokers and non-smokers. A two-sample t-test resulted in no significant differences in average  $k_r$  multiplier values between male subjects and female subjects. This was not surprising based on the large inter-subject variability observed in the  $k_r$  multiplier values.

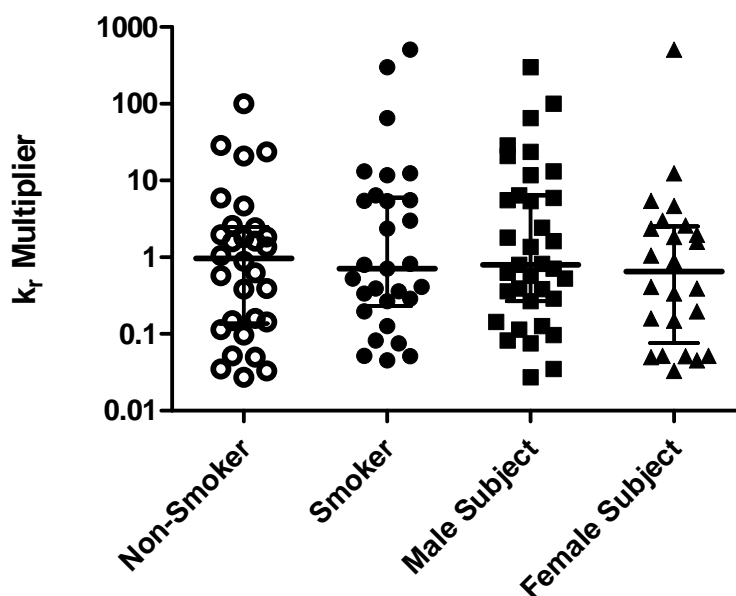


Figure 5-13: Subject Specific  $k_r$  Values by Smoking Category and by Gender. Horizontal bars are population median value. Error bars are interquartile range.

Sixty-four percent of the subject specific values are within an order of magnitude of the base value and 95% of the subject specific values are within two orders of magnitude of the base value. The subjects that have multipliers greater than 10 skew the population mean value upward

as observed. These results are consistent with the subject-specific  $k_r$  multipliers determined by Reeser on healthy non-smoking subjects, in which two-thirds of his population had multipliers within an order of magnitude of the base value [Reeser, 2007].

The proportion of “outlying subjects” that exhibited a multiplier less than 0.1 was uniformly distributed among the subpopulations: 3 male non-smokers, 2 male smokers, 3 female non-smokers, and 3 female smokers. The proportion of outlying subjects that exhibited a multiplier of greater than 10 was non-uniformly distributed among the subpopulations: 4 male non-smokers, 4 male smokers, 0 female non-smokers and 2 female smokers.

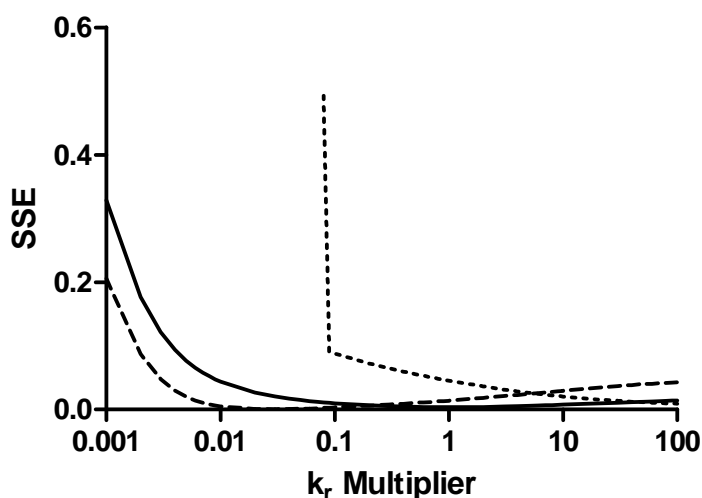


Figure 5-14: SSE Function for Sample Subjects with High (FPM114S, short-dashed line), Average (FPM074N, solid line), and Low (MPM069N, long-dashed line) Fitted  $k_r$  Multipliers.

The sum squared error (SSE) for three sample subjects was computed using simulations over a range of  $k_r$ -multiplier values from 0.001 to 100. The subjects were chosen so that their optimum  $k_r$ -multiplier (i.e., minimum SSE) would be either high, average, and low. The SSE functions for these subjects are presented in Figure 5-14. This figure demonstrates that the SSE does not always exhibit an absolute minimum. For subjects MPM069N and FPM074N, who exhibited low and average values of the optimal  $k_r$ -multiplier there was a distinct minimum for

the SSE function. This was not the case for the subject FPM114S, whose SSE function exhibited a continual shallow reduction with increasing value of  $k_r$  over the range of multiplier values presented in Figure 5-14. In particular with increasing  $k_r$ , the slope of the SSE function fell from 0.27 immediately after the initial reduction to  $2.9E-5$  at  $k_r$  values closer to 100. This suggests that an estimated  $k_r$ -multiplier should be no larger than the value at which the slope of the SSE function falls below  $1 \times 10^{-4}$ .

The simulation was previously shown to be sensitive to changes to  $k_r$  over a range of values. However, there was a saturation point in the sensitivity analysis where increasing the  $k_r$  multiplier resulted in minimal increases in  $O_3$  uptake efficiency (Figure 2-10). The saturation would correspond to the limit in which the reaction of  $O_3$  within the liquid-phase is rapid, reducing the concentration of  $O_3$  in the liquid-phase to essentially zero.

Asplund and colleagues observed a dose dependent decrease in the absorption efficiency of  $O_3$  after exposure to  $O_3$  through the bolus inhalation technique [Asplund et al., 1996]. The significant decrease of UE over the course of  $O_3$  exposure found in the current study (Figure 4-7) is consistent with Asplund's observations. Part of the reason for this progressive UE decline could have been the parallel decline in  $V_T$  that was also observed (Figure 4-3). It is also possible that  $k_r$  was progressively reduced during the course of  $O_3$  exposure. Simulations using a fixed  $k_r$ -multiplier but the known multiple-breath breathing pattern for subject FPM074N indicate that there are still deviations in UE from the simulation, particularly early in the exposure period (Figure 5-12). This suggests that  $k_r$  may, in fact, have initially varied in the subject's lungs.

To determine what changes in  $k_r$  are necessary to bring the simulations of subject FPM074N in line with her UE data, separate  $k_r$ -multiplier estimates (based on UE and breathing pattern data averaged over 5-minute intervals) were determined at eleven time points during  $O_3$  exposure (Figure 5-15). Because the fitted  $k_r$  value for the 15-minute time point did not exhibit a minimum SSE,  $k_r$  was identified as that simulation where the slope of the SSE function with

respect to the  $k_r$ -multiplier dropped below  $1 \times 10^{-4}$ . The session-averaged  $k_r$  value (broken line in the figure) under-predicted the initial time-specific  $O_3$  reaction rate constants for this subject and tended to over-predict the time specific reaction rate constants later in the session. The pattern of decreasing reaction rate constant over the time course of the  $O_3$  exposure session is consistent with a progressive depletion of reactive substrates.

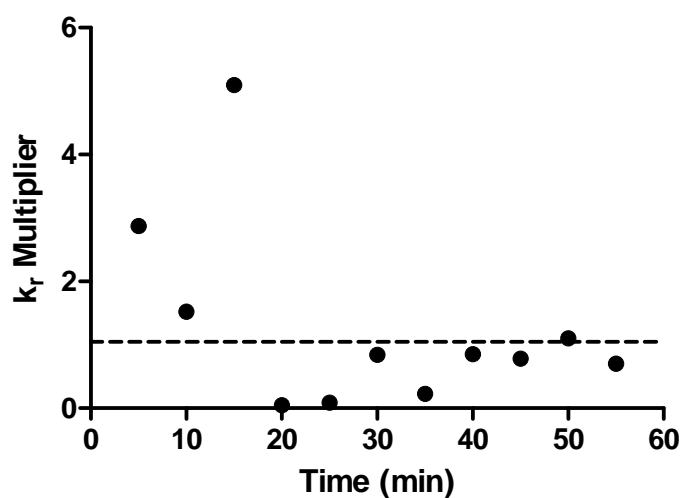


Figure 5-15: Time Course of  $k_r$  Value for Subject FPM074N.  $k_r$  multiplier determined through the single point fitting technique using the subject specific average values for each 5 minute time interval. The dashed line represents the subject specific  $k_r$  value determined through multiple point fitting.

The uptake efficiency simulated using the time-specific  $k_r$  values for this subject is compared to the simulation using the session-averaged  $k_r$  estimate throughout the exposure is presented in Figure 5-16. The simulation that used the time-specific  $k_r$  values showed better agreement between the simulated values and the experimental measurements of uptake efficiency. The SSEs of these simulations were 0.0098 when time-specific  $k_r$  values were used and 0.0258 when the session-averaged  $k_r$  estimate was employed.

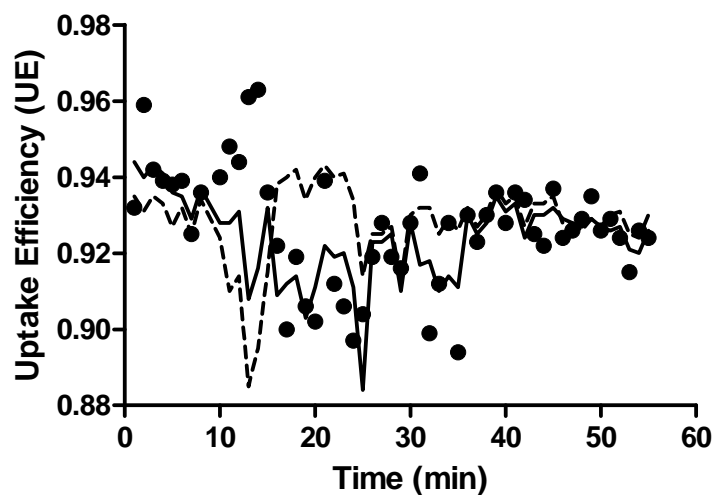


Figure 5-16: Comparison of Time Specific  $k_r$  and Multiple Point Fitted  $k_r$  Simulations for Subject FPM074N. Presented as a comparison to the one minute averaged uptake efficiency measurement ( $\bullet$ ). Simulation of the uptake efficiency for multiple point fitted  $k_r$  value (dashed line) and time-specific  $k_r$  value (solid line).

### 5.3.4 Regional Dose of $O_3$

The single-path model was used to partition the inhaled dose between various local respiratory compartments. By distributing the retained dose in this manner, the relationship between a localized dose and pulmonary responses can be elucidated. Presented in this section are: the method used to partition the retained dose into specific respiratory compartments; the subject-specific and population retained dose partitioning; and an analysis of the localized dose with static pulmonary response measurements.

### 5.3.4.1 Partitioning Retained Dose Using Single-Path Model

The partitioning of the  $D_T$  into regional components required additional modifications to the single-path model. The previous version of the model determined the cumulative uptake of  $O_3$  as:

$$D_T = \int_0^L \int_0^t K \left( \frac{4}{d} \right) C A dt dy \quad [5-17]$$

where:

- L is the length of the respiratory tract;
- t is the total time of the breath, inhalation and exhalation;
- K is the overall mass transfer coefficient which takes into account both the convective-diffusion through the gas boundary layer adjacent to the air-liquid interface and the reactive-diffusion through the liquid lining the epithelial cells;
- d is the hydraulic diameter;
- C is the concentration of  $O_3$  in the air; and
- A is the airspace cross-sectional area.

The numerical integration with respect to length in Equation 5-17 was modified to incorporate specific length ranges that corresponded to localized regions in the respiratory tract. The specific locations selected were the upper airways (UA), the proximal conducting airways ( $CA_P$ ), the distal conducting airways ( $CA_D$ ), and the respiratory airspaces (RA). Included in the single path model are the base values and scaling factors for the 23-generation Weibel model [Weible, 1963]. The UA included the oral cavity, pharynx and larynx. The  $CA_P$  included the trachea and the first 4 generations based on the Weibel model. The  $CA_D$  included generations 5 to 16. The RA included all the generations distal to generation 16.

The finite difference solution of the species conservation equation (Equation 5-1) decomposes the total longitudinal distance of the respiratory tract into a finite number of

elements. At each finite element (i) the flux of O<sub>3</sub> into the liquid lining layer (F<sub>i</sub>) was determined as:

$$F_i = \left[ \int_0^t K_i \left( \frac{4}{d_i} \right) C_i A_i dt \right] \times \Delta y_i \quad [5-18]$$

where:  $i$  is the finite element number; and  
 $\Delta y_i$  is the longitudinal length associated with finite element i.

The regional flux (F<sub>a</sub>) was then determined as:

$$F_a = \sum_{i=i_0}^{i_f} F_i \quad [5-19]$$

where:  $a$  is the region of interest, either UA, CA, or RA;  
 $i_0$  is the finite element corresponding to the start of the localized respiratory region; and  
 $i_f$  is the finite element corresponding to the end of the localized respiratory region.

Finally, the regional partitioning factors (P<sub>a</sub>) were calculated by:

$$P_a = \frac{F_a}{\sum F_a} \quad [5-20]$$

The partitioning factors were simulated for each minute-averaged breathing pattern to account for variations in tidal volume and frequency. The regional dose was determined by multiplying the D<sub>R</sub> by the subject-specific, time-specific P<sub>a</sub>.

#### ***5.3.4.2 Results of Retained Dose Partitioning***

The single-path simulations were conducted with the anthropomorphic data for the subject, the baseline value of V<sub>D</sub> for the subject, the V<sub>T</sub> and RR of the subject based on minute-averaged values, and the subject-specific k<sub>r</sub> value that was determined through the multiple-breath fitting procedure. This resulted in regional partitioning factors for the minute-averaged set

of breathing pattern data for each subject. The time-course of the partitioning factors for one subject during the one-hour O<sub>3</sub> exposure period are provided in Figure 5-17. The regional doses over the entire exposure period and pooled within the subject subpopulations are summarized in Table 5-2.

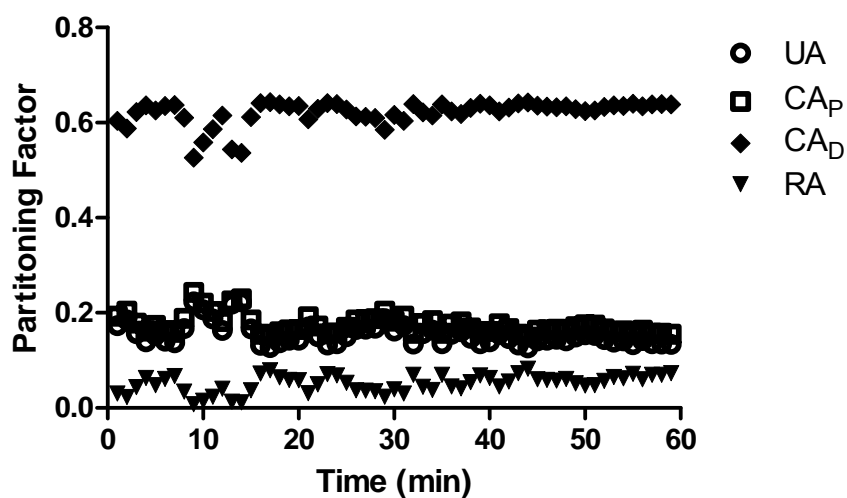


Figure 5-17: Partitioning Factor for Regional Respiratory Compartment. Presented for subject FPM074N.

Table 5-2: Retained Dose Partitioned into Lung Regions.

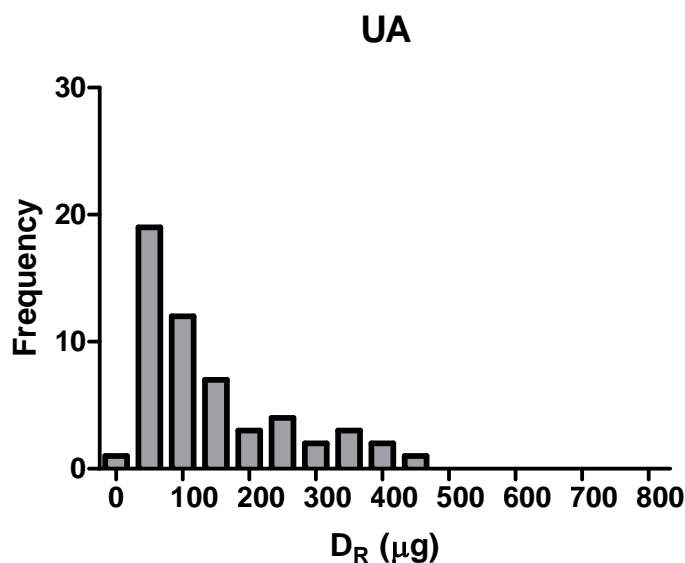
Subject Category	D <sub>R</sub> (μg)			
	UA	CA <sub>p</sub>	CA <sub>D</sub>	RA
Female	109 ± 90.5	109 ± 55.1 <sup>#</sup>	378 ± 73.4 <sup>#</sup>	91.1 ± 97.3
Male	163 ± 124	149 ± 77.4 <sup>#</sup>	440 ± 107 <sup>#</sup>	101 ± 123
Smoker	132 ± 110	129 ± 74.5	423 ± 83.7	105 ± 126
Non-Smoker	153 ± 120	137 ± 69.9	409 ± 115	88.7 ± 98.1

Determination of compartment partitioning failed for 5 subjects (2 female non-smokers, 1 female smoker, and 2 male smokers). These subjects have not been included in the above table or further analyses discussed in this section.

<sup>#</sup> Significant difference from opposite subject category.

The regional dose of  $O_3$  for the total subject population was greater in the total conducting airway region ( $CA = CA_P + CA_D$ ) ( $549 \pm 115 \mu\text{g}$ , mean  $\pm$  SD) than in either the UA ( $142 \pm 114 \mu\text{g}$ ) or RA ( $97 \pm 113 \mu\text{g}$ ) regions. A two-sample t-test indicated that smoking status was not a significant factor in the  $O_3$  dose to any of the airway regions. A two-sample t-test indicated that gender was a significant factor in the regional dose of  $O_3$  in the CA ( $P = 0.001$ ) but not in UA or RA. This gender difference existed in both  $CA_P$  ( $P = 0.031$ ) and  $CA_D$  ( $P = 0.015$ ). Gender was also a significant factor in  $D_R$  as mentioned in Section 4.3. Although there were significant differences between genders in the CA regional dose, the percentage of the  $D_R$  retained in the CA is not significantly different based on gender;  $71 \pm 10\%$  for female subjects and  $69 \pm 10\%$  for male subjects. This supports the notion that the localized retention of  $O_3$  was size dependent.

The distributions of the regional doses are shown in Figure 5-18. The distribution in the UA and the RA are skewed toward lower doses compared to the more uniform doses in the CA where the largest dose of  $O_3$  is retained.



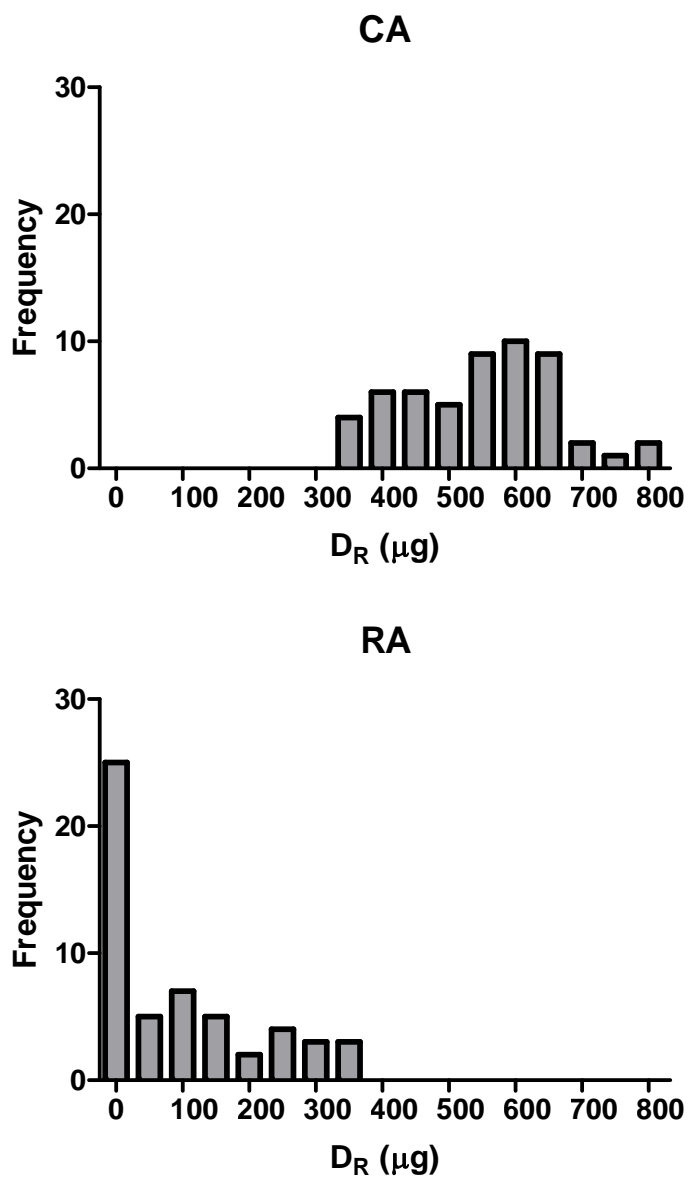
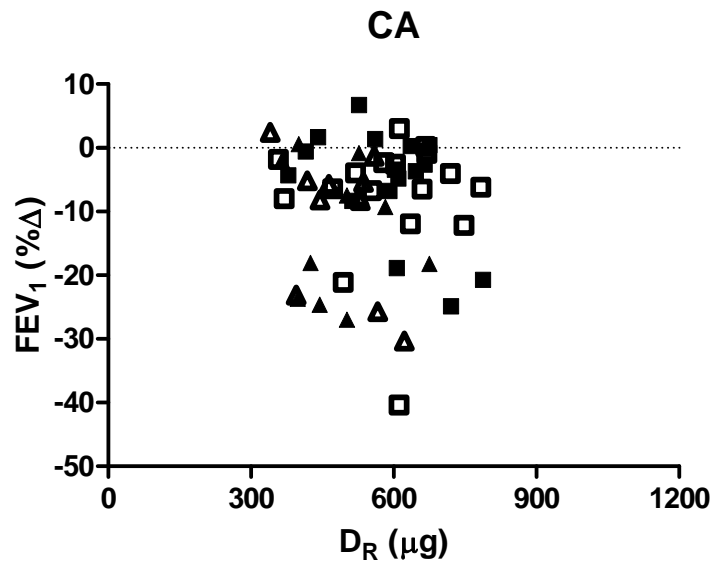
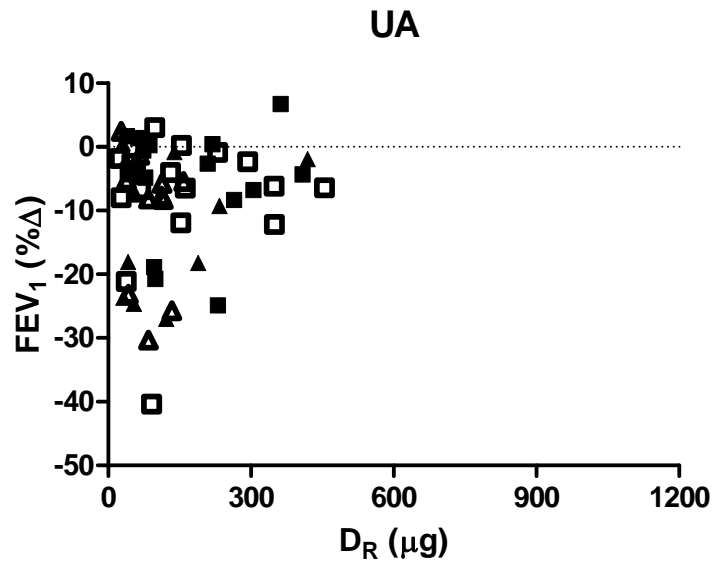


Figure 5-18: Population Distribution of Retained Dose by Lung Region.

#### 5.3.4.3 Comparison of Regional Dose to Pulmonary Response

The regional dose of  $\text{O}_3$  was compared to the static response measurements on a subject-specific basis. The subject-specific regional dose of  $\text{O}_3$  in the UA, the CA, and the RA is

presented with the percent change in  $FEV_1$  in Figure 5-19, the percent change in  $V_D$  in Figure 5-20, and the percent change in  $S_N$  in Figure 5-21.



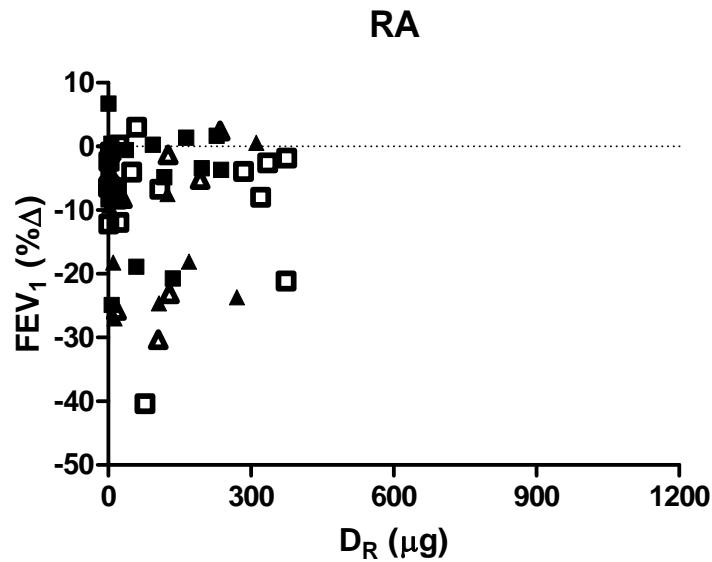
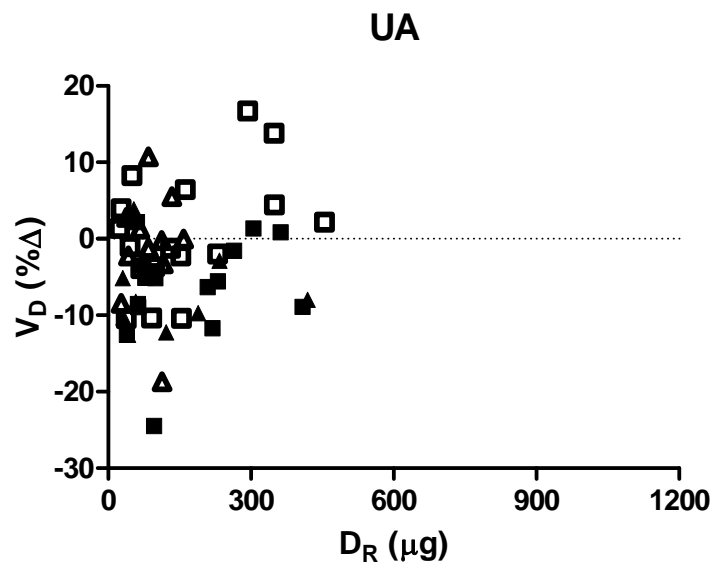


Figure 5-19: Percent Change in FEV<sub>1</sub> with Respect to Regional Retained Dose of O<sub>3</sub> (D<sub>R</sub>) for Male Non-Smoking Subjects (□), Female Non-Smoking Subjects (Δ), Male Smoking Subjects (■) and Female Smoking Subjects (▲). Each symbol represents an individual subject. Percent change in FEV<sub>1</sub> (%Δ) calculated as (post-exposure – pre-exposure)/ pre-exposure.



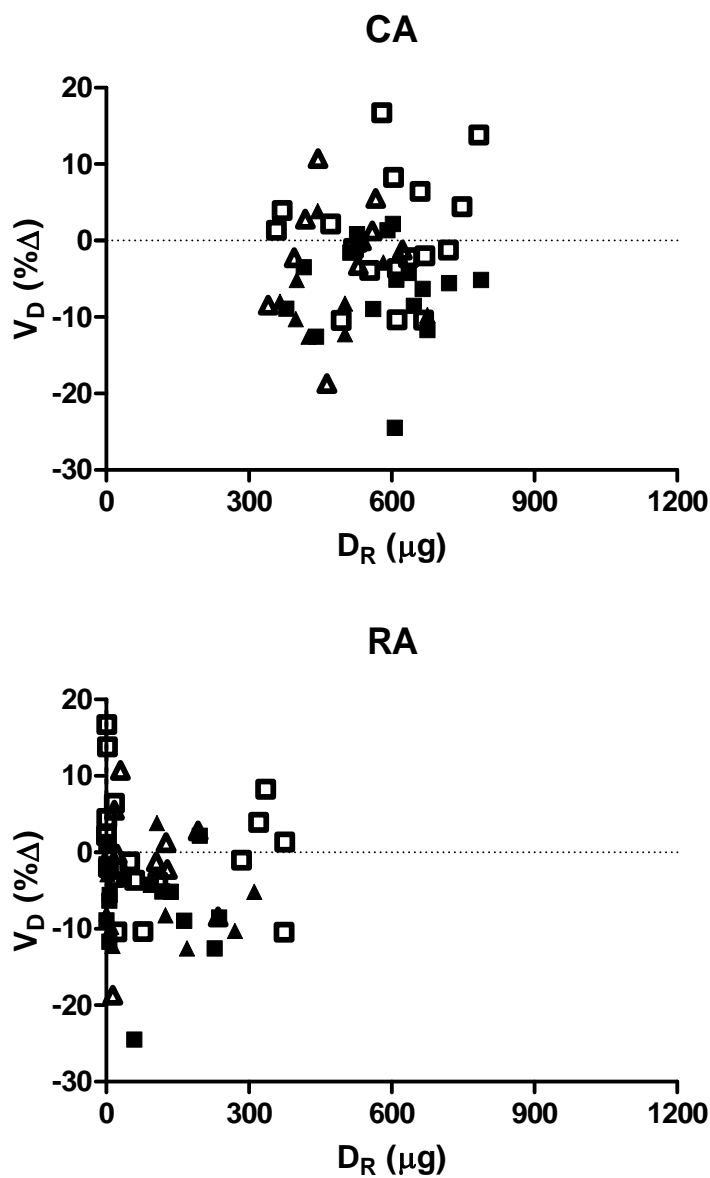
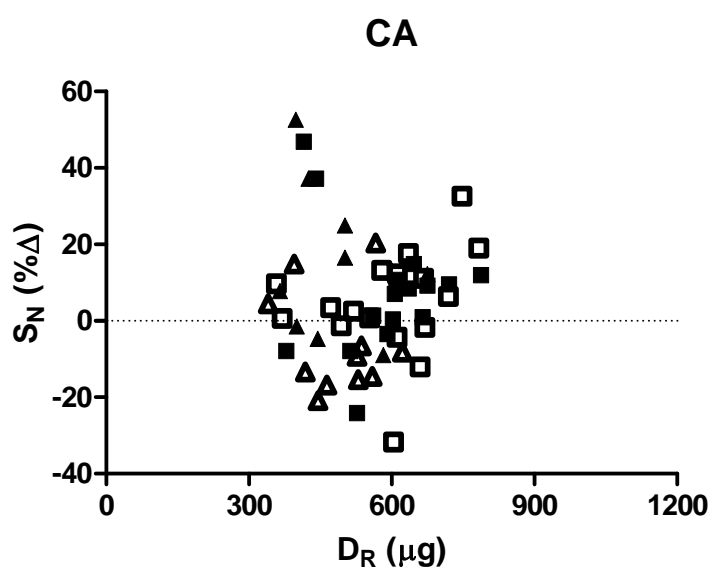
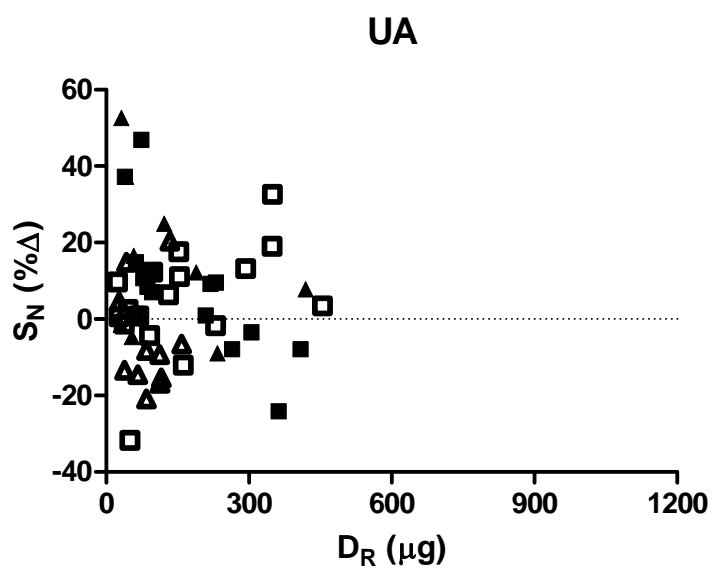


Figure 5-20: Percent Change in  $V_D$  with Respect to Regional Retained Dose of  $O_3$  ( $D_R$ ) for Male Non-Smoking Subjects ( $\square$ ), Female Non-Smoking Subjects ( $\Delta$ ), Male Smoking Subjects ( $\blacksquare$ ) and Female Smoking Subjects ( $\blacktriangle$ ). Each symbol represents an individual subject. Percent change in  $FEV_1$  (% $\Delta$ ) calculated as (post-exposure – pre-exposure)/ pre-exposure.



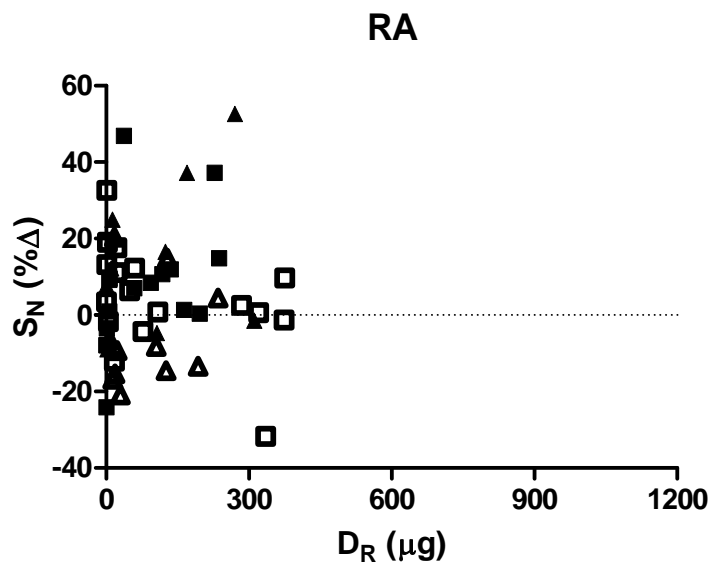


Figure 5-21: Percent Change in  $S_N$  with Respect to Regional Retained Dose of  $O_3$  ( $D_R$ ) for Male Non-Smoking Subjects ( $\square$ ), Female Non-Smoking Subjects ( $\Delta$ ), Male Smoking Subjects ( $\blacksquare$ ) and Female Smoking Subjects ( $\blacktriangle$ ). Each symbol represents an individual subject. Percent change in  $FEV_1$  ( $\% \Delta$ ) calculated as  $(\text{post-exposure} - \text{pre-exposure}) / \text{pre-exposure}$ .

A high degree of inter-subject variability in all three static response measurements was observed for the range of regional retained dose. Pearson correlation tests confirmed that the dose of  $O_3$  in the local respiratory compartments was not correlated to the pulmonary function parameters  $FEV_1$ ,  $V_D$ , and  $S_N$ .

## Chapter 6

### Summary and Future Work

#### 6.1 Dose and Dose-Response Relationships

The main objective of this work was to determine the dose response relationship for O<sub>3</sub> exposure. Several O<sub>3</sub> dose metrics were considered: the inhaled dose (D<sub>I</sub>); the cumulative retained dose (D<sub>T</sub>); and the retained dose partitioned into contributions from the upper airway (UA), the conducting airway (CA), and the respiratory airspace (RA) regions. Pulmonary response was measured by both static and dynamic methods. The static pulmonary response measurements were taken prior to and just after the O<sub>3</sub> exposure session at a fixed breathing condition, whereas the dynamic pulmonary response was measured simultaneous to the exposure. The statically measured parameters consisted of the forced expired volume (FEV<sub>1</sub>), the CO<sub>2</sub> dead space volume (V<sub>D</sub>), and the normalized slope of the CO<sub>2</sub> alveolar plateau (S<sub>N</sub>). The dynamically measured parameters included the tidal volume (V<sub>T</sub>), respiratory rate (RR), V<sub>D</sub>, and S<sub>N</sub>.

The D<sub>I</sub> administered to the 60 subjects in this study ranged from 534 to 1149 μg O<sub>3</sub> with an average of 794 μg O<sub>3</sub>. The resulting static response of %ΔFEV<sub>1</sub> ranged from 6.71 to -40.37 consistent with the meta-analysis of McDonnell and colleagues (1997) on 485 subjects. The D<sub>T</sub> was strongly correlated with the D<sub>I</sub> indicating a population-averaged uptake efficiency (UE) of 0.971. The static capnometry parameters, V<sub>D</sub> and S<sub>N</sub>, were compared to cumulative D<sub>T</sub> and the regional D<sub>R</sub>. Neither V<sub>D</sub> nor S<sub>N</sub> were correlated with either dose metrics.

The breathing pattern of the subject populations changed over the time course of the continuous air and continuous O<sub>3</sub> sessions. In both sessions breathing frequency increased and V<sub>T</sub> decreased. The V<sub>T</sub> decrease in the O<sub>3</sub> session was greater than that in the air session, and the

time course of this difference ( $\Delta V_T$ ) was significantly correlated with cumulative  $D_T$ . Linear regression analysis determined the rate of change in  $\Delta V_T$  with cumulative  $D_T$  for the population of  $-0.11 \pm 0.03$  mL/ $\mu$ g.

Real time capnometry data were analyzed to determine if the time course of  $V_D$  and  $S_N$  were correlated with cumulative  $D_T$ . For the  $O_3$  exposure session  $\Delta V_D$  was negatively correlated with cumulative  $D_R$  and  $\Delta S_N$  was not correlated with cumulative  $D_T$ . Linear regression analysis determined the rate of change in  $\Delta V_D$  with cumulative  $D_R$  of  $-0.014 \pm 0.005$  mL/ $\mu$ g.

## 6.2 Influence of Smoking Status

An additional goal was the determination of differences in the dose response relationship between smoking subjects and non-smoking subjects. Primarily using  $FEV_1$  as an end-point, previous studies of the relative sensitivity of smokers and non-smokers to  $O_3$  exposure were inconsistent. The current study found that changes in static  $FEV_1$  were, in fact, quite similar in smokers and non-smokers.

The percent change in  $V_D$  was the only static pulmonary function measurement that was significantly different between smokers ( $-6.02 \pm 6.40$  % $\Delta V_D$ ) and non-smokers ( $-0.13 \pm 7.40$  % $\Delta V_D$ ). Regression analysis of the time course rate of change in the dynamic parameters  $V_M$ ,  $V_T$ ,  $RR$ ,  $V_D$  and  $S_N$  and the uptake parameters  $UR$  and  $UE$  resulted in no significant differences based on smoking status. However, significant differences in  $UE$ ,  $VD$ , and  $SN$  parameters attributable to smoking status did exist very early during  $O_3$  exposure. Similarly significant differences in  $VD$  and  $SN$  due to smoking status also occurred during the air exposure. This suggests that smoking affected the initial pulmonary response to exercise. The magnitude of the difference determined in  $UE$  did not result in significant differences in the cumulative retained dose.

There were no observed differences in cumulative  $D_R$  or regional DR which could be used to explain the significant  $\% \Delta V_D$  difference based on smoking status.

### 6.3 Gender Differences

The difference in the dose-response relationship between male and female subjects was also investigated. Previous studies suggest that gender differences in response can be attributed to the size difference between genders. The protocol for this study normalized the target minute volume based on the subject BSA, which normalizes the inhaled dose of  $O_3$  by size.

No significant gender differences were observed in the static pulmonary function measurements of  $FEV_1$ ,  $V_D$ , and  $S_N$ . Gender was a significant factor for the initial values of the dynamic response variables.  $V_T$  was the only dynamic response variable that exhibited a significant gender difference in the time rate of change during the  $O_3$  exposure session, with the male subjects decreasing  $V_T$  more rapidly. However, gender was not a significant factor in determining the relationship between  $D_T$  and  $\Delta V_T$ .

### 6.4 Future Work

In this work, the regional dose of  $O_3$  was compared to the static pulmonary response measurements of  $FEV_1$ ,  $V_D$ , and  $S_N$ . The dynamic respiratory measurements for  $V_T$  have been analyzed as a continuous function of time and dose. The identification and analysis of the time-to-onset of tachypnea by Schelegle and colleagues, provides a method of analysis that should be applied to both the time-course and dose-course measurements of the dynamic parameters in this study.

In this thesis, the reaction rate constant was used as an adjustable parameter in a single-path model to fit experimentally measured uptake efficiency during the course of an O<sub>3</sub> exposure session. The time course change in the reaction rate constant measurement was analyzed for one subject, presented in Figures 5-15 and 5-16. The result of that analysis suggested that the reaction rate constant may be dependent upon the time course of the exposure. The time course changes in reaction rate constant for the subject population in this study should be evaluated further.

Capnometry measurements were evaluated over the time course of the air session and O<sub>3</sub> session. Time course response measurements have the advantage of corresponding to the time course of the retained dose in this experimental protocol, which enables analysis at multiple cumulative dose levels from one exposure session. However, the time course measurements can be influenced by the dynamic nature of the breathing pattern during the session [Neufeld et al., 1991; Kars et al., 1997]. Scherer and colleagues used a single-path model to simulate experimental CO<sub>2</sub> expirogram data [Scherer et al., 1988]. This model was then used to determine the effect of differing acinar structure on the capnometry parameters V<sub>D</sub> and S<sub>N</sub> [Neufeld et al., 1992]. Future efforts in applying a single-path model to the dynamic capnometry measurement would help quantify the meaning of the dynamic parameters V<sub>D</sub> and S<sub>N</sub>.

## Bibliography

- Adams, W. C., W. M. Savin, and A. E. Christo. Detection of ozone toxicity during continuous exercise via the effective dose concept. *J. Appl. Physiol.:Respirat. Exercise Physiol.* 51(2): 415-422, 1981.
- Aitken, R. S., and A. E. Clarke-Kennedy. On the fluctuation in the composition of the alveolar air during a respiratory cycle in the muscular exercise. *J. Physiol. (London)* 65: 389-411, 1928.
- Asplund, P. T., A. Ben-Jebria, M. L. Rigas, and J. S. Ultman. Longitudinal distribution of ozone absorption in the lung: effect of continuous inhalation exposure. *Arch. Environ. Health.* 51(6): 431-438, 1996.
- Bates, D. V., G. M. Bell, C. D. Burnham, M. Hazucha, J. Mantha, L. D. Pengelly, and F. Silverman. Short-term effects of ozone on the lung. *J. Appl. Physiol.* 32(2): 176-181, 1972.
- Bell, M. L., A. McDermott, S. L. Zeger, J. M. Samet, and F. Dominici. Ozone and short-term mortality in 95 US urban communities, 1987-2000. *JAMA* 292: 2372-2378, 2004.
- Ben-Jebria, A., G. Bedig, B. Mensch, and C. Hatzfeld. Dispersin d'un emboli radioactive dans l'oropharynx et le larynx: recherché de la fonction de transfer. *J. Biophys. Med. Nucl.* 6: 51-57, 1982.
- Ben-Jebria, A., S. C. Hu, E. L. Kitzmiller, and J. S. Ultman. Ozone absorption into excised porcine and sheep tracheae by a bolus-response method. *Environ. Res.* 56: 144-157, 1991.
- Bush, M. L., P. T. Asplund, K. A. Miles, A. Ben-Jebria, and J. S., Ultman. Longitudinal distribution of O<sub>3</sub> absorption in the lung: gender differences and intersubject variability. *J. Appl. Physiol.* 81(4): 1651-1657, 1996.
- Bush, M. L., T. Raybold, S. Abeles, S. C. Hu, A. Ben-Jebria, and J. S. Ultman. Longitudinal distribution of ozone absorption in the lung: simulation with a single-path model. *Toxicol. Appl. Pharmacol.* 140: 219-226, 1996B.
- Bush, M. L. Ozone absorption in the human respiratory tract: A study in intersubject variability. Doctor Thesis: The Pennsylvania State University, University Park, PA 16802. Department of Chemical Engineering. 1999.
- Bush, M. L., W. Zhang, A. Ben-Jebria, and J. S. Ultman. Longitudinal distribution of ozone and chlorine in the human respiratory tract: simulation of nasal and oral breathing with the single-path diffusion model. *Toxicol. Appl. Pharmacol.* 173: 137-145, 2001.
- Condorelli, P. and S. C. George. Theoretical gas phase mass transfer coefficients for endogenous gases in the lungs. *Ann. Biomed. Eng.* 27: 326-339, 1999.

- Cotes, J.E. Lung Function: Assessment and Application in Medicine. 5<sup>th</sup> Ed. Blackwell Scientific Publications, Oxford. 1993.
- Cussler, E. L. Diffusion Mass Transfer in Fluid Systems. Cambridge University Press, London. 1984.
- Cvitas, T., L. Klasinc, N. Kezele, S. P. McGlynn, and W. A. Pryor. New directions: how dangerous is ozone? *Atmos. Environ.* 39: 4607-4608, 2005.
- Farmery, A. D. Volumetric capnography and lung growth in children, a simple model validated. *Anesthesiology* 83 (6): 1377-1379, 1995.
- Fowler, W. S. Lung function studies: II. The respiratory dead space. *Am. J. Physiol.* 154: 405-416, 1948.
- Frampton, M. W., P. E. Morrow, A. Torres, C. Cox, K. Z. Voter, and M. J. Utell. Ozone responsiveness in smokers and nonsmokers. *Am. J. Respir. Crit. Care Med.* 155: 116-121, 1997.
- Gerrity, T. R., F. Biscardi, A. Strong, A. R. Garlington, J. S. Brown, and P. A. Bromberg. Bronchoscopic determination of ozone uptake in humans. *J. Appl. Physiol.* 79(3): 852-860, 1995.
- Gibbons, S. I., and W. C. Adams. Combined effects of ozone exposure and ambient heat on exercising females. *J. Appl. Physiol.:Respirat. Exercise Physiol.* 57(2): 450-456, 1984.
- Hazucha, M., F. Silverman, C. Parent, S. Field, and D. V. Bates. Pulmonary function in man after short-term exposure to ozone. *Arch. Environ. Health.* 27: 183-188, 1973.
- Hazucha, M. J., L. J. Folinsbee, and P. A. Bromberg. Distribution and reproducibility of spirometric response to ozone by gender and age. *J. Appl. Physiol.* 95: 1917-1925, 2003.
- Hu, S. C., A. Ben-Jebria, and J. S. Ultman. Longitudinal distribution of ozone absorption in the lung: quiet respiration in healthy subjects. *J. Appl. Physiol.* 73(4): 1655-1661, 1992.
- Hu, S. C., A. Ben-Jebria, and J. S. Ultman. Longitudinal distribution of ozone absorption in the lung: effects of respiratory flow. *J. Appl. Physiol.* 77(2): 574-583, 1994.
- Kabel, J. R., A. Ben-Jebria, and J. S. Ultman. Longitudinal distribution of ozone absorption in the lung: comparison of nasal and oral quiet breathing. *J. Appl. Physiol.* 77(6): 2584-2592, 1994.
- Kars, A. H., J. M. Bogaard, T. Stijnen, J. de Vries, A. F. M. Verbraak, and C. Hilvering. Dead space and slope indices from the expiratory carbon dioxide tension-volume curve. *Eur. Respir. J.* 10: 1829-1836, 1997.
- Kerr, H. D., T. J. Kulle, M. L. McIlhany, and P. Swidersky. Effects of ozone on pulmonary function in normal subjects. *Am. Rev. Resp. Disease* 3: 763-773, 1975.

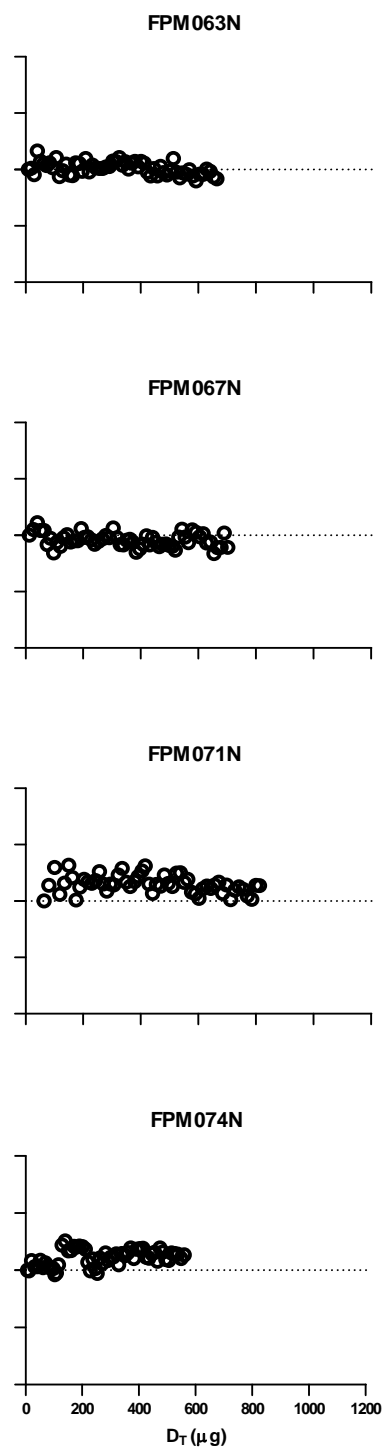
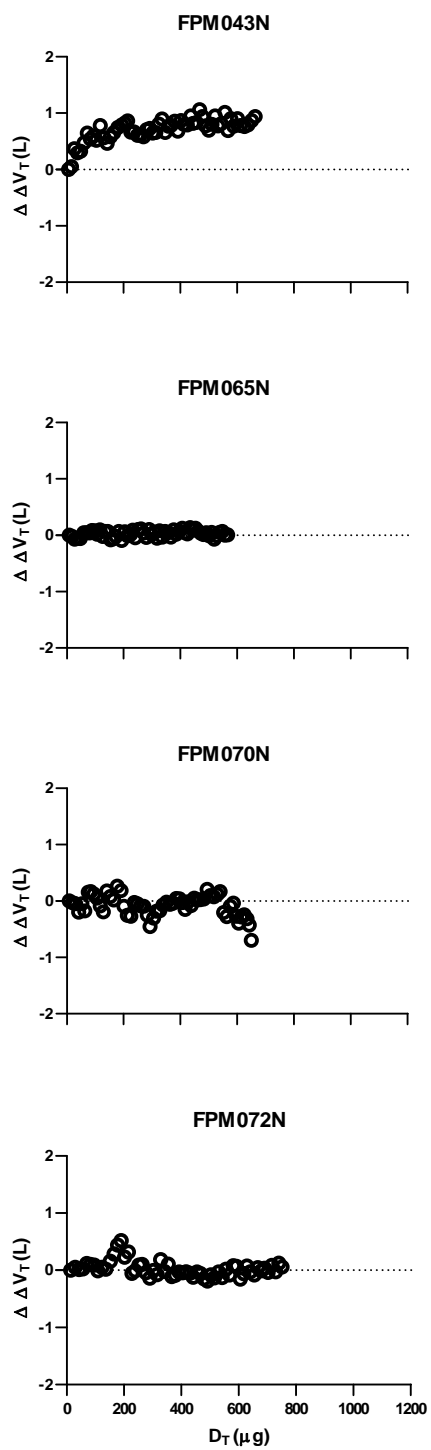
- Knudsen, R. J., R. C., Slatin, D. Lebowitz, and B. Burrows. The maximal expiratory flow volume curve: normal standards, variability, and effects of age. *Amer. Rev. of Resp. Dis.* 113: 587-600, 1976.
- Lauritzen, S. K., and W. C. Adams. Ozone inhalation effects consequent to continuous exercise in females: comparison to males. *J. Appl. Physiol.* 59(5): 1601-1606, 1985.
- MacDougal, C. S., M. L. Rigas, A. Ben-Jebria, and J. S. Ultman. A respiratory ozone analyzer optimized for high resolution and swift dynamic response during exercise conditions. *Arch. Environ. Health.* 53(2): 161-174, 1998.
- McDonnell, W. F., D. H. Horstman, M. J. Hazucha, E. Seal Jr., E. D. Haak, S. A. Salaam, and D. E. House. Pulmonary effects of ozone exposure during exercise: dose-response characteristics. *J. Appl. Physiol.:Respirat. Exercise Physiol.* 54(5): 1345-1352, 1983.
- McDonnell, W. F., P. W. Stewart, S. Anderoni, El Seal, Jr., H. R. Kehrl, D. H. Horstman, L. J. Folinsbee, and M. V. Smith. Prediction of ozone-induced FEV1 changes. *Am. J. Respir. Crit. Care. Med.* 156: 715-722, 1997.
- Messineo, T. D., and W. C. Adams. Ozone inhalation effects in females varying widely in lung size: comparison with males. *J. Appl. Physiol.* 69(1): 96-103, 1990.
- Neufeld, G. R., S. Gobran, J. E. Baumgardner, S. J. Aukburg, M. Schreiner, and P. W. Scherer. Diffusivity, respiratory rate and tidal volume influence inert gas expirograms. *Resp. Physiol.* 84: 31-47, 1991.
- Neufeld, G. R., J. D. Schwardt, S. R. Gobran, J. E. Baumgardner, M. S. Schreiner, S. K. Aukburg, and P. W. Scherer. Modeling steady state pulmonary elimination of He, SF<sub>6</sub>, and CO<sub>2</sub>: effect of morphometry. *Respir. Physiol.* 88: 257-275, 1992.
- Nuckols, M. L. Heat and water vapor transfer in the human respiratory system at hyperbaric conditions. Doctoral dissertation. Duke University, 1981.
- Peng, C.-K., J. E. Mietus, Y. Liu, C. Lee, J. M. Hausdorff, H. E. Stanley, A. L. Goldberger, and L. A. Lipsitz. Quantifying fractal dynamics of human respiration: age and gender effects. *Ann. Biomed. Eng.* 30: 683-692, 2002.
- Pryor, W. A. Mechanisms of radical formation from reaction of ozone with target molecules in the lung. *Free Rad. Biol. And Med.* 17: 451-465, 1994.
- Ratto, J., H. Wong, J. Liu, J. Fahy, H. Boushey, C. Solomon, and J. Balmes. Effects of multiday exposure to ozone on airway inflammation as determined using sputum induction. *Environ. Health Perspect.* 114: 209-212, 2006.
- Reeser, W. H., G. M. Lee, A. Taylor, L. Wang, S. F. Arnold, J. S. Ultman, and A. Ben-Jebria. Uptake of ozone in human lungs and its relationship to local physiological response. *Inhl. Tox.* 17: 699-707, 2005.

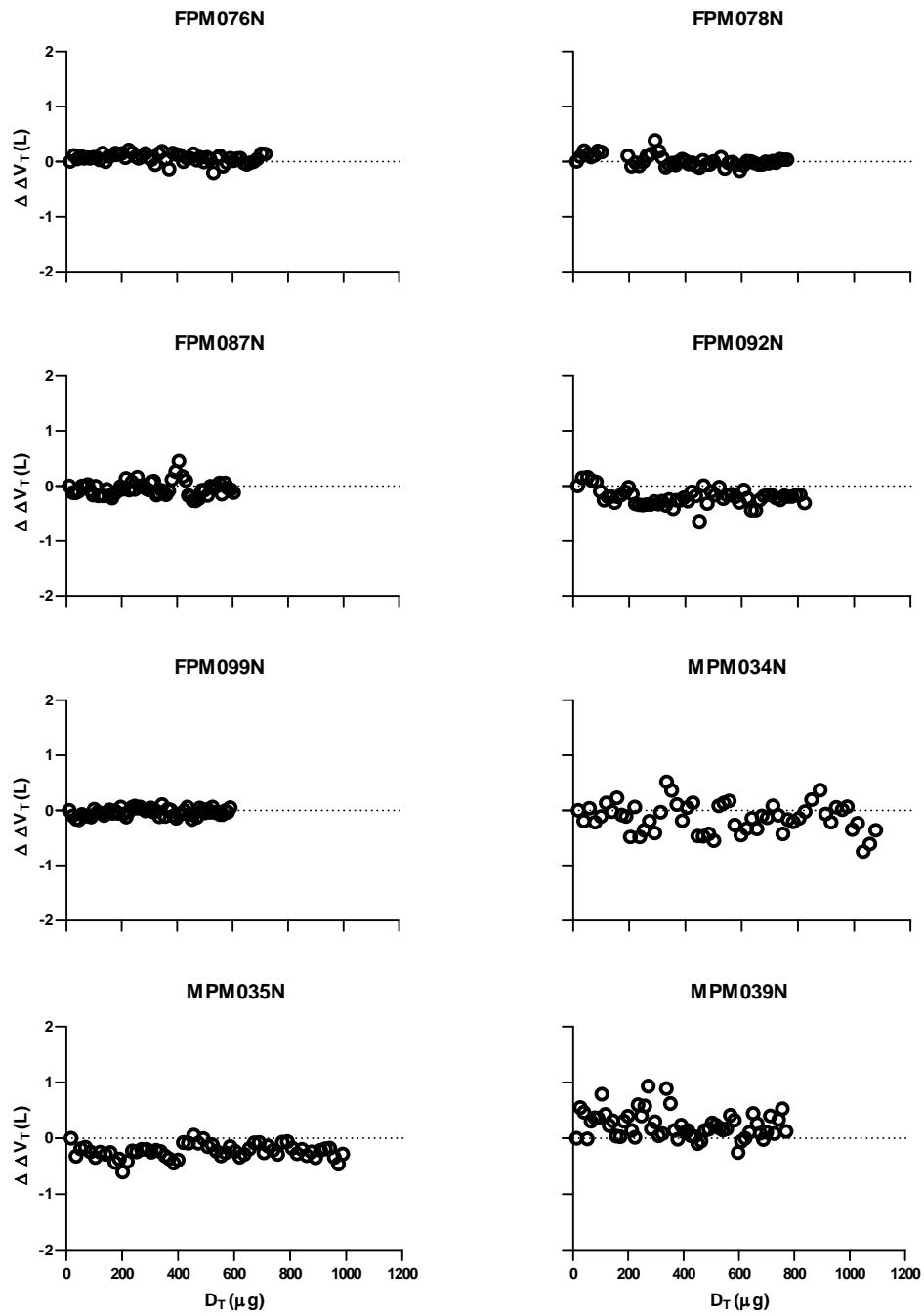
- Reeser, W. H. Intersubject variability in ozone uptake in the human lung. Doctor Thesis: The Pennsylvania State University, University Park, PA 16802. Department of Bioengineering. 2007.
- Rigas, M. L., S. N. Catlin, A. Ben-Jebria, and J. S. Ultman. Ozone uptake in the intact human respiratory tract: relationship between inhaled dose and actual dose. *J. Appl. Physiol.* 88: 2015-2022, 2000.
- Schelegle, E. S., W. F. Walby, and W. C. Adams. Time course of ozone-induced changes in breathing pattern in healthy exercising humans. *J. Appl. Physiol.* 102: 688-697, 2007.
- Scherer, P. W., L. H. Shendalman, and N. M. Grene. Simultaneous diffusion and convection in a single-breath lung washout. *Bull. Math. Biol.* 34: 393-412, 1972.
- Scherer, P. W., L. H. Shendalman, N. M. Greene, and A. Bouhuys. Measurement of axial diffusivities in a model of the bronchial airways. *J. Appl. Physiol.* 38: 719-723, 1975.
- Scherer, P. W., S. Gobran, S. J. Aukburg, J. E. Baumgardner, R. Bartkowski, and G. R. Neufeld. Numerical and experimental study of steady-state CO<sub>2</sub> and inert gas washout. *J. Appl. Physiol.* 64(3): 1022-1029, 1988.
- Schwardt, J. D., G. R. Neufeld, J. E. Baumgardner, and P. W. Scherer. Noninvasive recovery of acinar anatomic information from CO<sub>2</sub> expirograms. *Ann. Biomed. Eng.* 22: 293-306, 1994.
- Shephard, R. J., B. Urch, F. Silverman, and N. J. Corey. Interaction of ozone and cigarette smoke exposure. *Environ. Res.* 31: 125-137, 1983.
- Silverman, F., L. J. Folinsbee, J. Barnard, and R. J. Shephard. Pulmonary function changes in ozone – interaction of concentration and ventilation. *J. Appl. Physiol.* 41(6): 859-864.
- Taulbee, D. B., and C. P. Yu. A theory of aerosol deposition in the human respiratory tract. *J. Appl. Physiol.* 38: 77-85, 1975.
- Taylor, A. B., G. M. Lee, K. Nellore, A. Ben-Jebria, and J. S. Ultman. Changes in the carbon dioxide expirogram in response to ozone exposure. *Toxicol. Appl. Pharmacol.* 213: 1-9, 2006.
- Ultman, J. S., A. Ben-Jebria, and S. F. Arnold. Uptake distribution of ozone in human lungs: intersubject variability in physiologic response. *Res Rep Health Eff Inst.* 125: 1-30, 2004. (Data in Figure 2-6 not published in original report, but was personally transmitted by J. S. Ultman.)
- Weibel, E. R. Morphometry of the Human Lung. Academic Press, New York, 1963.
- Wiester, M. J., M. A. Stevens, M. G. Menache, J. L. McKee Jr., and T. R. Gerrity. Ozone uptake in healthy adult males during quiet breathing. *Fundam. Appl. Toxicol.* 29: 102-109, 1996.

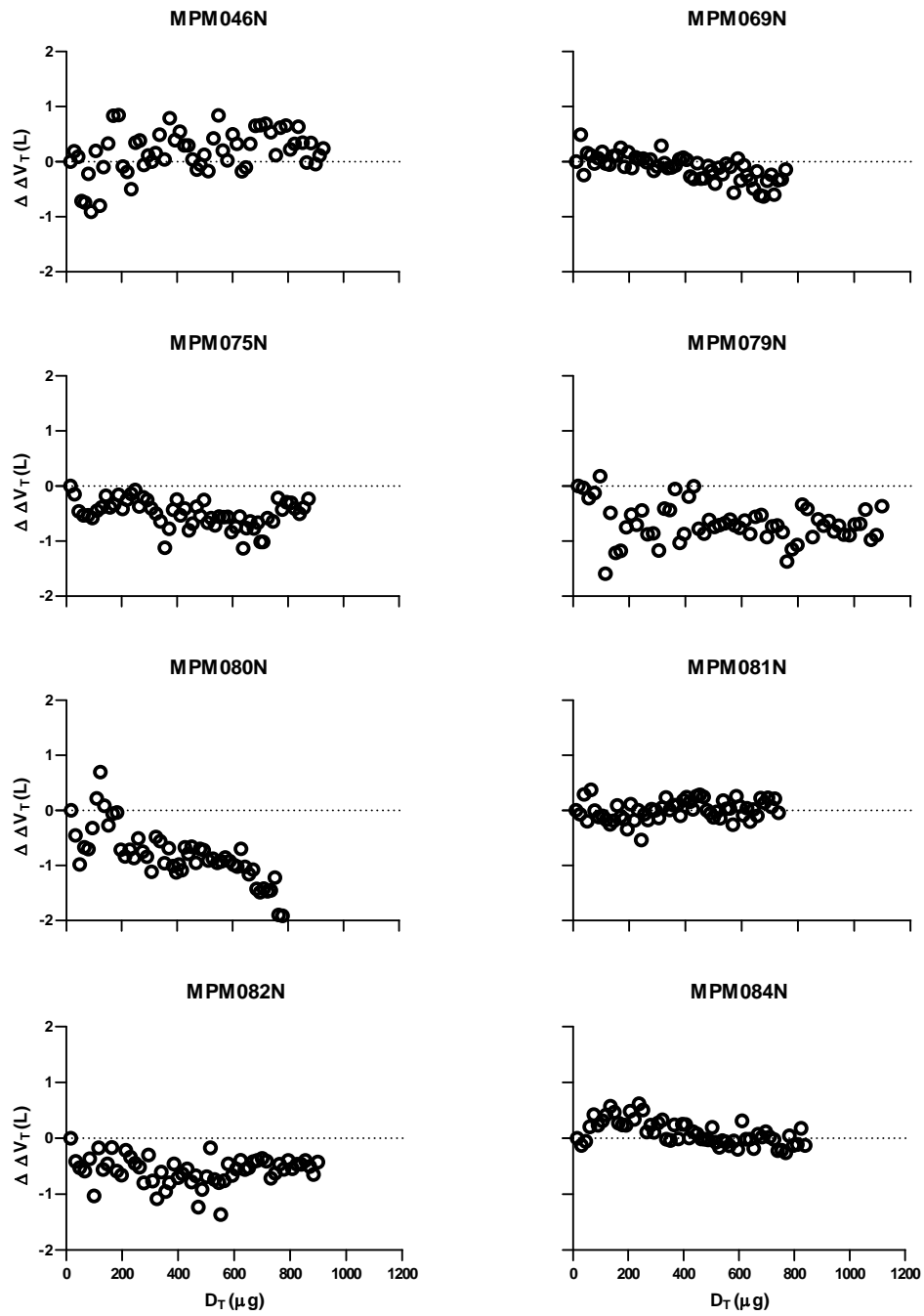
Young, W. A., D. B. Shaw, and D. V. Bates. Effect of low concentrations of ozone on pulmonary function in man. *J. Appl. Physiol.* 19(4): 765-768, 1964.

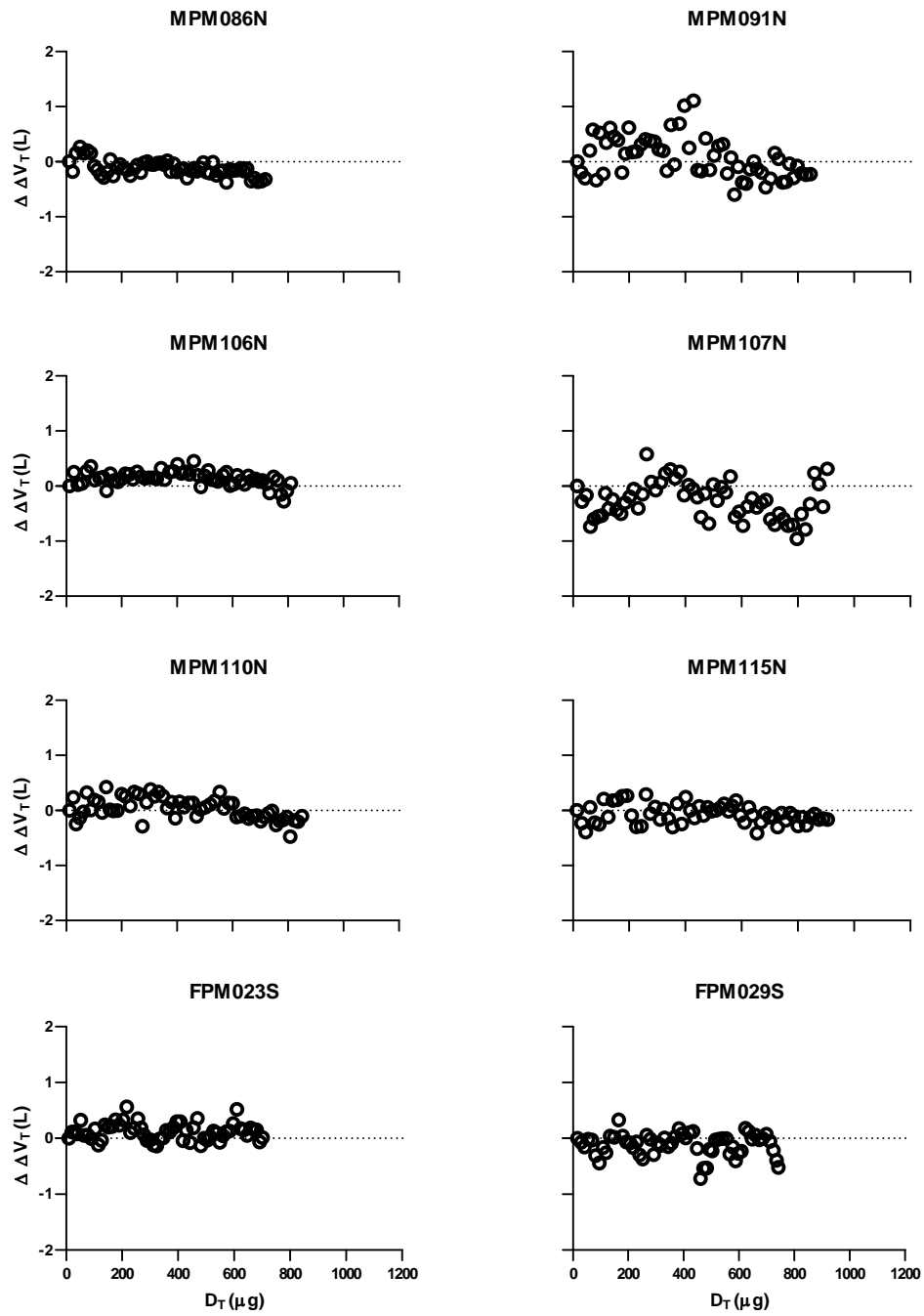
Zhang, W. Longitudinal distribution of chlorine and oone absorption in the human respiratory system: simulation with the single-path model. Master Thesis: The Pennsylvania State University, University Park, PA 16802. Department of Chemical Engineering. 2000.

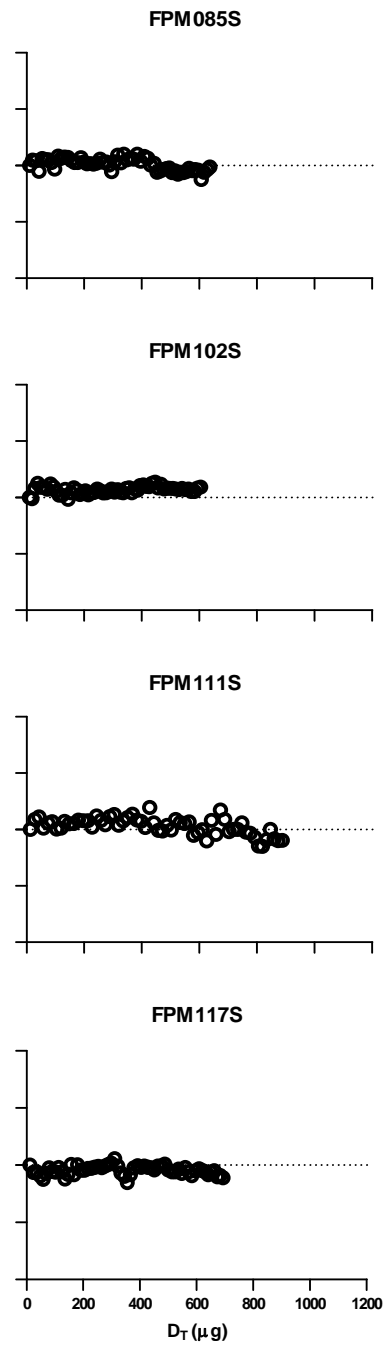
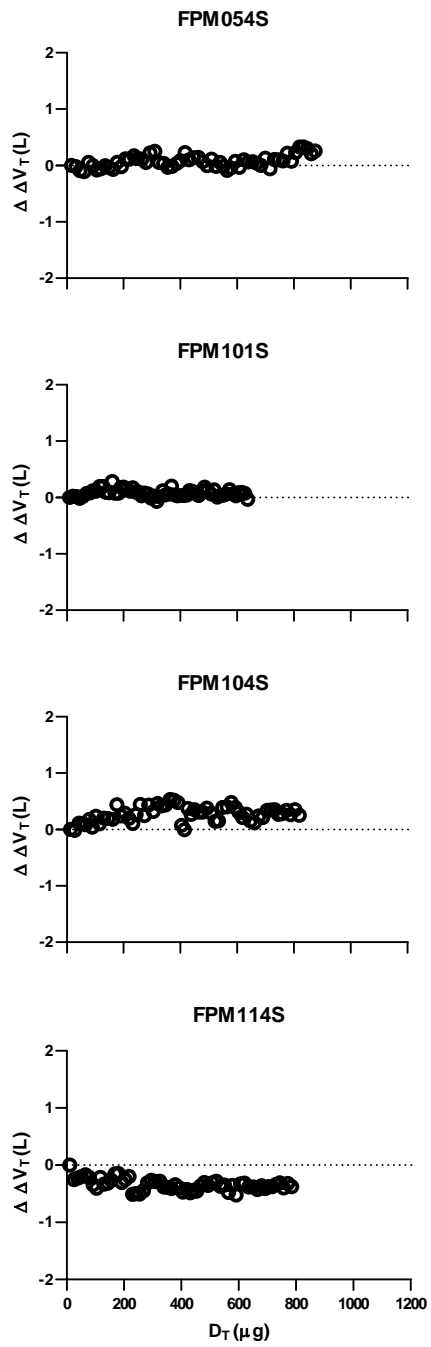
**Appendix A****Subject Specific Change in Tidal Volume ( $V_T$ ) with****Respect to Retained Dose of  $O_3$**

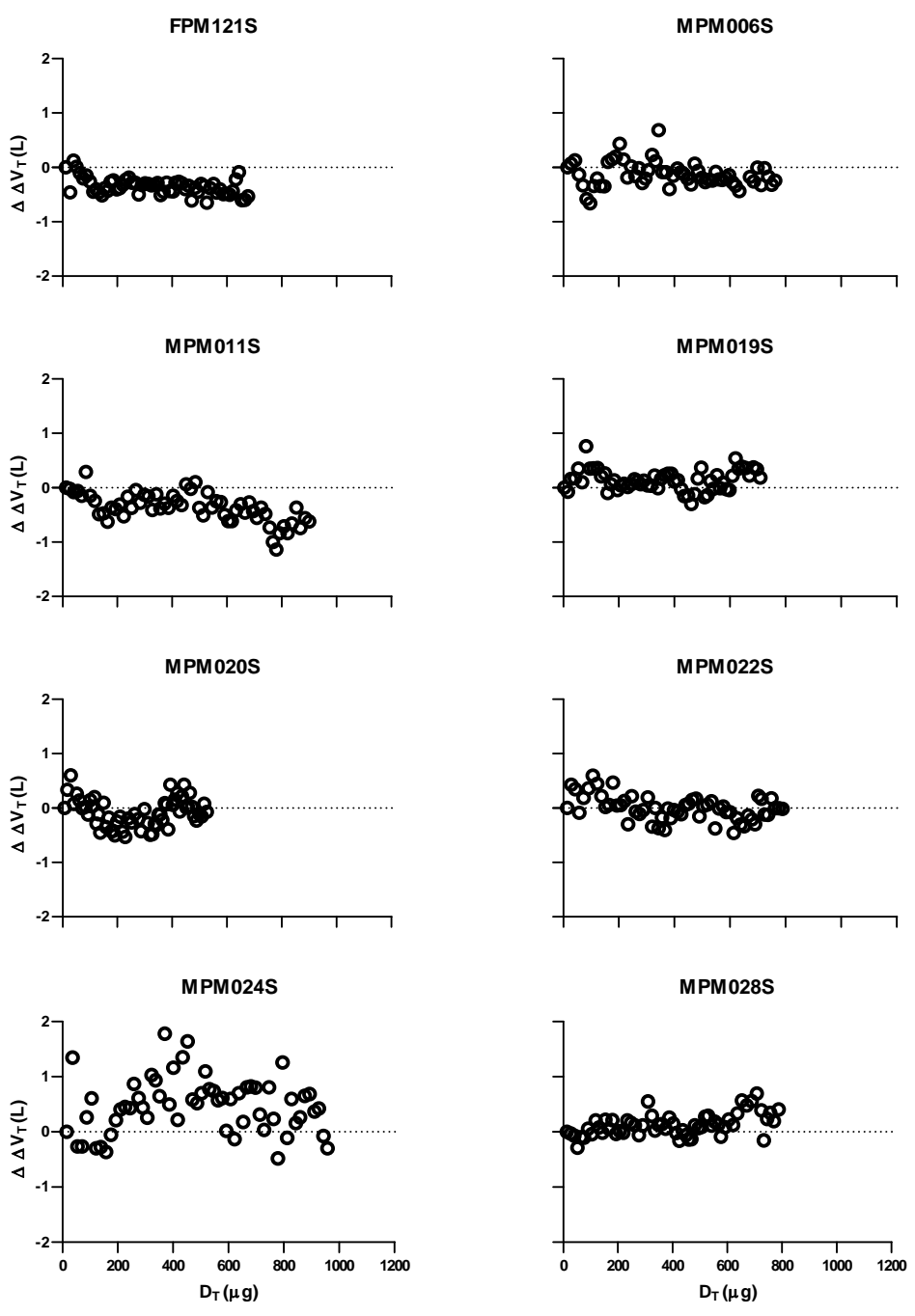


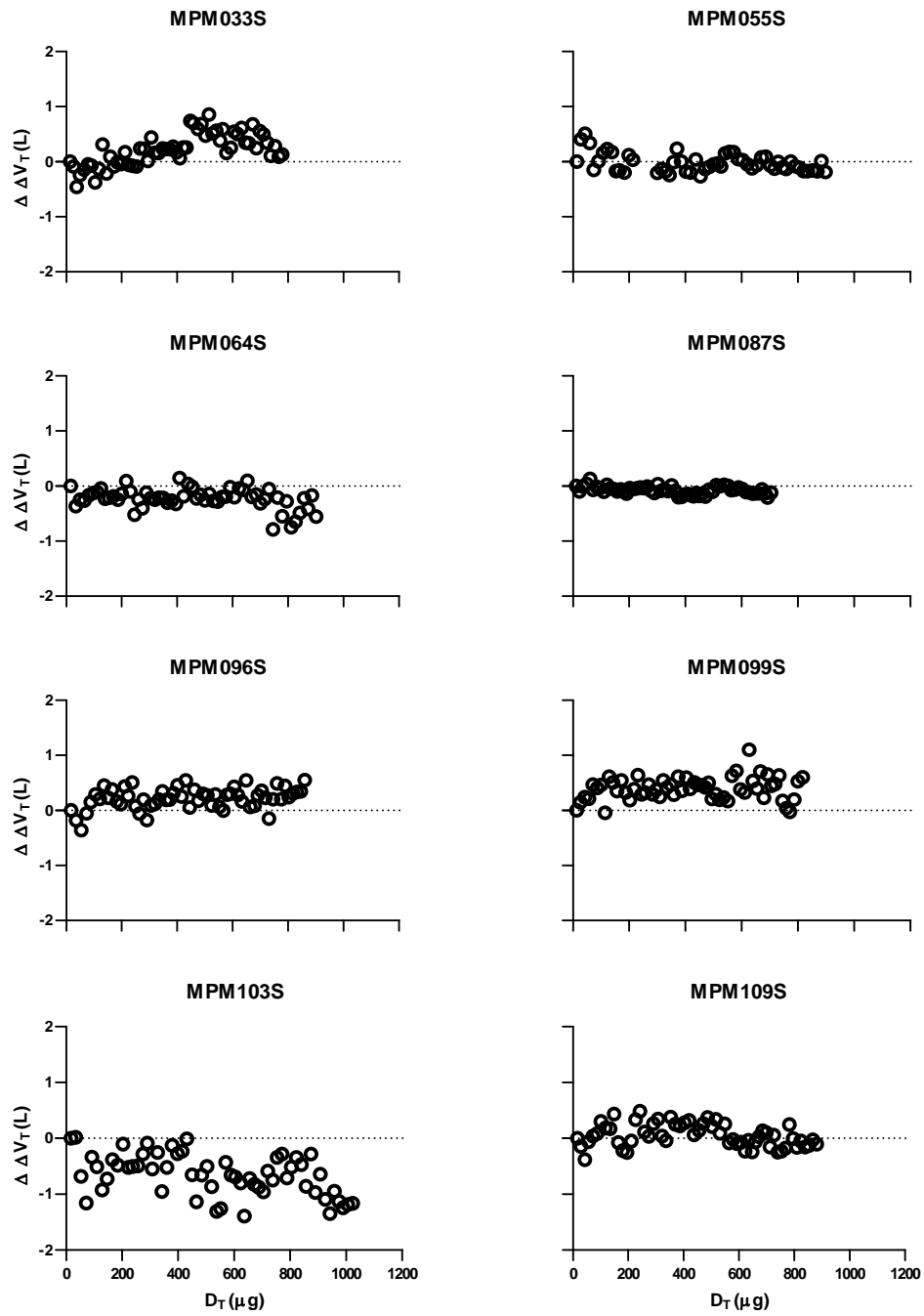


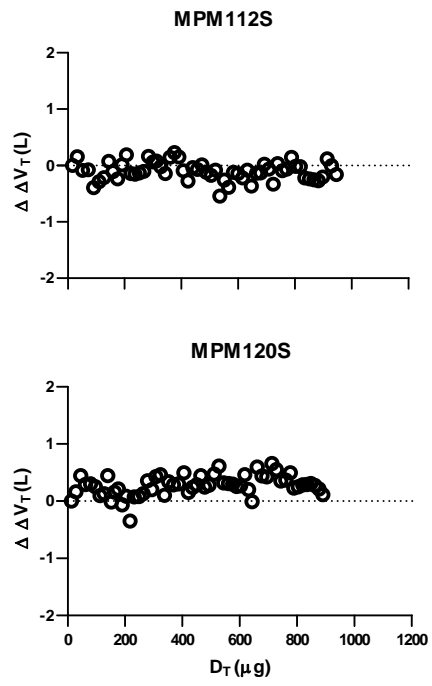




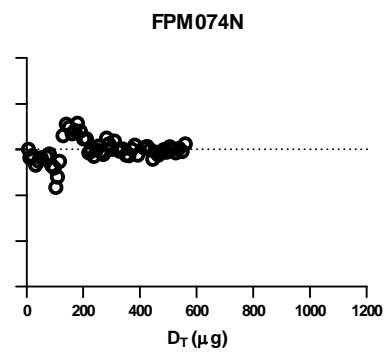
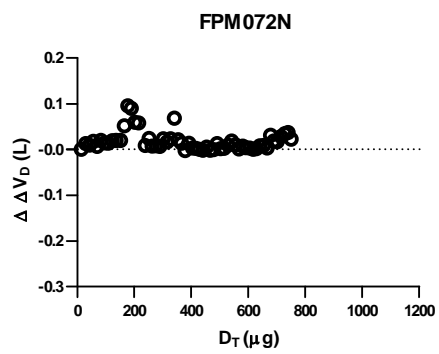
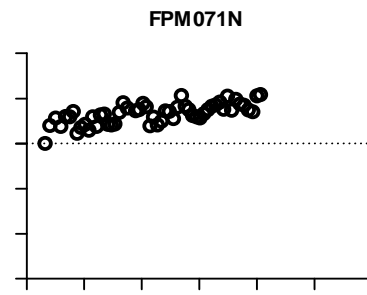
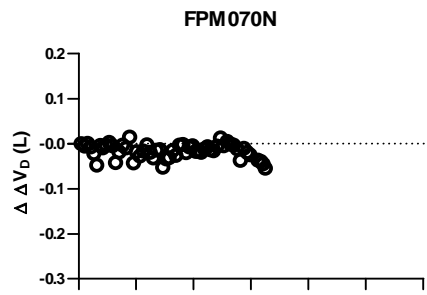
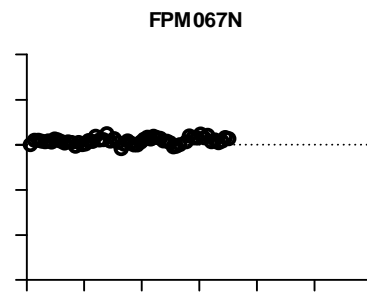
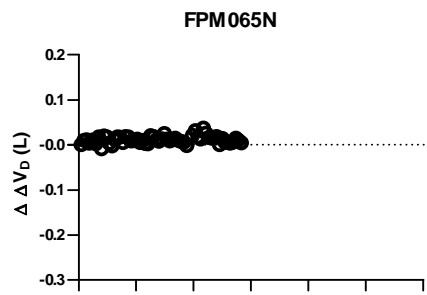
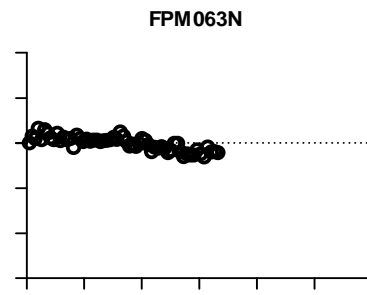
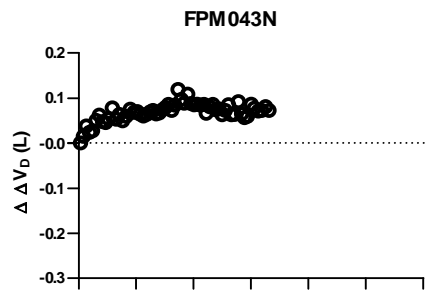


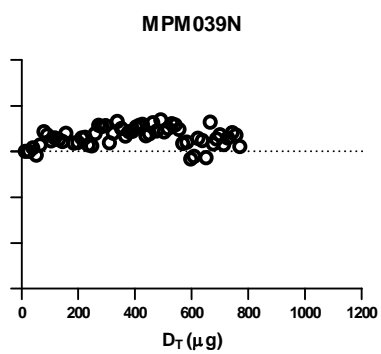
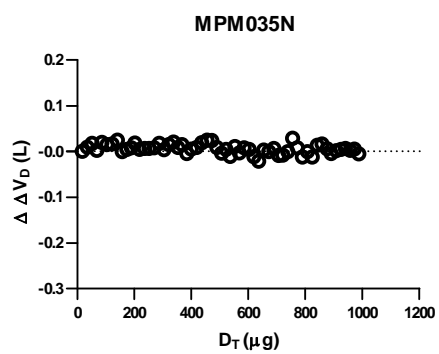
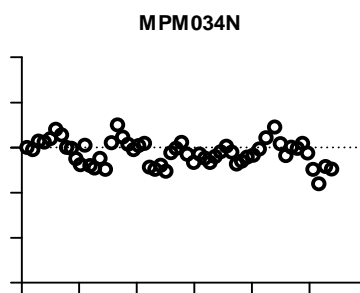
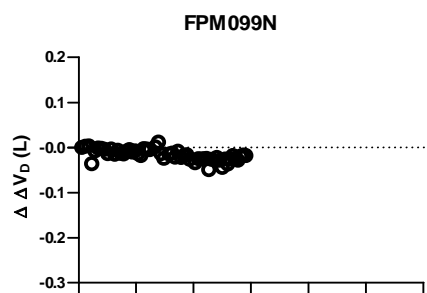
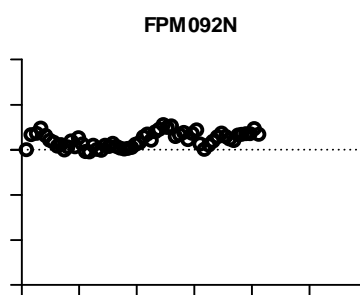
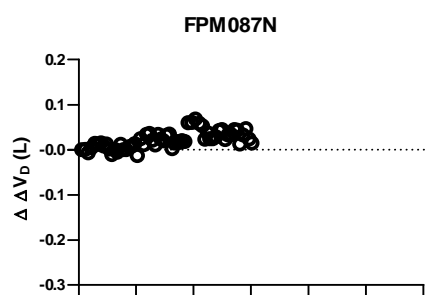
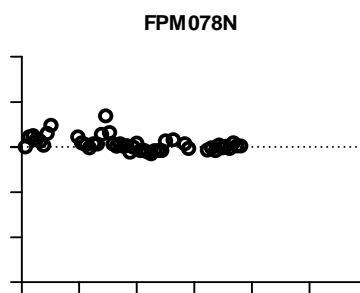
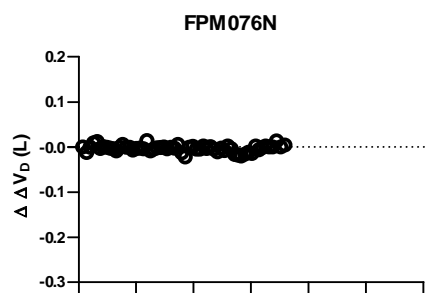


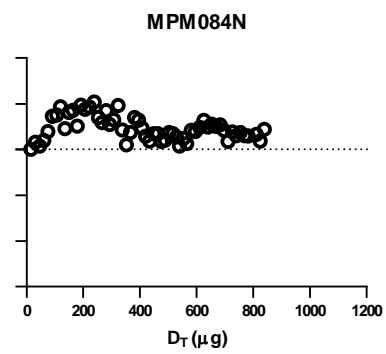
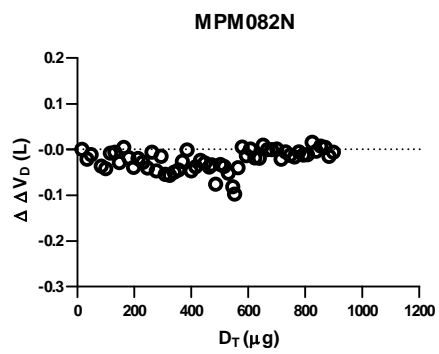
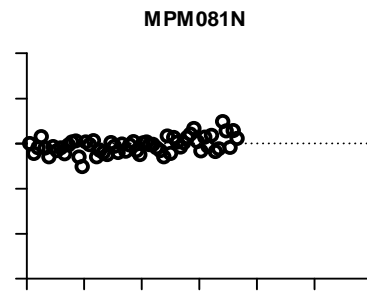
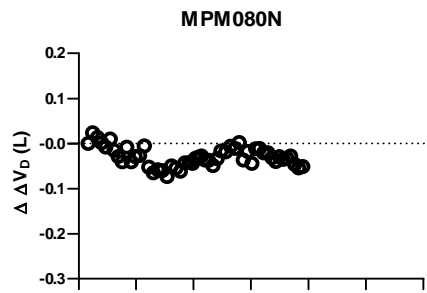
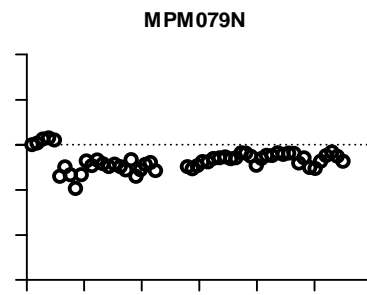
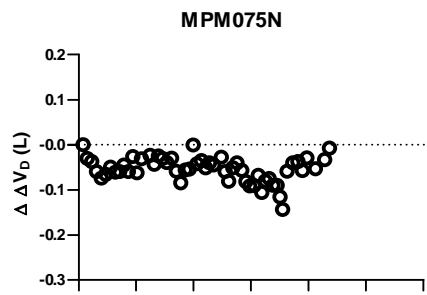
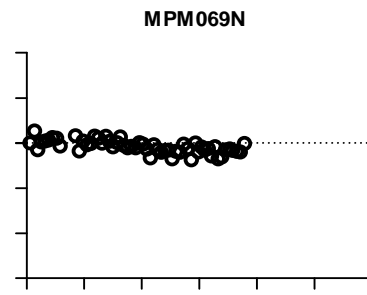
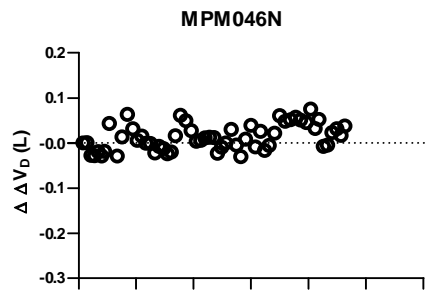


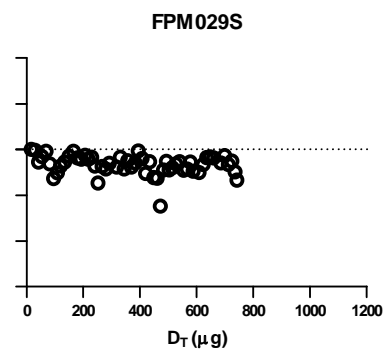
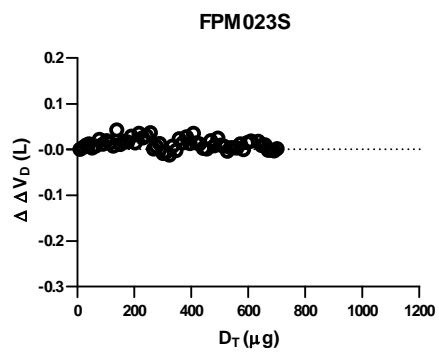
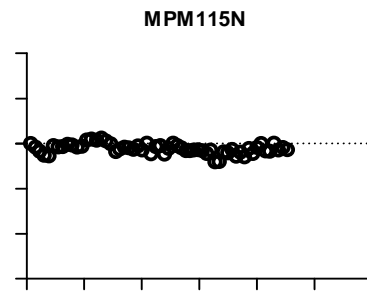
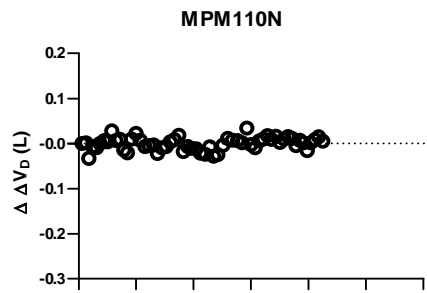
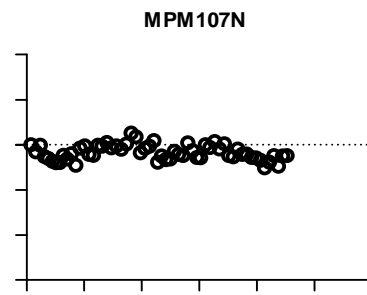
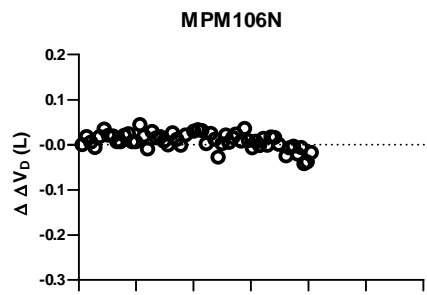
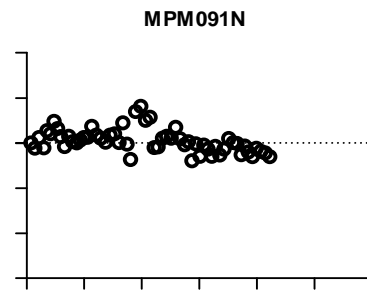
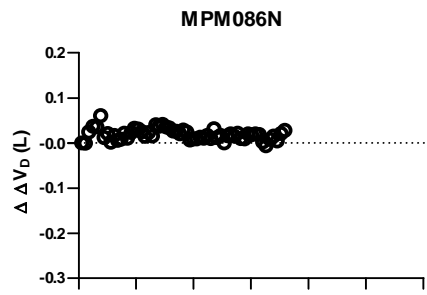


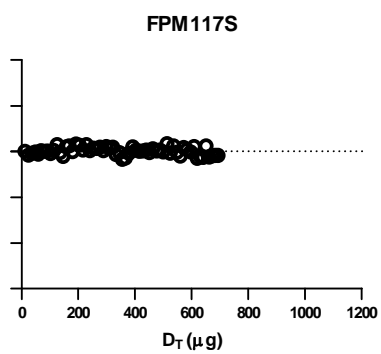
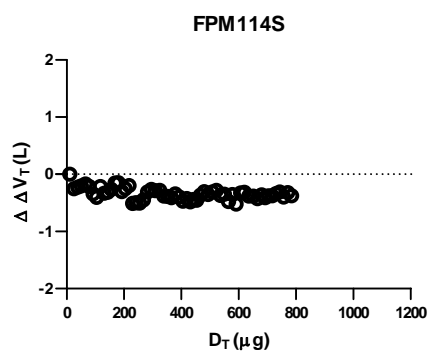
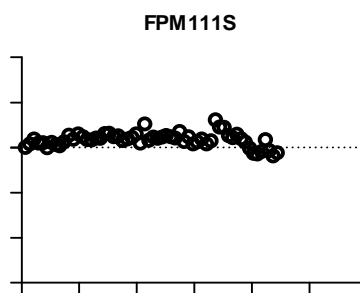
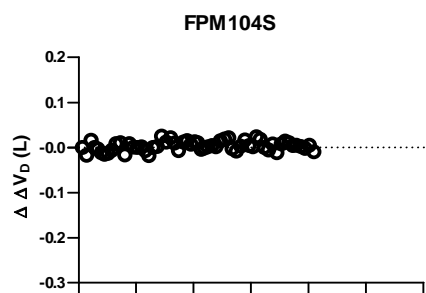
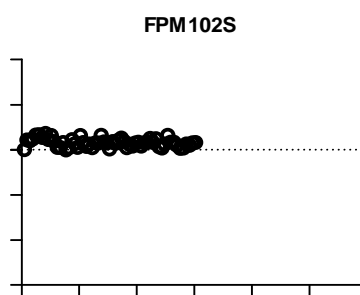
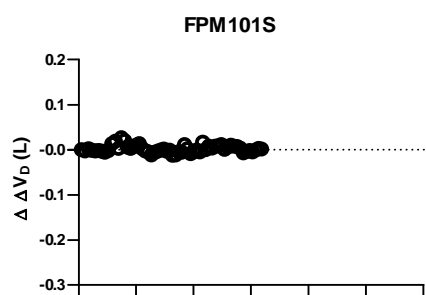
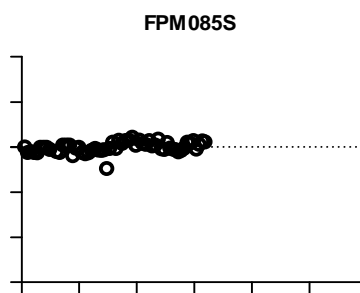
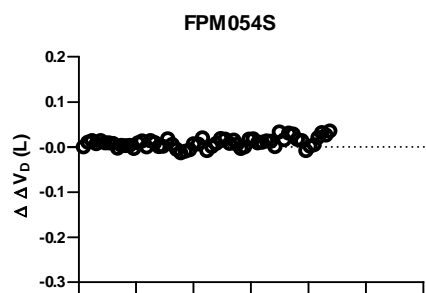
**Appendix B****Subject Specific Change in Dead Space Volume ( $V_D$ ) with****Respect to Retained Dose of  $O_3$**

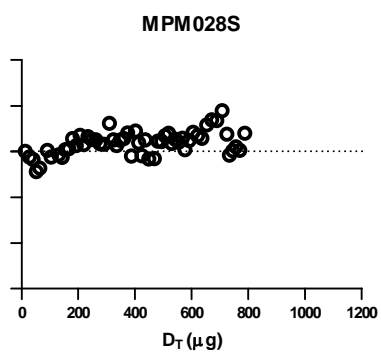
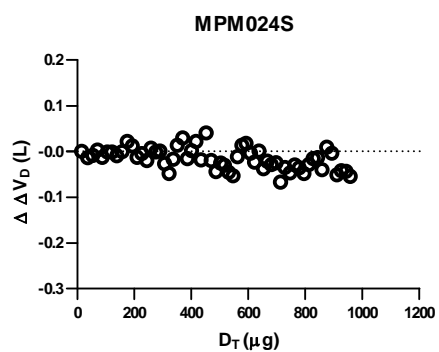
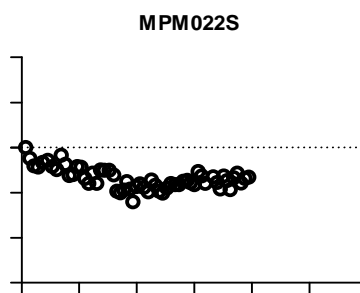
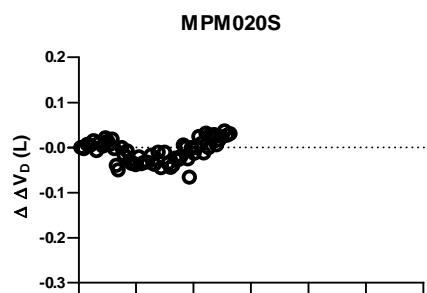
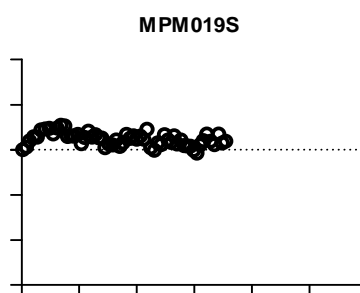
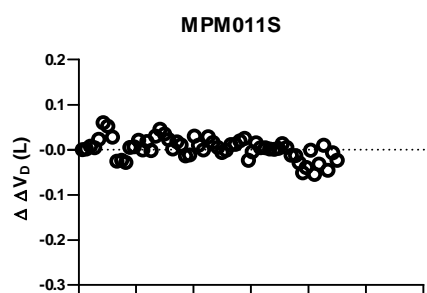
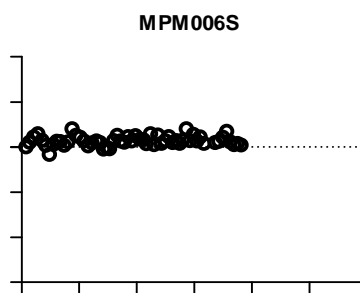
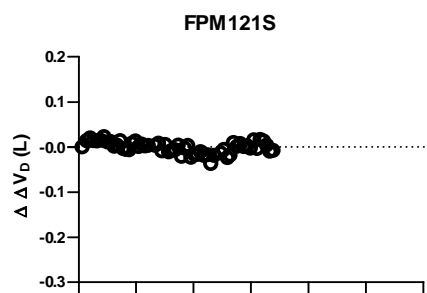


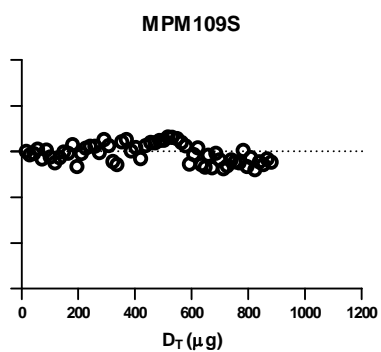
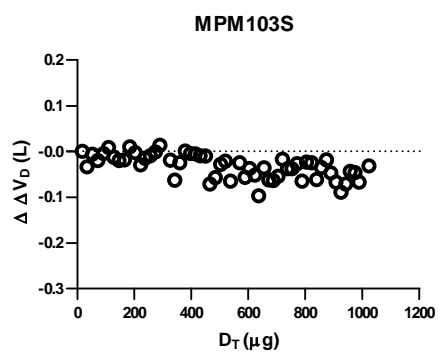
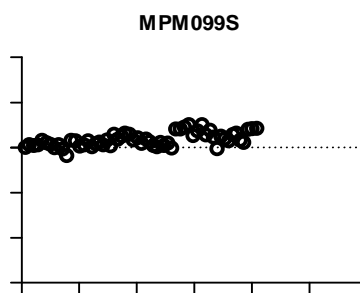
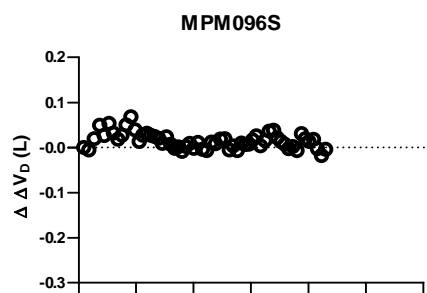
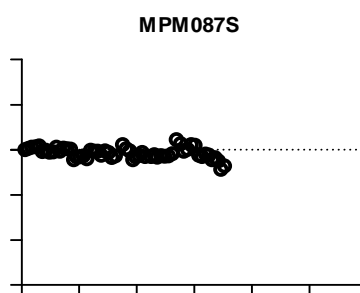
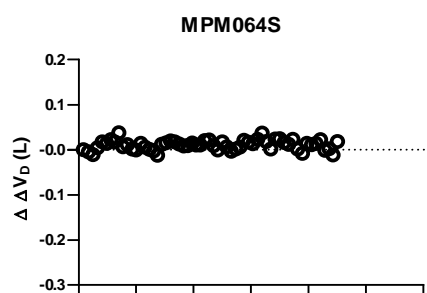
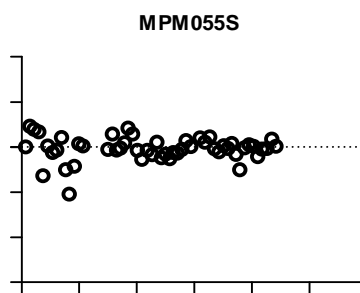
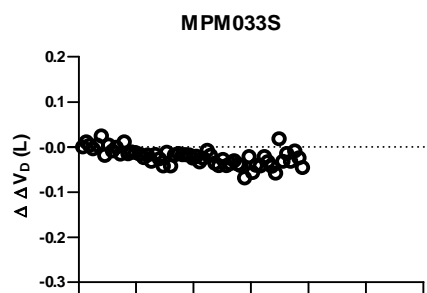


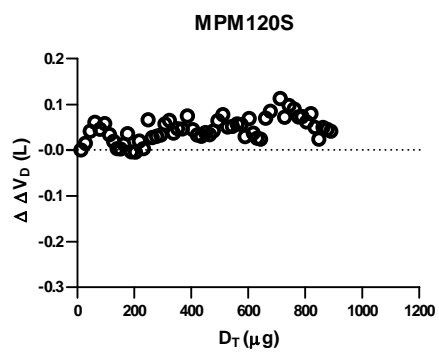
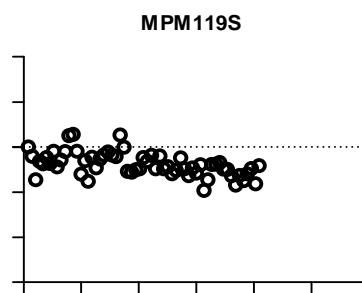
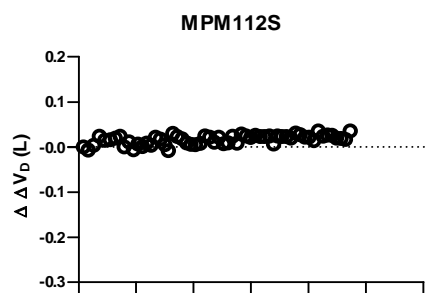












## Vita

### Timothy Michael Brenza

#### Education:

**Ph.D., Chemical Engineering**

The Pennsylvania State University      Fall 2008 (expected)

**B.S., Chemical Engineering**

The Pennsylvania State University      1996

#### Presentations:

**T. Brenza**, M.L. Bates, A. Ben-Jebria and J.S. Ultman (2007). Dynamic Changes in Response to Ozone Exposure. The American Institute of Chemical Engineers (AIChE) Annual Meeting. Salt Lake city, UT.

**T. Brenza**, M.L. Bates, A. Ben-Jebria and J.S. Ultman (2007). Determination of Ozone Uptake in Human Lungs: Study of the Effects of Smoking. The American Institute of Chemical Engineers (AIChE) Annual Meeting. Salt Lake city, UT.

**Timothy Brenza** (2007). Respiratory Measurements with Exposure to Ozone. Chemical Engineering Department Research Symposium, State College, PA.

**T. Brenza**, M.L. Bates, A. Ben-Jebria and J.S. Ultman (2006). The Effects of Smoking on Ozone Uptake in Human Lungs. Podium presentation at the Biomedical Engineering Society (BMES) Annual Meeting, Chicago, IL.

**Tim Brenza** and Melissa Bates (2006). Determination of Ozone Uptake in Human Lungs: Study of the Effects of Smoking. Paper presented at the College of Engineering Research Symposium, University Park, PA

#### Publications:

**T. Brenza**, M.L. Bates, A. Ben-Jebria and J.S. Ultman. "Dynamic Changes in Response to Ozone Exposure." AIChE Annual Meeting (CD). New York, NY: AIChE. 2007.

M. L. Bates, **T. M. Brenza**, A. Ben-Jebria, R. Bascom, and J. S. Ultman. Longitudinal Distribution of Ozone Absorption in the Lung: Comparison of Cigarette Smokers and Nonsmokers. (in submission).

#### Awards:

Student Poster Award for Foods, Pharmaceuticals, and Bioengineering (FPBE) Division at the American Institute of Chemical Engineers (AIChE) Annual Meeting, Salt Lake City (2007)

Third Place Award at the College of Engineering Research Symposium at the Pennsylvania State University (2006)